[AMERICAN JOURNAL OF SCIENCE, VOL. 291, JUNE, 1991, P. 541–648]

American Journal of Science

JUNE 1991

CRITICAL PHENOMENA IN HYDROTHERMAL SYSTEMS: STATE, THERMODYNAMIC, ELECTROSTATIC, AND TRANSPORT PROPERTIES OF H_2O IN THE CRITICAL REGION

JAMES W. JOHNSON* and DENIS NORTON
Department of Geosciences, University of Arizona, Tucson, Arizona 85721

ABSTRACT. The critical point defines the vertex of the near-parabolic H_2O vaporization boundary; hence, geometric considerations ensure that specific partial derivatives of any representative H_2O equation of state will diverge to $\pm\infty$ at criticality. This inherent divergency of isothermal compressibility, isobaric expansivity, and higher-order derivatives effectively controls not only thermodynamic, electrostatic, and transport properties of H_2O, but also dependent transport and chemical processes in hydrothermal systems.

The Gibbs-Duhem equation provides several thermodynamically-equivalent functional expressions for P–V_m–T and μ–ρ–T equations of state. Specific statements of these expressions, however, are distinguished by their mathematical representation of the critical point as either analytic or an isolated singularity, a distinction that leads to, respectively, so-called classical or nonclassical asymptotic behavior of equation-of-state derivatives. In the critical region, nonclassical μ–ρ–T formulations are preferred because they closely approximate experimental observations in the context of statistical mechanics descriptions of critical-point phase transition.

The nonclassical equation of state for H_2O developed by Levelt Sengers and others (1983) from modern theories of revised and extended scaling affords accurate prediction of state and thermodynamic properties in the critical region. This formulation has been used together with the classical, empirically-augmented virial equation proposed by Haar, Gallagher, and Kell (1984) and predictive equations for the dielectric constant (this study), thermal conductivity (Sengers and others, 1984), and dynamic viscosity (Sengers and Kamgar-Parsi, 1984; Watson, Basu, and Sengers, 1980b) to present a comprehensive summary of fluid H_2O properties within and near the critical region. Specifically, predictive formulations and computed values for twenty-three properties are presented as a series of equations, three-dimensional P–T surfaces, isothermal and isobaric cross sections, and skeleton tables from 350° to 475°C and 200 to 450 *bars*. The properties considered are density, isothermal compressibility, isobaric expansivity and its isobaric temperature derivative, Helmholtz and Gibbs free

* Present address: Earth Sciences Department, Lawrence Livermore National Laboratory, L-219, P.O. Box 808, Livermore, California 94550

energies, internal energy, enthalpy, entropy, isochoric and isobaric heat capacities, the dielectric constant, Z, Q, Y, and X Born functions, dynamic and kinematic viscosity, thermal conductivity, thermal diffusivity, the Prandtl number, the isochoric expansivity-compressibility coefficient, and sound velocity.

The equations and surfaces are analyzed with particular emphasis on functional form in the near-critical region and resultant extrema that persist well beyond the critical region. Such extrema in isobaric expansivity, isobaric heat capacity, and kinematic viscosity delineate state conditions that define local maxima in fluid and convective heat fluxes in hydrothermal systems; in permeable media, these fluxes diverge to ∞ at the critical point. Extrema in the *Q*, *Y*, and *X* Born functions delineate state conditions that define local maxima or minima in the standard partial molal volumes, enthalpies, entropies, and heat capacities of aqueous ions, complexes, and electrolytes; these properties diverge to ±∞ at criticality. Because these fluxes and thermodynamic properties diverge to ±∞ at the critical point, seemingly trivial variations in near-critical state conditions cause large variations in fluid flow velocity, thermal energy transfer rates, and the state of chemical equilibrium.

INTRODUCTION

Permeable-media transport theory and modern theoretical geochemistry demonstrate that transport and chemical processes in magma-hydrothermal systems are largely controlled by thermophysical and electrostatic properties of the universal solvent, H_2O (Norton and Knight, 1977; Norton, 1984; Helgeson and Kirkham, 1976; Helgeson, Kirkham, and Flowers, 1981). Of particular importance is the dependence of fluid flux, thermal energy convection, and the thermodynamic effects of ion solvation on derivative properties of the H_2O equation of state. This dependence causes fluid and convective heat fluxes and most standard partial molal properties of aqueous solutes to asymptotically approach ±∞ at the H_2O critical point; moreover, they maintain anomalous values within a restricted sector of the equation-of-state surface known as the *critical region.* In practice (Levelt Sengers and others, 1983), this sector is delineated by the 421.85°*C* isotherm, 0.20 and 0.42 g/cm^3 isochores, and vaporization-boundary segment that bridges these isochores. In P–T coordinates, these conditions are intermediate to those of magma solidi and ambient geothermal gradients in the upper crust. As a result, the P–T evolution of shallow intrusive bodies and their proximate host rocks invariably includes traversal of the aqueous-phase critical region.[1] Be-

[1] We refer here to the effective critical region of fluid compositions thought to occur in magma-hydrothermal systems. It is important to recognize that although the following discussion focuses on the near-critical divergent behavior of pure H_2O as a limiting case, such anomalous behavior is in fact characteristic of all dilute fluid mixtures (Chang, Morrison, and Levelt Sengers, 1984; Levelt Sengers and others, 1984, 1986; Chang and Levelt Sengers, 1986) and thus relevant to many of the aqueous electrolyte solutions inferred to be present in magma-hydrothermal environments (Helgeson, 1964, 1970; Roedder, 1972, 1979, 1984). The primary difference between the effects of critical phenomena in pure H_2O and in natural hydrothermal solutions is the composition-dependent

cause all epizonal subsurface and submarine magma-hydrothermal systems attain critical-region conditions, description and analysis of the transport and chemical consequences of critical phenomena is fundamental to our understanding of these environments.

Numerous equations of state for H_2O have been proposed since the late nineteenth century; although conceptually varied, one common theme emerges: unique treatment of the critical region where partial derivatives of the $\rho(P, T)$ surface diverge to $\pm\infty$ at the critical point. Because this divergence has proved difficult to represent accurately with traditional theoretical descriptions, such formulations typically require augmentation with an appropriate difference function near the critical point: a theoretically unsatisfactory and computationally inconvenient approach. Moreover, regression coefficients used in such difference functions must be derived from experimental volumetric data, the abundance and resolution of which diminishes as the critical state is approached. Hence, this procedure has necessarily resulted in predictions of the *near-critical region* (a subset of the critical region restricted to within a few degrees and bars of the critical point) that are inferior to those elsewhere. Recently, however, the modern theory of critical phenomena has led to development of an equation of state that describes the critical-region surface with a level of accuracy comparable to that attained for the *global region* (state conditions of fluid H_2O stability excluding the critical region). This advancement makes possible quantitative assessment of transport and chemical processes in the H_2O critical region.

The purpose of this communication is to: (1) summarize the theoretical development of an accurate critical-region equation of state, (2) present a comprehensive set of equations and data (Levelt Sengers and others, 1983; Haar, Gallagher, and Kell, 1984; Sengers and others, 1984; Sengers and Kamgar-Parsi, 1984; those proposed in the present study) that facilitate calculation of the thermophysical and electrostatic properties of H_2O required for numerical modeling of transport and geochemical processes in hydrothermal systems, (3) analyze the functional form of these properties within and near the critical region, and (4) present a set of illustrations that will continue to facilitate visual appreciation of the functional behavior discussed herein long after the precision of far-decimal places reported in the associated skeleton tables has been superseded. Property values are given below in the context of independent-variable, triple-point, and unit conventions commensurate with those

criticality condition. A well-studied and particularly relevant example is the H_2O-*NaCl* system. Here, as with most single electrolyte aqueous solutions (Marshall and Jones, 1974), criticality shifts to progressively higher temperatures and pressures with increasing electrolyte concentration. The critical point for a mixture containing 4 wt percent *NaCl*, an example composition which approximates (in bulk) that of many hydrothermal fluids (Roedder, 1972, 1979), is located at approx 415°C, 320 *bars* (Bischoff and Rosenbauer, 1988). Hence, the critical region for this particular H_2O–*NaCl* solution will occur at correspondingly higher P–T conditions than those of pure H_2O, but the anomolous divergent behavior of solvent (and solute) properties and their effect on transport and chemical processes will, of course, persist.

most often used in modern theoretical geochemistry and transport modeling. The values were computed, tabulated, and illustrated using a software package designed and developed by the senior author in the course of this investigation. This package implements equations and data from the above references, incorporates modified versions of several routines given by Levelt Sengers and others (1983) and Haar, Gallagher, and Kell (1984), and, at the drafting stage, utilizes an Evans & Sutherland PS-300 graphics workstation together with graphics software developed by L. Steve Sorenson.

To some extent, this contribution represents an update and refinement of Helgeson and Kirkham's (1974a) pioneering summary of the thermodynamic and electrostatic properties of H_2O at elevated temperatures and pressures. Relative to their work, however, the scope of the present discussion has been focused on the critical region and property extrema, while expanded to include transport properties and theoretical development of the critical-region equation of state. Accurate prediction of the thermophysical and electrostatic properties of H_2O within and near the critical region is of paramount importance in numerical modeling of transport and chemical processes in hydrothermal systems. It is hoped that the present communication will provide a comprehensive summary of equations and data that facilitate such prediction.

THEORETICAL DEVELOPMENT

Because of their importance in all branches of engineering and natural science, no substances have been more thoroughly investigated by the scientific community than the fluid phases of H_2O. The myriad experimental and theoretical studies involving measurement and description of various properties of these phases have produced a data base and set of predictive equations whose comprehensive and precise nature is unsurpassed by those of all other substances. At the core of these equations is the equation of state: derived from theory, but implemented with inseparable dependence on experiment.

The following discussion presents a review of thermodynamic and mathematical considerations in developing such an equation, theoretical and predictive distinctions between so-called classical and nonclassical equations of state, and the specific formulations from which fluid H_2O properties are evaluated in this study: in the global region, the classical virial equation developed by Haar, Gallagher, and Kell (1984) —hereinafter referred to as the HGK equation; in the critical region, the nonclassical scaled description proposed by Levelt Sengers and others (1983) —hereinafter referred to as the LS equation.

Thermodynamic and mathematical considerations.—An equation of state defines the functional relationship among intensive variables for a given substance and its physical surroundings. In general, the mathematical form and related parameters of such an equation are completely unrestricted. If, however, the state function is to serve as the fundamental equation from which *thermodynamic* status of the substance is described, then specific constraints on both its functional form and set of interre-

lated intensive variables are imposed by the Gibbs-Duhem equation, which relates differential changes in these variables. The Gibbs-Duhem relation for a one-component substance of constant mass can be expressed as

$$nd\mu = -SdT + CVdP, \tag{1}$$

where $n\,(mol)$ stands for the number of moles, μ (cal/mol) denotes chemical potential, S $(cal/°K)$ refers to entropy, $C(0.02390054\ cal\ bar^{-1}\ cm^{-3})$ represents a conversion factor, and $T(°K)$, $P(bars)$, and $V(cm^3)$ correspond to temperature, pressure, and volume. Normalization of eq (1) with respect to n or V and subsequent optional Legendre transformation of state variables in the T-independent term yields four equivalent expressions from which all thermodynamic and state properties can be obtained from appropriate partial differentiation. These expressions, often refered to as fundamental equations owing to their thermodynamic versatility, are given by

$$d\mu = -S_m dT + CV_m dP, \tag{2}$$

$$dA_m = -S_m\, dT - CPdV_m, \tag{3}$$

$$dP = \frac{1}{C}\left(S_v\, dT + \frac{\rho}{M}\, d\mu\right), \tag{4}$$

and

$$dA_v = -S_v\, dT + \frac{\mu}{M}\, d\rho, \tag{5}$$

where m-subscripts denote *molar* (mol^{-1}) properties, v-subscripts refer to *specific* (cm^{-3}) quantities, A defines the subscripted Helmholtz free energy, and $M\,(18.0152\ g/mol)$ corresponds to the molecular weight of H_2O.

Equations of state derived from eqs (2) through (5) are, respectively,

$$V_m(T, P) = \frac{1}{C}\left(\frac{\partial \mu}{\partial P}\right)_T, \tag{6}$$

$$P(T, V_m) = -\frac{1}{C}\left(\frac{\partial A_m}{\partial V_m}\right)_T, \tag{7}$$

$$\rho(T, \mu) = MC\left(\frac{\partial P}{\partial \mu}\right)_T, \tag{8}$$

and

$$\mu(T, \rho) = M\left(\frac{\partial A_v}{\partial \rho}\right)_T. \tag{9}$$

Because eqs (6) through (9) are thermodynamically equivalent, choice of variable set, P–V_m–T or μ–ρ–T, within which to case an equation of state is

unrestricted in a thermodynamic sense. From a mathematical standpoint, however, thermodynamic utility of theoretical or empirical expressions that represent specific statements of eqs (6) through (9) requires their formulation as readily integrable expressions.

An additional prerequisite is the existence of experimental P–V_m–T or μ–ρ–T data, from which the adjustable coefficients characteristic of all

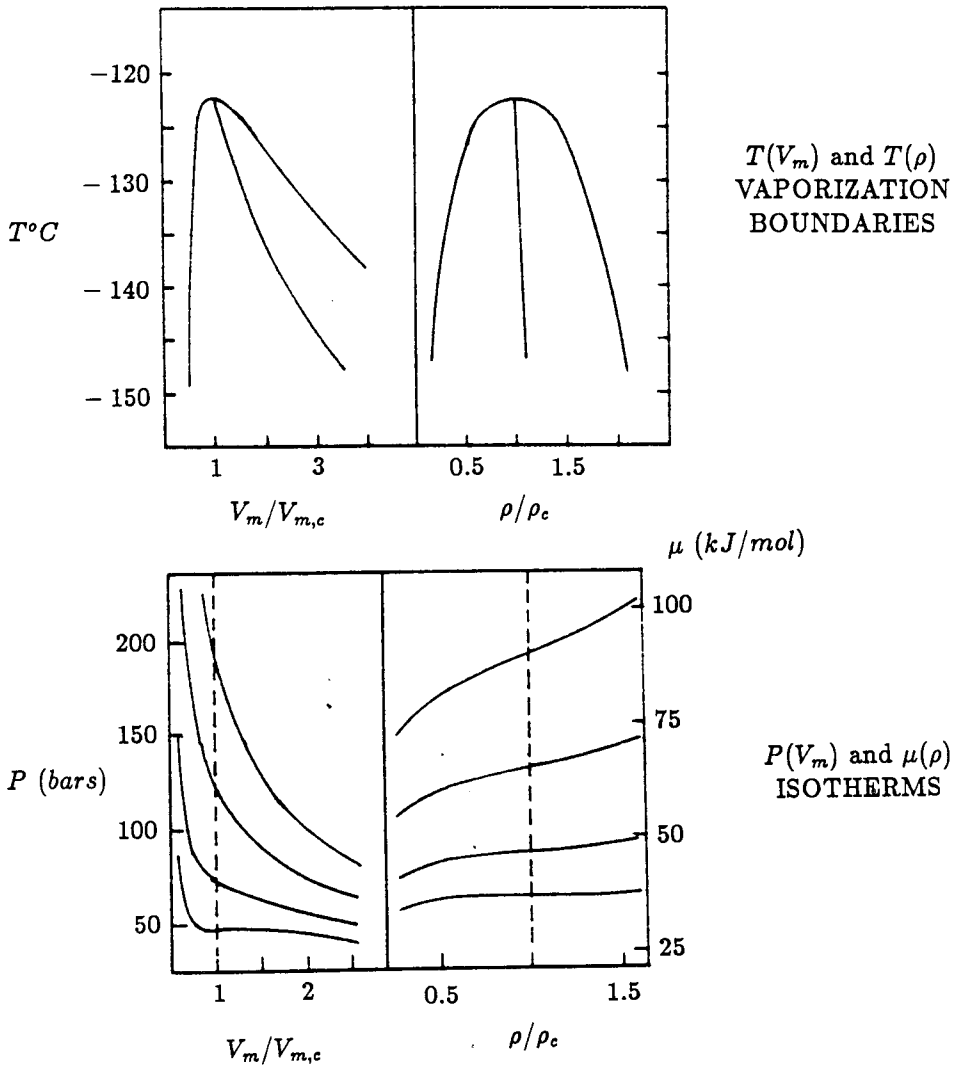

Fig. 1. The argon vaporization boundary and isotherms in thermodynamically equivalent state variables: P–V_m–T and μ–ρ–T. Note preferred symmetry of the vaporization boundary and preferred antisymmetry of isotherms with respect to the critical isochore in μ–ρ–T coordinates. Modified from Levelt Sengers, Greer, and Sengers (fig. 1, 1976).

such expressions are obtained through regression analysis. Because these data are invariably reported as P–V_m–T measurements, the overwhelming majority of fluid equations of state are implicitly based on eq (6) or (7). Included among this class of functions are all virial (Onnes, 1901) and van der Waals (ms) equations; notable examples include the formulation given by Keenan and others (1969) and the HGK equation, both of which define *molar* Helmholtz free energy, eq (3), from integration of an empirically-augmented virial expansion that represents the associated state function, eq (7).

Although convenience dictates implementation of most state functions in P–V_m–T space, intrinsic symmetry properties of the thermodynamically equivalent μ–ρ–T coordinate system necessitate use of this latter variable set in formulating an accurate equation of state for the critical region. In particular, μ–ρ–T coordinates provide perfect symmetry of the $\rho(T)$ vaporization boundary and anti-symmetry of $\mu(\rho)$-isotherms with respect to the critical isochore (Callitet and Mathias, 1886; Michels, Blaisse, and Michels, 1937; Michels, Levelt, and Graaff, 1958; Guggenheim, 1945; Tisza and Chase, 1965; Roach, 1968; Vicentini-Missoni, Levelt Sengers, and Green, 1969b; Wallace and Meyer, 1970b). These symmetry features, decidedly lacking in P–V_m–T space (fig. 1), are also present in the lattice-gas model of critical-point phase transition (Lee and Yang, 1952; Fisher, 1964; Brush, 1967; Levelt Sengers, 1970, 1974; Sengers and Levelt Sengers, 1978; Levelt Sengers and Greer, 1972), a statistical mechanics description (based on the Ising model of analogous transition at the ferromagnet Curie point: Ising, 1925; Onsager, 1944) that affords close approximation of anomolous, near-critical thermodynamic behavior (Levelt Sengers, 1970; Sengers and Levelt Sengers, 1978). As a result, most equations of state designed to represent such anomalies are cast in terms of $\rho(T, \mu)$ or $\mu(T, \rho)$, experimental values of which can be obtained from numerical integration of their $V_m(T, P)$ and $P(T, V_m)$ counterparts (Vicentini-Missoni, Levelt Sengers, and Green, 1969b). State functions of this type include virtually all scaled equations of state developed from the modern theory of critical phenomena; notable examples include the formulation proposed by Widom (1965) and the LS equation, both of which can be viewed as modified versions of eqs (4) and (8).

As outlined above, thermodynamics provides several equivalent functional expressions within which to cast an equation of state. Specific statements of these expressions, however, are subdivided into two behaviorally distinct catagories based on their functional representation of the critical point: the P–V_m–T (and μ–ρ–T) coordinate that bridges the vaporization boundary and confluent critical isochore, thereby uniquely satisfying

$$\left(\frac{\partial P}{\partial V_m}\right)_T^{-1} \equiv -\left(\frac{\partial^2 A_m}{\partial V_m^2}\right)_T^{-1} = \infty = \left(\frac{\partial^2 P}{\partial V_m^2}\right)_T^{-1} \equiv -\left(\frac{\partial^3 A_m}{\partial V_m^3}\right)_T^{-1}$$

and

$$\left(\frac{\partial \mu}{\partial \rho}\right)_T^{-1} \equiv -\left(\frac{\partial^2 A_v}{\partial \rho^2}\right)_T^{-1} = \infty = \left(\frac{\partial^2 \mu}{\partial \rho^2}\right)_T^{-1} \equiv -\left(\frac{\partial^3 A_v}{\partial \rho^3}\right)_T^{-1}. \tag{10}$$

The criticality condition implicitly ensures that specific first- and second-derivative properties of *any representative* equation of state will be divergent. If such an equation is *analytic* at the critical point, then by definition all derivatives of the dependent state variable exist here and can be represented as Taylor series in their independent variables, which in practice are typically reduced and normalized relative to their critical values. Lower-order approximations to these Taylor series produce a corresponding set of exponents that govern the divergence of derivative properties to $\pm\infty$ with approach to criticality. All equations of state having implicit critical-point analyticity (van der Waals and virial equations), and therefore a restricted set of possible divergence-governing exponents, yield similar, so-called *classical,* asymptotic behavior in their derivative properties (Fisher, 1964; Griffiths, 1967; Levelt Sengers, 1970, 1974; Levelt Sengers, Greer, and Sengers, 1976; Levelt Sengers, Morrison, and Chang, 1983; Sengers and Levelt Sengers, 1978).

There is, however, no mathematical advantage obtained by formulating the equation of state such that near-critical divergence of its derivative properties is governed by exponents consistent with approximated Taylor series. In fact, compelling experimental evidence argues for the alternative development. Equations of state belonging to this second category, that is, those that describe *nonanalytic* functions at the critical point, are characterized by so-called *nonclassical* asymptotic behavior of derivative properties (Griffiths, 1967; Levelt Sengers, 1970, 1974; Levelt Sengers and Greer, 1972; Sengers and Levelt Sengers, 1978).

This functional distinction of critical-point analyticity and nonanalyticity between classical and nonclassical equations of state leads to significant differences in their representation and prediction of near-critical thermodynamic anomolies.

Classical equations in the near-critical region.—Critical-point Taylor expansions for classical equations of state are most conveniently expressed in terms of dimensionless properties reduced by normalization with respect to the appropriate critical parameter(s). In the μ–ρ–T coordinate system, these properties are defined as (Levelt Sengers, 1970; Sengers and Levelt Sengers, 1978)

$$\begin{aligned} T^* &= T/T_c, & \Delta T^* &= T^* - 1 = (T - T_c)/T_c, \\ \rho^* &= \rho/\rho_c, & \Delta\rho^* &= \rho^* - 1 = (\rho - \rho_c)/\rho_c, \\ \mu^* &= \mu\rho_c/(CP_c), & \Delta\mu^* &= [\mu(\rho, T) - \mu(\rho_c, T)]\rho_c/(CP_c), \text{ and} \\ A_v^* &= A_v/(CP_c), \end{aligned} \tag{11}$$

where c-subscripts denote critical parameters, and $\mu(T, \rho_c)_{T<T_c} \equiv \mu_{[l,v]}(T)$, in accord with critical-point slope continuity between the vaporization

boundary and critical isochore. The Taylor series for A_v^* and μ^* in $(\Delta T^*, \Delta\rho^*)$ can be expressed as

$$[A_v, \mu]^* = \sum_{i=0}^{\infty}\sum_{j=0}^{\infty} \frac{[A_v, \mu]_{ij}}{i!j!} (\Delta\rho^*)^i (\Delta T^*)^j, \tag{12}$$

where the $[A_v, \mu]_{ij}$ coefficients are given by

$$[A_v, \mu]_{ij} = \left(\frac{\partial^{i+j}[A_v, \mu]^*}{\partial(\Delta\rho^*)^i \partial(\Delta T^*)^j}\right), \tag{13}$$

and interrelated by $\mu_{ij} = A_{v(i+1)j}$ for $i \geq 1$ (Sengers and Levelt Sengers, 1978).

Very near the critical point, eq (12) and its derivatives are closely approximated by lowest-order terms, and critical-point identities $A_{v20} = A_{v30} = \mu_{10} = \mu_{20} = 0$ can be considered valid. In this region, the expansions reduce to simple power laws that represent classical asymptotic behavior of thermodynamic functions along specific paths of critical-point approach: the *critical isotherm* $(\Delta T^* = 0)$, *vaporization boundary* $(\Delta\mu^* = 0)$, and *critical isochore* $(\Delta\rho^* = 0)$, (Levelt Sengers, 1970, 1974; Levelt Sengers, Greer, and Sengers, 1976; Sengers and Levelt Sengers, 1978):

$$\Delta\mu^* = D_{ca}(\Delta\rho^*)|\Delta\rho^*|^{\delta_{ce}-1} \quad (\Delta T^* = 0), \tag{14}$$

$$|\Delta\rho^*_{[l,v]}| = B_{ca,[l,v]}|\Delta T^*|^{\beta_{ce}} \quad (\Delta\mu^* = 0), \tag{15}$$

$$\chi_T^* = \Gamma_{ca}|\Delta T^*|^{-\gamma_{ce}} \quad (\Delta\rho^* = 0), \tag{16}$$

and

$$c_v^* = -A_{ca}(\Delta T^*)^{-\alpha_{ce}} \quad (\Delta\rho^* = 0), \tag{17}$$

where χ_T^* corresponds to dimensionless isothermal compressibility, $(\chi_T^*)^{-1} \equiv (\partial\mu^*/\partial\rho^*)_{T^*} \equiv (\partial^2 A_v^*/\partial\rho^{*2})_{T^*}$, and c_v^* defines dimensionless isochoric heat capacity, $c_v^* \equiv -T^*(\partial^2 A_v^*/\partial T^{*2})_{\rho^*}$; *critical amplitudes* $[A, B, \Gamma, D]_{ca}$ are defined in terms of $[A_v, \mu]_{ij}$; and *critical exponents* $\alpha_{ce} = 0$, $\beta_{ce} = 1/2$, $\gamma_{ce} = 1$, and $\delta_{ce} = 3$ follow directly from first-order approximation to the Taylor series (Sengers and Levelt Sengers, 1978). The interested reader can derive power laws analogous to eqs (16) and (17) for all other first- and second-derivative properties of $\mu^*(\Delta\rho^*, \Delta T^*)$.

Although the power laws do not follow directly from thermodynamic or statistical mechanic principles (Griffiths, 1965a), consideration of thermodynamic stability does impose certain restrictions on interrelationships of the critical exponents (Griffiths, 1965a, b; Rushbrooke, 1963; Liberman, 1966; Mermin and Rehr, 1971; Rowlinson, 1969). Specifically,

$$2 - \alpha''_{ce} \leq \beta_{ce}(\delta_{ce} + 1),$$

and

$$\gamma'_{ce} \leq \beta_{ce}(\delta_{ce} - 1), \tag{18}$$

where γ'_{ce} controls the divergence of χ_T^* to ∞ (and α'_{ce} that of c_v^*) as the critical point is approached along either branch of the $\Delta\rho^*(\Delta T^*)$ vaporization boundary, α''_{ce} controls analogous divergency of c_v^* when criticality in the $\Delta T^* - \Delta\rho^*$ plane is approached from subcritical temperatures along the metastable critical isochore, $\alpha''_{ce} = \alpha'_{ce} = \alpha_{ce}$, and $\gamma'_{ce} = \gamma_{ce}$ (Levelt Sengers, Greer, and Sengers, 1976). Eq (18) holds with equality signs for both classical and nonclassical descriptions; hence, only two of the critical exponents are independent.

Eqs (14) through (17) summarize near-critical thermodynamic predictions of classical equations of state. In particular, to lowest-order approximation the asymptotic shape of the critical isotherm is cubic, that of the vaporization boundary is quadratic with symmetric top, and with approach to criticality along the critical isochore and vaporization boundary χ_T^* diverges logarithmically to ∞ while c_v^* converges to a finite value (Levelt Sengers, 1970, 1974; Levelt Sengers and Greer, 1972; Sengers and Levelt Sengers, 1978; Levelt Sengers, Greer, and Sengers, 1976). Associations between these special directions in the $\Delta T^* - \Delta\rho^*$ plane and derived power laws and critical exponents and amplitudes are summarized in figure 2.

Extensive experimental investigation of asymptotic power laws (14) through (17) has conclusively determined that although real one-component fluids do indeed obey such power laws, actual critical exponent values differ significantly from those predicted by classical equations. In particular, the vaporization boundary is closer to cubic than quadratic: $\beta_{ce} \approx 0.34$ to 0.36 (Verschaffelt, 1900; Eck, 1939; Michels, Blaisse, and Michels, 1937; Guggenheim, 1945; Lorentzen, 1953; Pings and Teague, 1968); the critical isotherm is somewhat higher-order than quadratic: $\delta_{ce} \approx 4.0$ to 4.6 (Widom and Rice, 1955; Wallace and Meyer, 1970b); divergence of isothermal compressibility is slightly stronger than logarithmic: $\gamma_{ce} \approx 1.1$ to 1.3 (Weber, 1970; Smith and Keyes, 1934; Smith, Keyes, and Gerry, 1934; Rivkin and Akhundov, 1962, 1963, 1966; Rivkin and Troianovskaia, 1964); and, most importantly, isochoric heat capacity does in fact diverge, albeit weakly, to ∞ at the critical point: $0 < \alpha_{ce} < 0.15$ (Voronel and others, 1964; Voronel, Snigirev, and Chashkin, 1965; Voronel, 1976; Moldover and Little, 1966; Moldover, 1969; Edwards, Lipa, and Buckingham, 1968; Kerimov, 1968; Gasparini and Moldover, 1969; Lipa, Edwards, and Buckingham, 1970).

Despite the multitude of constraints and difficulties inherent to critical-region experiments (for reviews, see Moldover, 1982; Greer and Moldover, 1981; Levelt Sengers, 1979; Fisher, 1964), the results summarized above clearly indicate quantitative failure of the classical theories near the critical point. In particular, the weak divergence of c_v to ∞ and the value of β_{ce} satisfying $\frac{1}{4} < \beta_{ce} < \frac{1}{2}$ are both irreconcilable with the

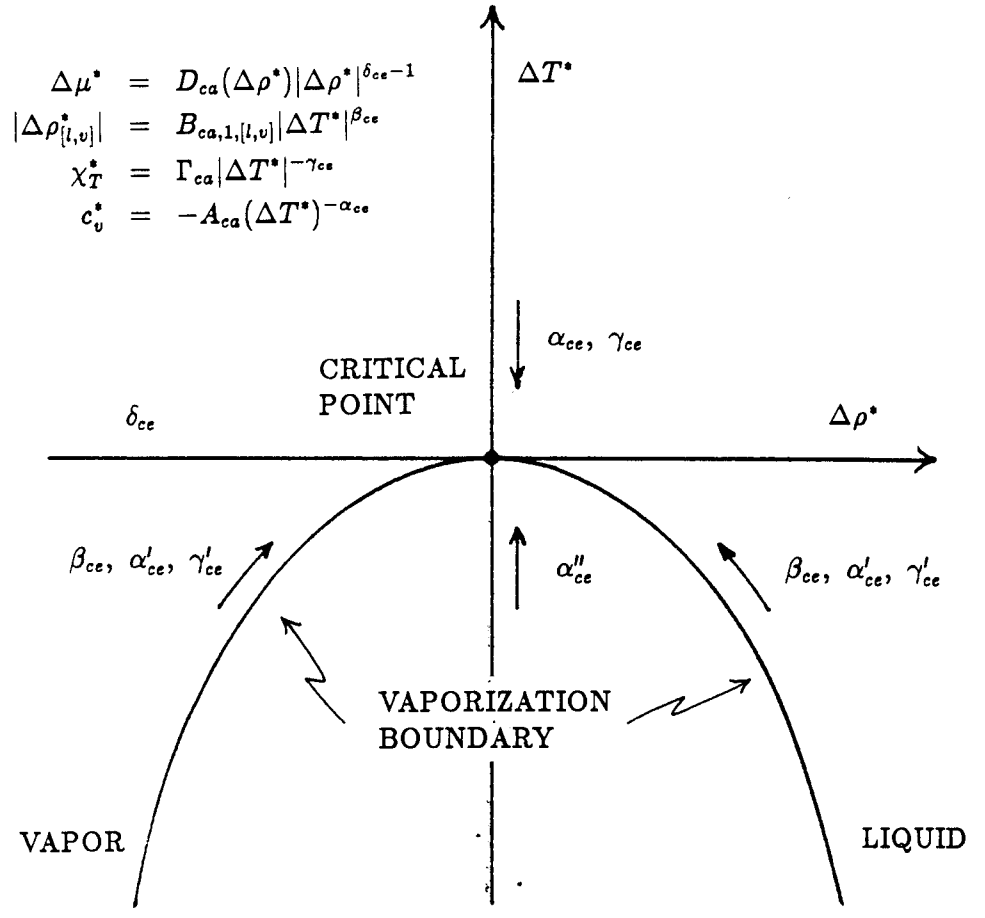

Fig. 2. Correlation among asymptotic power laws and paths of critical-point approach in the $\Delta T^* - \Delta\rho^*$ plane. Modified from Levelt Sengers, Greer, and Sengers (fig. 3, 1976).

existence of a Taylor expansion in $A_{[v,m]}$ at the critical point (Fisher, 1964; Levelt Sengers, 1970; Levelt Sengers and Greer, 1972).

The classical theories are also unsatisfactory from a theoretical viewpoint. Near-critical thermodynamic anomalies are produced by large and fluctuating variations in the density of juxtaposed molecular aggregates; hence, density homogeneity extends well beyond the scale of intermolecular spacing and the effective range of characteristic *short-ranged* attractive forces (Levelt Sengers, 1970, 1983; Levelt Sengers and Greer, 1972; Levelt Sengers, Greer, and Sengers, 1976; Levelt Sengers, Morrison, and Chang, 1983; Sengers and Levelt Sengers, 1978; Levelt Sengers and Sengers, 1981). However, classical equations of state implic-

itly assume *infinitely long-range* intermolecular attractive forces whose effective range exceeds the spatial dimensions of observed density homogeneities (Kac, Uhlenbeck, and Hemmer, 1963; Fisher, 1964; Griffiths, 1967; Levelt Sengers, 1970).

An outstanding contribution of the modern theory of critical phenomena is development of a nonclassical fluid equation of state that incorporates critical-point singularity, asymptotic power laws, and experimentally-observed critical exponent values in the context of statistical mechanics models of phase transitions implicitly based on short-ranged (finite) intermolecular attractive forces.

Nonclassical equations in the near-critical region.—By predicating near-critical, power-law behavior of thermodynamic functions on critical-point analyticity, exponents governing this behavior are necessarily constrained to classical values atypical of real one-component fluids. If, alternatively, the power laws implicitly account both for critical-point singularity and homogeneity of functions that represent these singular contributions, then their behavior is governed by nonclassical exponent values that are consistent with both experimental results and theoretical models of critical-point phase transitions.

Presuming that the singular component of the chemical potential is homogeneous (Widom, 1965, 1974; Kadanoff, 1966), its contribution to eq (9), cast in reduced variables, $\Delta\mu^*(\Delta\rho^*, \Delta T^*)$, can be expressed as (Stanley, 1971; Sengers and Levelt Sengers, 1978)

$$\Delta\mu^*(\lambda_h^{a_\rho}\,\Delta\rho^*, \lambda_h^{a_T}\,\Delta T^*) = \lambda_h \Delta\mu^*(\Delta\rho^*, \Delta T^*), \tag{19}$$

where a_ρ, a_T, and λ_h are unspecified constants. By appropriate choice of these parameters, namely $\lambda_h^{a_\rho} = \rho^{-1}$, $\lambda_h = \rho^{1/a_\rho}$, $a_\rho = 1/\delta_{ce}$, and $\alpha_T = (\beta_{ce}\delta_{ce})^{-1}$, eq (19) can be rearranged to

$$\frac{\Delta\mu^*(\Delta\rho^*, \Delta T^*)}{\Delta\rho^*\,|\Delta\rho^*|^{\delta_{ce}^{-1}}} = h(1, x/x_o). \tag{20}$$

This set of parameters scales the equation of state by a factor of $(\Delta\rho^*)^{\delta_{ce}}$, reducing its functional dependence, $h(1, x/x_o) \equiv \Delta\mu^*(1, x)$, to a single *scaling variable*, $x = \Delta T^*/\Delta\rho^{*1/\beta_{ce}}$. This choice of scaling variable is convenient because it yields a scaled equation of state, eq (9), whose classical counterpart follows directly from combination of eqs (12), (14), and (15), in which case $\delta_{ce} = 3$, $\beta_{ce} = \frac{1}{2}$, $x_o = B_{ca,[l,v]}^{-1/\beta_{ce}}$, and $h(x/x_o) = D_{ca}(1 + x/x_o)$. Thus, the nonclassical scaling law (20) can be viewed as a convenient mathematical framework that embodies all experimentally-observed power laws predicted by classical equations —yet it is not restricted to incorporation of classical exponent values that contradict experimental evidence.

Nonclassical critical exponents in close agreement with their experimentally-deduced counterparts are predicted by the statistical mechanics lattice-gas model of phase transition at the fluid critical point (Lee and Yang, 1952), the three-dimensional Ising model of analogous ferromag-

netic transition at the Curie point (Domb, 1974; Camp and others, 1976; Gaunt and Sykes, 1979), and the renormalization group theory of critical phenomena (Wilson, 1971a, b, 1983; Baker, 1977; Zinn-Justin, 1979; Le Guillou and Zinn-Justin, 1980) (table 1). Moreover, the lattice-gas model presumes short-range molecular interaction; the lattice-gas and Ising models predict critical-point singularity of Helmholtz functions (3) and (5); and the Ising model and renormalization group theory both confirm Widom's (1965) homogeneity postulate for these fundamental properties and their derived equations of state.

Hence, nonclassical equations of state accurately predict the observed macroscopic behavior of fluids in the context of several independent theories of near-critical molecular interactions. This successful coupling of theoretical prediction on macroscopic and microscopic scales is consistent with the *universality* concept. Within this conceptual model, the *long-range* character of near-critical density fluctuations (Levelt Sengers, 1970, 1983; Levelt Sengers and Greer, 1972; Levelt Sengers, Greer, and Sengers, 1976; Levelt Sengers, Morrison, and Chang, 1983; Sengers and Levelt Sengers, 1978; and Levelt Sengers and Sengers, 1981) implies that asymptotic behavior of all fluid (and other) systems having the same symmetry features is governed by a single set of universal critical exponents and scaling functions (Jasnow and Wortis, 1968; Griffiths, 1970; Kadanoff, 1971; Levelt Sengers and Sengers, 1975; Sengers, 1982). These universal exponents are predicted from the theoretical lattice-gas and Ising models and confirmed by renormalization group theory, which also gives the asymptotic form of the associated scaling function (Sengers and Levelt Sengers, 1986). In practice, however, the scaling function must also be formulated such that several constraints imposed by thermodynamic stability are satisfied (Widom, 1965; Griffiths, 1970). These include (1) analyticity throughout the one-phase region with singularity restricted to the critical point, (2) $h(1, -1) = 0$ on the vaporization

TABLE 1

Comparison of critical exponent values derived from experimental data and those predicted for classical equations of state, the three-dimensional Ising model, and from renormalization group theory

Critical Exponent	Classical Eqn. State*	Experiment**	3-D Ising Model***	Renorm. group†
α_{ce}	0	0–0.15	0.125 ± 0.02	0.110 ± 0.02
β_{ce}	0.5	0.34–0.36	0.312 ± 0.02	0.110 ± 0.005
γ_{ce}	1	1.1–1.3	1.25 ± 0.003	1.241 ± 0.002
δ_{ce}	3	4.0–4.6	5.01††	4.82††
Δ_i	—	—	0.50 ± 0.08	0.50 ± 0.02

*Levelt Sengers (1970, 1974), Sengers and Levelt Sengers (1978)
**Numerous sources; see text
***Domb (1974), Camp and others (1976)
†LeGuillou and Zinn-Justin (1980)
††Estimated from α_{ce}, β_{ce}, γ_{ce} values and equation (18)

boundary, (3) $h(1, 0) = D_{ca}$ on the critical isotherm, and (4) $h(1, \infty) = \infty$ on the critical isochore. In addition, consideration of subsequent integration to obtain the Helmholtz free energy requires that $h(1, x/x_a)$ be expressed in closed form.

A scaling function that satisfies the foregoing thermodynamic and integration constraints can be provided *implicitly* by transforming the physical variables ΔT^*, $\Delta\rho^*$ into parametric variables r, θ where r represents a measure of distance from the critical point, and θ specifies an r-contour location (Schofield, 1969; Josephson, 1969). The scaling function becomes implicit by isolating power-law behavior as an r-dependence, keeping θ-dependence analytic, and formulating the transformations such that ratios of the physical variables that define scaling function (20) and the scaling variable (x) are solely θ-dependent. These constraints are satisfied by $\Delta T^* = rT(\theta)$, $\Delta\rho^* = r^{\beta_{ce}} R(\theta)$, and $\Delta\mu^* = r^{\beta_{ce}\delta_{ce}} M(\theta)$, where $T(\theta)$ and $[R, M](\theta)$ are, respectively, symmetric and antisymmetric functions of θ in accord with symmetry features of the μ–ρ–T coordinate system (Sengers and Levelt Sengers, 1978).

The actual transformation functions are not unique (Fisher, 1971); the following set, known as the *linear-model parametric description* (Schofield, 1969), satisfies all requisite thermodynamic and scaling constraints and provides reasonable agreement with present-day theoretical knowledge (Sengers and Levelt Sengers, 1978):

$$\begin{aligned} \Delta T^* &= r(1 - b_{sc}^2\theta^2), \\ \Delta\rho^* &= r^{\beta_{ce}} k_{sc,o}\theta, \text{ and} \\ \Delta\mu^* &= r^{\beta_{ce}\delta_{ce}} a_{sc}\theta(1 - \theta^2), \end{aligned} \tag{21}$$

where θ is specified such that it equals $\pm$ 1 on the vapor and liquid branches of the vaporization boundary, $\pm$ $1/b_{sc}$ on the critical isotherm, and 0 on the critical isochore (fig. 3). Substance-specific adjustable constants a_{sc} and $k_{sc,o}$ are determined from numerical regression of (21) with μ–ρ–T data; b_{sc} is a universal constant (Schofield, 1969; Sengers and Levelt Sengers, 1978; Levelt Sengers and others, 1983). Although computationally nontrivial (Moldover, 1978), this transformation provides a scaled equation of state that is singular only at the critical point ($r = 0$) and is readily integrated in closed form to yield the associated fundamental property, A_v (Hohenberg and Barmatz, 1972; Schofield, 1969).

The parametric scaling law, (21), accurately describes near-critical thermodynamic anomalies within the region where its implicit symmetry features and power laws are valid. From symmetry considerations, this region is rather large; although slight asymmetry of the vaporization boundary in real fluids is of some concern, experimentially determined antisymmetry of $\mu(\rho)$-isotherms appears valid to at least $\pm$ 30 percent of ρ_c (Vicentini-Missoni, Levelt Sengers, and Green, 1969a, b). In contrast, experimental evidence (Hocken and Moldover, 1976) suggests that precise validity of the asymptotic power laws, implemented with theoretical

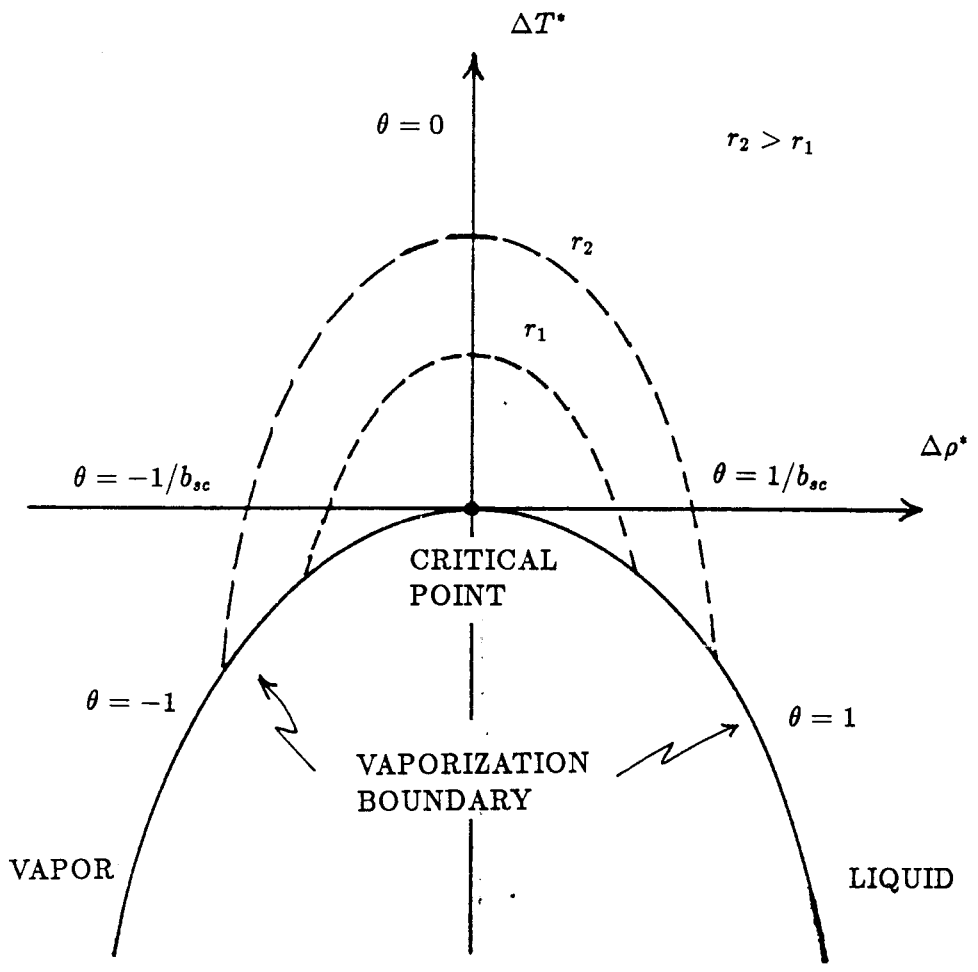

Fig. 3. Definition of parametric variables, r and θ, in the $\Delta T^*-\Delta\rho^*$ plane. Modified from Levelt Sengers, Greer, and Sengers (fig. 4, 1976) and Levelt Sengers, Morrison, and Chang (fig. 5, 1983).

exponent values, is restricted to within a fractional degree of the critical point (Levelt Sengers and Sengers; 1981). As a result, incorporation of correction terms is necessary in order to formulate a practical, so-called *extended* (Green, Cooper, and Levelt Sengers, 1971) scaled equation of state.

Renormalization group theory provides estimates of both the functional form and magnitude of such correction terms (Wegner, 1972; Ley-Koo and Sengers, 1982; Sengers and Levelt Sengers, 1978). Ley-Koo and Green (1977, 1981) implemented the extended scaling concept by

translating Wegner's (1972) Gibbs free energy formulation for ferromagnetic systems into an analogous thermodynamic potential for fluids: $\tilde{P}(\tilde{T}, \tilde{\mu})$, where

$$\tilde{P} = \frac{P^*}{T^*} = \frac{T_c}{P_c}\left(\frac{P}{T}\right),$$

$$\tilde{\mu} = \frac{\mu^*}{T^*} = \frac{\rho_c T_c}{P_c}\left(\frac{\mu}{T}\right),$$

and

$$\tilde{T} = -\frac{1}{T^*} = -T_c\left(\frac{1}{T}\right). \tag{22}$$

This potential, a temperature-normalized version of eq (4), can be expressed as the sum of analytic ($\tilde{P}_{reg}$), scaling ($\tilde{P}_{sc}$), and correction-to-scaling ($\tilde{P}_{corr}$) contributions:

$$\tilde{P} = \tilde{P}_{reg} + \tilde{P}_{sc} + \tilde{P}_{corr}, \tag{23}$$

where

$$\tilde{P}_{reg} = \tilde{P}_{reg}(u_t, u_\mu), \tag{24}$$

$$\tilde{P}_{sc} = a_{sc}|u_t|^{2-a_{ce}} k_{sc,o}\, h_o(x), \tag{25}$$

$$\tilde{P}_{corr} = a_{sc}|u_t|^{2-a_{ce}} \sum_{i=1}^{\infty} k_{sc,i}|u_t|^{\Delta_i} h_i(x), \text{ and} \tag{26}$$

$$x = u_\mu/|u_t|^{\delta_{ce}\beta_{ce}}. \tag{27}$$

The *scaling fields* u_μ and u_t are analytic functions of $\tilde{\mu}$ and $\tilde{T}$ that are equivalent in coexisting liquid and vapor phases. The u_t-axis defines the vaporization boundary and its analytic continuation into the one-phase region; the u_μ-axis intersects the vaporization boundary at an angle chosen such that experimentally-observed asymmetry is introduced into the T–ρ vaporization boundary (fig. 4) (Levelt Sengers and Sengers, 1981; Levelt Sengers, Morrison, and Chang, 1983). In *revised* scaling, the desired angle between u_μ and u_t axes is achieved by defining u_t as a linear combination of $\tilde{T}$ and $\tilde{\mu}$, and u_μ as a function of $\tilde{\mu}$ only (Rehr and Mermin, 1973; Balfour and others, 1978; Levelt Sengers and Sengers, 1981).

In the context of linear-model parametric representation (21), scaling and correction-to-scaling functions $h_o(x)$ and $h_i(x)$ become simple polynomials in θ^2; a_{sc}, $k_{sc,o}$, and $k_{sc,i}$ are substance-specific adjustable constants obtained from numerical fitting to experimental data; and the Δ_i represent corrections-to-scaling or "gap" exponents obtained from renormalization group theory (Levelt Sengers and Sengers, 1981).

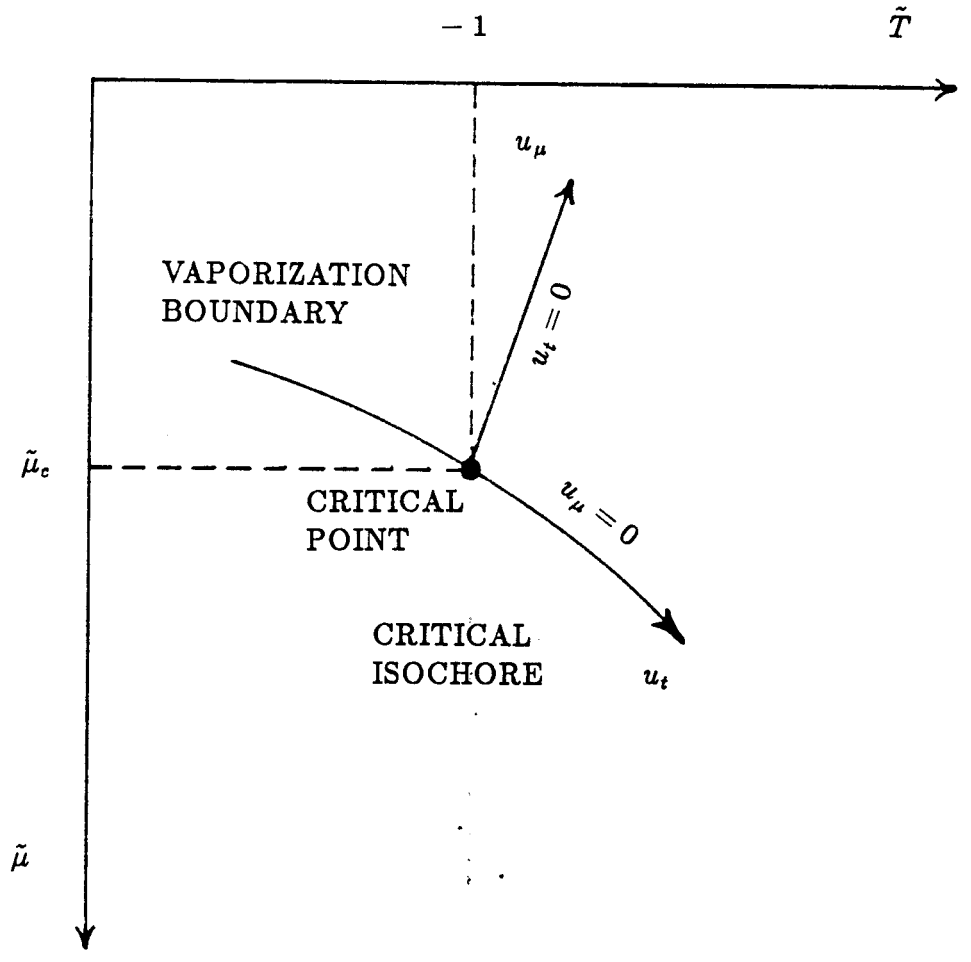

Fig. 4. Definition of scaling fields, u_t and u_u, in the $\tilde{T}-\tilde{\mu}$ plane. Modified from Levelt Sengers, Morrison, and Chang (fig. 6, 1983).

The $\tilde{P}(\tilde{\mu}, \tilde{T})$ surface is continuous everywhere with the vaporization boundary being defined by slope discontinuity. As the critical point is approached, the magnitude of this discontinuity diminishes while curvature of the vaporization boundary increases. At the critical point, the slopes are equivalent and finite, and the curvature infinite. Consequently, first derivative properties of the surface, reduced dimensionless density and internal energy, are unequal in coexisting liquid and vapor and converge to finite values at the critical point. Second derivative properties, reduced dimensionless isothermal compressibility and isochoric heat capacity, are also unequal in coexisting liquid-vapor but diverge

to ∞ at the critical point (Ley-Koo and Green, 1977, 1981; Levelt Sengers and Sengers, 1981).

Eq (23) with incorporation of nonclassical exponent values and extended (one corrections-to-scaling term) and revised scaling has been used successfully to predict near-critical thermodynamic anomalies of several one-component fluids, including H_2O (Balfour and others, 1978; Balfour, Sengers, and Levelt Sengers, 1980; Levelt Sengers and others, 1983), over the approximate range of $\pm$ 35 percent in ρ_c and from -1 to $+8$ percent in T_c (Levelt Sengers, 1983).

The classical-nonclassical boundary.—Although classical and nonclassical equations of state provide accurate representation of state and thermodynamic properties over the global and critical regions of the state-variable surface, it has proved difficult to develop a theoretically-sound, experimentally-verified algorithm for smoothly meshing the two descriptions across overlapping regions of their applicability. Development of a single continuous function that combines asymptotic scaling predictions in the critical region and classical predictions elsewhere has also proved elusive.

There have been several attempts to formulate a differentiable *crossover* or *switching* function that, through some linear combination of classical and nonclassical Helmholtz predictions, yields a third intermediate value within an appropriately-specified crossover region (Chapela and Rowlinson, 1974; Woolley, 1983). Unfortunately, the switch-function concept is intrinsically flawed by the inherent inability of any such function to produce intermediate values for, simultaneously, the Helmholtz function and its first and second derivatives (Wooley, 1983).

Of greater practical utility is an alternate approach that involves augmenting the experimental data used for regression fitting of both (if possible) the classical and nonclassical description with values predicted by the alternate equation within overlapping regions of their applicability. Levelt Sengers, Kamgar-Parsi, and Sengers (1983) utilized this technique in developing a scaled equation of state for isobutane. They incorporated data predicted by the corresponding analytic equation (Waxman and Gallagher, 1983) and in so doing obtained very close agreement, on the order of 1 percent in isochoric heat capacity, with this classical description where both formulations were valid (Levelt Sengers, Morrison, and Chang, 1983).

Another empirical algorithm (Fox, 1983) accomplishes smooth classical/nonclassical crossover by introducing "distance" and "damping" functions that are used to reformulate the classical equation and in principle facilitate smooth transition across the boundary. In essence, the distance function represents geometric distance from the critical point, and the dependent damping function, which increases monotonically from zero at criticality to one far from the critical point, balances classical and nonclassical contributions. This approach overcomes difficulties inherent to the "third-function" concept (Woolley, 1983) and is more attractive than the simple augmented, re-regression model (Levelt Sengers, Kamgar-Parsi, and Sengers, 1983). However, Fox (1983) notes two

present difficulties: the proposed damping function is not applicable to global equations of state, and the algorithm does not predict accurately the nonclassical divergence of asymptotic properties.

Arguably the most successful crossover procedure developed to date is that given by Albright and others (1986). This method, derived from renormalization group theory, introduces two substance-specific constants that effectively delimit the validity boundaries of asymptotic scaling and corrections-to-scaling and explicitly accounts for the apparent shift of critical-point state parameters between classical and nonclassical equations. The authors demonstrate application of their algorithm to van der Waals equations but remark in summary that the theory has yet to be tested against experimental data.

FUNDAMENTAL EQUATIONS

The HGK equation has been approved by the IAPS for use to 1000°C and 15,000 *bars*, excepting a small T–ρ region near the critical point where the formulation does not provide sufficiently close approximation of divergent properties (Kestin and others, 1984; Kestin and Sengers, 1986). This near-critical asymptotic behavior can, however, be accurately represented using the LS equation, whose T–ρ validity region extends well beyond the immediate vicinity of critical point where the HGK equation is suspect. These two formulations are presented below in the context of the foregoing overview of theoretical development.

The HGK equation.—The HGK equation represents a specific statement of eq (7): an empirically-augmented, theoretically-modified Ursell-Mayer virial expansion ($[P/\rho\overline{R}T](\rho)$; Mayer and Mayer, 1940) whose functional form represents over a decade of evolutionary development (Haar and Shenker, 1971; Wardell and others, 1975; Powell and others, 1979; Haar, Gallagher, and Kell, 1980, 1982a, b). The equation can be expressed as the sum of base and residual contributions to $P(T, \rho)$; the base function, P_{base}, implements a hard-ellipse equation of state (Few and Rigby, 1973; Gibbons, 1969) modified by a two-term approximation to intermolecular attraction contributions (Percus and Yevick, 1958; Thiele, 1963; Wertheim, 1963, 1964); the residual function, P_{resid}, is an empirical formulation (Haar, Gallagher, and Kell, 1980, 1982a, b; 1984) that accounts for discrepancies between base-function and experimental values in regions where quantitative accuracy of the base function diminishes (most importantly, for $T > 1.4\ T_c$: Wardell and others, 1975; Powell and others, 1979). The complete formulation is (Haar, Gallagher, and Kell, 1984):

$$P = P_{base} + P_{resid}, \text{ where} \tag{28}$$

$$P_{base} = \rho\overline{R}T\left\{\frac{1 + (\hat{\gamma} - 2)y + (1 - \hat{\gamma} + \hat{\gamma}^2/3)y^2}{(1 + y)^3} + 4y^*\left(\frac{B_{v,2}}{b_{v,2}} - \frac{1 + \hat{\gamma}}{4}\right)\right\}, \tag{29}$$

$$P_{resid} = \frac{k_\rho}{C\hat{C}} \left\{ \sum_{i=1}^{36} g(i) \left(\frac{T_o}{T}\right)^{l(i)} \rho^2 (1 - exp(-k_\rho \rho))\, exp(-k_\rho \rho) \right.$$

$$+ \sum_{i=37}^{40} g(i) \rho_i^{-1}\, \rho^2\, exp(-\alpha_i \delta_i^{k(i)} - \beta_i \tau_i^2)$$

$$\left. \{ l(i) \delta_i^{l(i)-1} - a_i\, k(i) \delta_i^{k(i)+l(i)-1} \} \right\}, \tag{30}$$

$$b_{v,2} = B_1\, ln\left(\frac{T}{T_o}\right) + \sum_{j=0,1,3,5} b_j \left(\frac{T_o}{T}\right)^j, \text{ and} \tag{31}$$

$$B_{v,2} = \sum_{j=0,1,2,4} B_j \left(\frac{T_o}{T}\right)^j. \tag{32}$$

For the base function, $y = b_{v,2}\, \rho/4$, $\overline{R}$ (4.6152 *bar* $cm^3\, g^{-1} {}^oK^{-1}$) stands for the gas constant, $\hat{\gamma}$ designates an empirically-determined geometric constant representing eccentricity of the ellipsoids (Powell and others, 1979), $B_{v,2}$ and $b_{v,2}$ correspond to second virial coefficients for the actual and hard-ellipse equations of state, T_o = 647.074°*K*, and the $[b, B]_j$ represent adjustable coefficients (table 2) obtained from regression of experimental volumetric data to eqs (29) through (32). For the residual function, the $g(i)$ represent fit coefficients, $l(i)$, $k(i)$, α_i, β_i, and k_ρ are integer constants, C and $\hat{C}$ are conversion factors, $\delta_i = (\rho - \rho_i)/(\rho_i)$, $\tau_i = (T - T_i)/T_i$, and the ρ_i and T_i represent density and temperature constants. The adjustable coefficients and integer, density, and temperature constants are given in table 3.

The first summation term in eq (30) represents a global, least-squares fit to residuals between eq (29) predictions and their experimental counterparts, the latter pooled from numerous sources (see Haar, Gallagher, and Kell, 1984). The first three terms of the second summation represent a least-squares fit to *two* near-critical isotherms (roughly 31

TABLE 2

Coefficients b_j *and* B_j *in eqs (29), (32), and (34). Modified from Haar, Gallagher, and Kell (1984, table A.1)*

j	b_j (cm^3/g)	B_j (cm^3/g)
0	0.7478629	1.1278334
1	–0.3540782	–0.5944001
2	0	–5.010996
3	0.007159876	0
4	0	0.63684256
5	–0.003528426	0

TABLE 3

Coefficients g(i), l(i), k(i), ρ_i, α_i, β_i, and T_i in eqs (30) and (35). From Haar, Gallagher, and Kell (1984, table A.2)

i	$k(i)$	$l(i)$	$g(i)$ (J/g)	i	$k(i)$	$l(i)$	$g(i)$ (J/g)
1	1	1	$-5.3062968529023(10^2)$	19	5	4	$-1.3802577177877(10^6)$
2	1	2	$2.2744901424408(10^3)$	20	5	6	$-2.5109914369001(10^5)$
3	1	4	$7.8779333020687(10^2)$	21	6	1	$4.6561826115608(10^6)$
4	1	6	$-6.9830527374994(10^1)$	22	6	2	$-7.2752773275387(10^6)$
5	2	1	$1.7863832875422(10^4)$	23	6	4	$4.1774246148294(10^5)$
6	2	2	$-3.9514731563338(10^4)$	24	6	6	$1.4016358244614(10^6)$
7	2	4	$3.3803884280753(10^4)$	25	7	1	$-3.1555231392127(10^6)$
8	2	6	$-1.3855050202703(10^4)$	26	7	2	$4.7929666384584(10^6)$
9	3	1	$-2.5637436613260(10^5)$	27	7	4	$4.0912664781209(10^5)$
10	3	2	$4.8212575981415(10^5)$	28	7	6	$-1.3626369388386(10^6)$
11	3	4	$-3.4183016969660(10^5)$	29	9	1	$6.9625220862664(10^5)$
12	3	6	$1.2223156417448(10^5)$	30	9	2	$-1.0834900096447(10^6)$
13	4	1	$1.1797433655832(10^6)$	31	9	4	$-2.2722827401688(10^5)$
14	4	2	$-2.1734810110373(10^6)$	32	9	6	$3.8365486000660(10^5)$
15	4	4	$1.0829952168620(10^6)$	33	3	0	$6.8833257944332(10^3)$
16	4	6	$-2.5441998064049(10^5)$	34	3	3	$2.1757245522644(10^4)$
17	5	1	$-3.1377774947767(10^6)$	35	1	3	$-2.6627944829770(10^3)$
18	5	2	$5.2911910757704(10^6)$	36	5	3	$-7.0730418082074(10^4)$

i	$k(i)$	$l(i)$	ρ_i (g/cm^3)	T_i $(°K)$	α_i	β_i	$g(i)$ (J/g)
37	2	0	0.319	640.	34	20000	$-2.25(10^{-1})$
38	2	2	0.319	640.	40	20000	$-1.68(10^0)$
39	2	0	0.319	641.6	30	40000	$5.50(10^{-2})$
40	4	0	1.55	270.	1050	25	$-2.25(10^{-1})$

$P(T, \rho)$ measurements) reported by Rivkin and Akhundov (1963, 1966); the last term contributes only in the high-pressure, low-temperature region (Haar, Gallagher, and Kell, 1984). Incorporation of this second summation term is the only differentiating feature between the 1980 and 1984 versions of the HGK equation. Moreover, all experimental data within the critical region were excluded from the regression procedure with the exception of the two isotherms mentioned above. *Note that the T–ρ region of data excluded by Haar, Gallagher, and Kell (1984) in their regression fit is closely approximated by the T– ρ validity region of the LS equation at $T < 395°C$ (fig. 5).* Presumably, this exclusion was necessitated by the

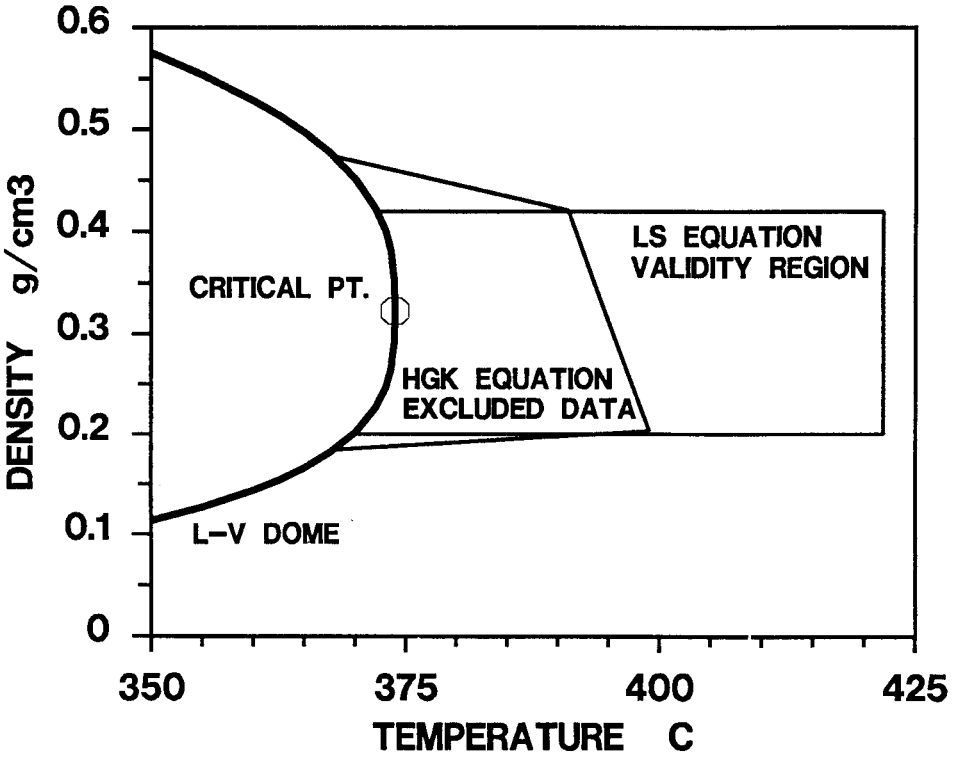

Fig. 5. The $T-\rho$ validity region of the LS equation and the $T-\rho$ region where experimental data were excluded from regression fitting of the HGK equation (sparce data along the 374 and 375°C isotherms (Rivkin and Akhundov, 1963, 1966) *were* included in the HGK fit — see text). Note close correspondence between the two regions for $T < 395$°C.

prohibitive computational expense of incorporating a sufficient number of terms to represent experimental data in the critical region with the accuracy achieved elsewhere (Levelt Sengers and Greer, 1972).

The fundamental *molar* Helmholtz function is readily obtained from integration of eq (28) with respect to density (Haar, Gallagher, and Kell, 1980, 1984):

$$A_m(\rho, T) = A_{m,base}(\rho, T) + A_{m,resid}(\rho, T) + A_{m,ideal}(T), \tag{33}$$

where

$$A_{m,base}(\rho, T) = CM\bar{R}T\left\{-ln(1-y) - \frac{\hat{\gamma}^2 - 3\gamma}{3(1-y)} + \frac{\hat{\gamma}^2}{6(1-y)^2} + 4y\left(\frac{B_{v,2}}{b_{v,2}} - \frac{1+\hat{\gamma}}{4}\right) - \frac{6\hat{\gamma} - \hat{\gamma}^2}{6} + ln\left(\frac{\rho RT}{P_o}\right)\right\}, \tag{34}$$

$$A_{m,resid}(\rho, T) = \frac{M}{\hat{C}} \left\{ \sum_{i=1}^{36} \frac{g(i)}{k(i)} \left(\frac{T_o}{T} \right)^{l(i)} (1 - exp(-k_\rho \rho))^{k(i)} + \sum_{i=37}^{40} g(i) \delta_i^{l(i)} exp(-\alpha_i \delta_i^{k(i)} - \beta_i \tau_i^2) \right\}, \text{ and} \quad (35)$$

$$A_{m,ideal}(T) = -CM\bar{R}T \left\{ 1 + \left(\frac{c_1}{T_R} + c_2 \right) ln\ T_R + \sum_{i=3}^{18} c_i T_R^{i-6} \right\}, \quad (36)$$

where $A_{m,ideal}$ represents the ideal-gas contribution that does not, as a consequence of its density independence, contribute to the equation of state (Woolley, 1980; Haar, Gallagher, and Kell, 1980, 1982a, b, 1984). In eq (36), $T_R = T/(100°K)$ and the adjustable coefficients c_i are given in table 4.

TABLE 4

Coefficients c_i for eq (36). Modified from Haar, Gallagher, and Kell (1984, table A.3)

i	c_i	i	c_i
1	$1.97302710180(10^{1})$	10	$4.1238460633(10^{-3})$
2	$2.09662681977(10^{1})$	11	$-2.7929052852(10^{-4})$
3	$-4.83429455355(10^{-1})$	12	$1.4481695261(10^{-5})$
4	$6.05743189245(10^{0})$	13	$-5.6473658748(10^{-7})$
5	$2.256023885(10^{1})$	14	$1.620044600(10^{-8})$
6	$-9.875324420(10^{0})$	15	$-3.3038227960(10^{-10})$
7	$-4.3135538513(10^{0})$	16	$4.51916067368(10^{-12})$
8	$4.581557810(10^{-1})$	17	$-3.70734122708(10^{-14})$
9	$-4.7754901883(10^{-2})$	18	$1.37546068238(10^{-16})$

The LS equation.—The thermodynamic potential for critical-region H_2O given by Levelt Sengers and others (1983) is both a temperature-normalized version of eq (4) and a specific statement of eq (23). The potential, $\tilde{P}(\tilde{\mu}, \tilde{T})$, is expressed as the sum of an analytic function, $\tilde{P}_{reg}$, which describes finite contributions to the surface and its derivatives, and an asymptotic potential, $\Delta\tilde{P}$, which represents scaling and correction-to-scaling contributions that account for divergence of second-derivative properties to $\pm\infty$ at the critical point (Levelt Sengers and others, 1983):

$$\tilde{P} = \tilde{P}_{reg} + \Delta\tilde{P},$$

where

$$\tilde{P}_{reg} = \tilde{P}_o(\tilde{T}) + \Delta\tilde{\mu} + \tilde{P}_{11}\Delta\tilde{\mu}\Delta\tilde{T},$$

and

$$\Delta\tilde{P} = a_{sc}|u_t|^{2-\alpha_{ce}} \sum_{i=0}^{1} k_{sc,i}|u_t|^{\Delta_i} g_i(x). \tag{37}$$

The analytic function is further defined by

$$\Delta\tilde{T} = \tilde{T} + 1 + \Delta T^*/T^* = (T - T_c)/T_c, \tag{38}$$

$$\Delta\tilde{\mu} = \tilde{\mu} - \tilde{\mu}_o(\tilde{T}) = \Delta\mu^*/T^* = \frac{\rho_c T_c}{CP_c T}(\mu(\rho, T) - \mu(\rho_c, T)), \tag{39}$$

$$\tilde{\mu}_o(\tilde{T}) = \tilde{\mu}_c + \sum_{i=1}^{3} \tilde{\mu}_i(\Delta\tilde{T})^i, \tag{40}$$

and

$$\tilde{P}_o(\tilde{T}) = 1 + \sum_{i=1}^{3} \tilde{P}_i(\Delta\tilde{T})^i, \tag{41}$$

where $\tilde{\mu}_o(\tilde{T})$ represents the $\mu(T)$ vaporization boundary and its analytic continuation into the one-phase region, and $\tilde{P}_o(\tilde{T})$ represents background $\tilde{P}$ for the analytic potential, $\tilde{P}_{reg}$.

For the asymptotic potential, the first and second summation terms define respective contributions of the asymptotic scaling law (hence, $\Delta_o = 0$) and the first Wegner correction-to-scaling term. The scaling and correction-to-scaling functions, g_o and g_1, are both dependent on the scaling variable, $x(u_t, u_\mu)$, where the two independent scaling fields, u_t and u_μ, are defined in the $\Delta\tilde{T} - \Delta\tilde{\mu}$ plane (fig. 6) such that experimentally-observed asymmetry is introduced into the vaporization boundary. The scaling and correction-to-scaling functions, scaling variable, and scaling fields are given in linear parametric form by

$$g_i(x) = \frac{p_i(\theta)}{1 - b_{sc}^2\theta^2} \quad (i = 0, 1), \tag{42}$$

$$x = \frac{u_\mu}{|u_t|^{\beta_{ce}\delta_{ce}}} = \frac{\theta(1 - \theta)^2}{1 - b_{sc}^2\theta^2}, \tag{43}$$

$$u_\mu = \Delta\tilde{\mu}/a_{sc} = r^{\beta_{ce}\delta_{ce}}\theta(1 - \theta^2), \tag{44}$$

and

$$u_t = \Delta\tilde{T} + c_{sc}\Delta\tilde{\mu}/a_{sc} = r(1 - b_{sc}^2\theta^2), \tag{45}$$

where

$$p_i(\theta) = p_{0i} + p_{2i}\theta^2 + p_{4i}\theta^4,$$

$$p_{0i} = \frac{\beta_{ce}\delta_{ce} - 3\beta_{ce,i} - b_{sc}^2\alpha_{ce,i}\gamma_{ce,i}}{2b_{sc}^4(2 - \alpha_{ce,i})(1 - \alpha_{ce,i})\,\alpha_{ce,i}}$$

$$p_{2i} = \frac{\beta_{ce}\delta_{ce} - 3\beta_{ce,i} - b_{sc}^2\alpha_{ce,i}(2\beta_{ce}\delta_{ce} - 1)}{2b_{sc}^2(1 - \alpha_{ce,i})\alpha_{ce,i}},$$

and

$$p_{4i} = \frac{2\beta_{ce}\delta_{ce} - 3}{2\alpha_{ce,i}}. \qquad (46)$$

Note that the scaling variable and scaling and correction-to-scaling functions are all independent of r and depend only on θ; this restricts nonanalyticity of the equation of state to the critical point itself (Balfour, Sengers, and Levelt Sengers, 1980; Levelt Sengers and others, 1983).

Implementation of eqs (37) through (46) requires values for three critical exponents (β_{ce}, δ_{ce}, and Δ_1) predicted by theory (LeGillou and Zinn-Justin, 1980) and sixteen substance-specific constants which must be determined from regression of various experimental data (Balfour, Sengers, and Levelt Sengers, 1980; Levelt Sengers and others, 1983): three critical parameters (P_c, ρ_c, and T_c), five scaling function parameters (a_{sc}, b_{sc}, c_{sc}, $k_{sc,o}$, and $k_{sc,1}$), four background pressure parameters ($\tilde{P}_1$, $\tilde{P}_2$, $\tilde{P}_3$, and $\tilde{P}_{11}$), and four chemical potential background parameters ($\tilde{\mu}_1$, $\tilde{\mu}_2$, $\tilde{\mu}_3$, and $\tilde{\mu}_c$). Values adopted by Levelt Sengers and others (1983) are given in table 5.

In the near-critical region, the thermodynamic potential, eq (37), and its derivatives are extremely sensitive to the value of T_c. The seemingly minute discrepancy between values utilized by Levelt Sengers and others (1983), 373.917°C, and Balfour, Sengers, and Levelt Sengers (1980), 373.848°C, is in fact the main distinguishing feature of the two equations (Levelt Sengers and others, 1983).

The HGK—LS equation boundary.—The validity region of the LS equation is bound by the 421.85°C isotherm, 0.20 and 0.42 g/cm^3 isochores, and vaporization-boundary segment that bridges these isochores. Along this validity perimeter, H_2O property values computed with reference to this scaled equation of state necessarily differ from their counterparts predicted on the HGK equation. Although for a given property these differences vary somewhat with perimeter location, their magnitude is primarily dependent upon the differentiation level of the fundamental equation required to represent the specified property. In general, properties predominantly dependent on the undifferentiated fundamental expressions or their first-order partials agree to within 0.15

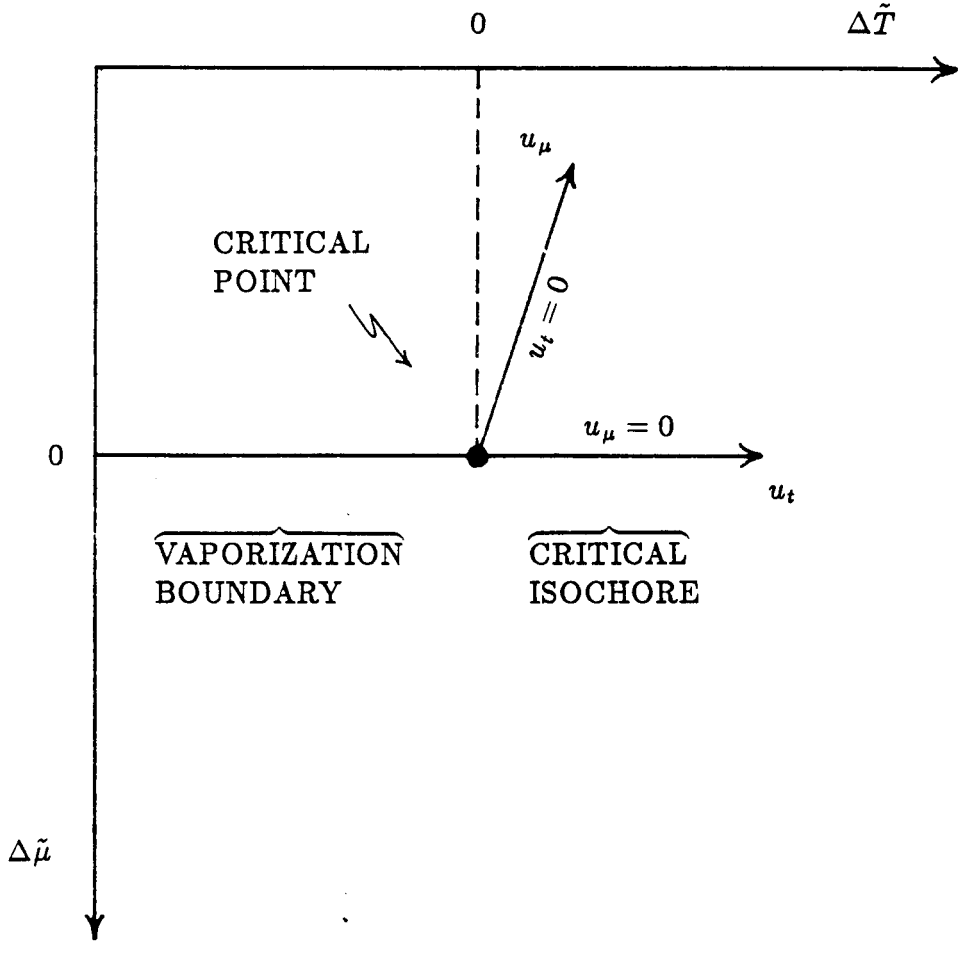

Fig. 6. Definition of scaling fields, u_t and u_μ, in the $\Delta T - \Delta\tilde{\mu}$ plane. Modified from Levelt Sengers, Morrison, and Chang (fig. 6, 1983).

percent; such properties include the dependent state variable (ρ or P), A, G, E, H, S, η, ν, ϵ, and Z (a glossary of symbols is given in the app.). These differences are sufficiently small to be considered negligible in most practical applications.

Boundary discrepancies for properties that require second- and third-order differentiation of the fundamental equations approach 3 and 15 percent, respectively, outside the near-critical region and exceed these values near the critical point. These second-derivative properties include α, β, c_v, c_p, Y, Q, and λ; third-derivative properties are limited to $(\partial\alpha/\partial T)_p$ and X in the present study. The magnitude of such discontinui-

TABLE 5

Summary of critical exponents, critical state parameters, scaling function parameters, background pressure parameters, and chemical potential background parameters for the scaled equation of state given by Levelt Sengers and others (1983); modified from their table B1)

	Parameter	Value
critical exponents	β_{cr}	0.325*
	δ_{cr}	4.82*
	Δ_1	0.50*
critical parameters	T_c	647.067°K**
	ρ_c	0.322778 g/cm^3***
	P_c	220.46 *bar*†
scaling function parameters	a_{sc}	23.667***
	$k_{sc,a}$	1.4403***
	$k_{sc,1}$	0.2942***
	c_{sc}	−0.01776***
	b_{sc}^2	1.3757***
pressure background parameters	P_1	6.8445***
	P_2	−25.4915***
	P_3	5.238***
	P_{11}	0.4918††
caloric background parameters	$\tilde{\mu}_c$	−11.233†††
	$\tilde{\mu}_1$	−22.655†††
	$\tilde{\mu}_2$	−17.888§
	$\tilde{\mu}_3$	−4.933§

*Fixed from theory
**From latent heat data of Osbourne and others (1933, 1937)
***From fit to *PVT* data of Rivkin and Akhundov (1962, 1963, 1966)
†Derived from vapor pressure curve
††From known coexistence curve diameter
†††From equating the scaled equation of state given by Levelt Sengers and others (1983) with the virial expansion of Haar, Gallagher, and Kell (1980) at 648.15°*K*, 0.23 g/cm^3.
§From fit to speed of sound data of Erokhin and Kal'yanov (1979, 1980)

ties in c_v, $(\partial\alpha/\partial T)_P$, and X, detailed below, are of potential concern in certain applications.

COMPUTATIONAL AND GRAPHICAL CONVENTIONS

Description and analysis of fluid H_2O properties computed with reference to the LS and HGK equations requires specification of unit and triple-point conventions, a suitable pressure-temperature reference frame, and an appropriate crossover function that bridges the two formulations across the validity boundary of the LS equation. The set of such specifications adopted in the present study is described below.

Unit conventions adopted for fluid H_2O properties are those most commonly used in geochemical calculations (Helgeson and Kirkham, 1974a) and fluid transport models (Norton and Knight, 1977). All property units are consistent with temperature in degree Kelvin (°*K*), pressure in *bars*, energy in thermochemical calories (*cal* or *kcal*), mass in

grams (g), and volume in cubic centimeters (cm^3). Energy properties are expressed as *per mole* quantities and density as g/cm^3. Units for specific properties are summarized in the glossary of symbols (app).

Energy properties tabulated by both Levelt Sengers and others (1983) and Haar, Gallagher, and Kell (1984) are referenced to the following triple point (tr) conventions: $S_{m,tr} \equiv E_{m,tr} \equiv 0$ which leads to $A_{m,tr} \equiv 0$ and $H_{m,tr} \equiv G_{m,tr} \approx 0$. This reference frame is useful in most engineering applications but inconsistent with standard state conventions in common use for calculating thermodynamic properties of minerals, gases, and aqueous ions (Helgeson and others, 1978; Helgeson, Kirkham, and Flowers, 1981; Tanger and Helgeson, 1988; Robie, Hemingway, and Fisher, 1978; Helgeson and Kirkham, 1974b, 1976). In order to attain consistency with these geochemical data, fluid H_2O energy properties computed from the LS and HGK equations (E_m, H_m, A_m, G_m, S_m) have been converted to apparent molal (ΔE_m, ΔH_m, ΔA_m, ΔG_m) and third law molal ($S_{m,tl}$) quantities of non-zero triple-point reference (Helgeson and Kirkham, 1974a):

$$
\begin{aligned}
S_{m,tl} &= S_m + S_{m,tr},\\
\Delta E_m &= E_m + E_{m,tr},\\
\Delta H_m &= H_m + H_{m,tr},\\
\Delta G_m &= H_m - TS_m + T_{tr}S_{m,tr} + G_{m,tr}\\
&= G_m + T_{tr}S_{m,tr} + G_{m,tr},
\end{aligned}
$$

and

$$
\begin{aligned}
\Delta A_m &= E_m - TS_m + T_{tr}S_{m,tr} + A_{m,tr}\\
&= A_m + T_{tr}S_{m,tr} + A_{m,tr},
\end{aligned}
\tag{47}
$$

where $S_{m,tr}$, $E_{m,tr}$, $H_{m,tr}$, $G_{m,tr}$, and $A_{m,tr}$ are given in table 6.

TABLE 6

Triple point values for A_m, G_m, E_m, and H_m in kcal/mol and S_m in cal/mol°K. Modified from Helgeson and Kirkham (1974a, table 2)

$A_{m,tr}$	$G_{m,tr}$	$E_{m,tr}$	$H_{m,tr}$	$S_{m,tr}$
−55.415	−56.290	−67.887	−68.767	15.132

The pressure-temperature grid within which fluid H_2O properties are presented below is of axis dimensions 200 to 450 *bars*, 350° to 465°*C* and granularity 6.25 *bars*, 3.125°*C* (fig. 7). Description and analysis of

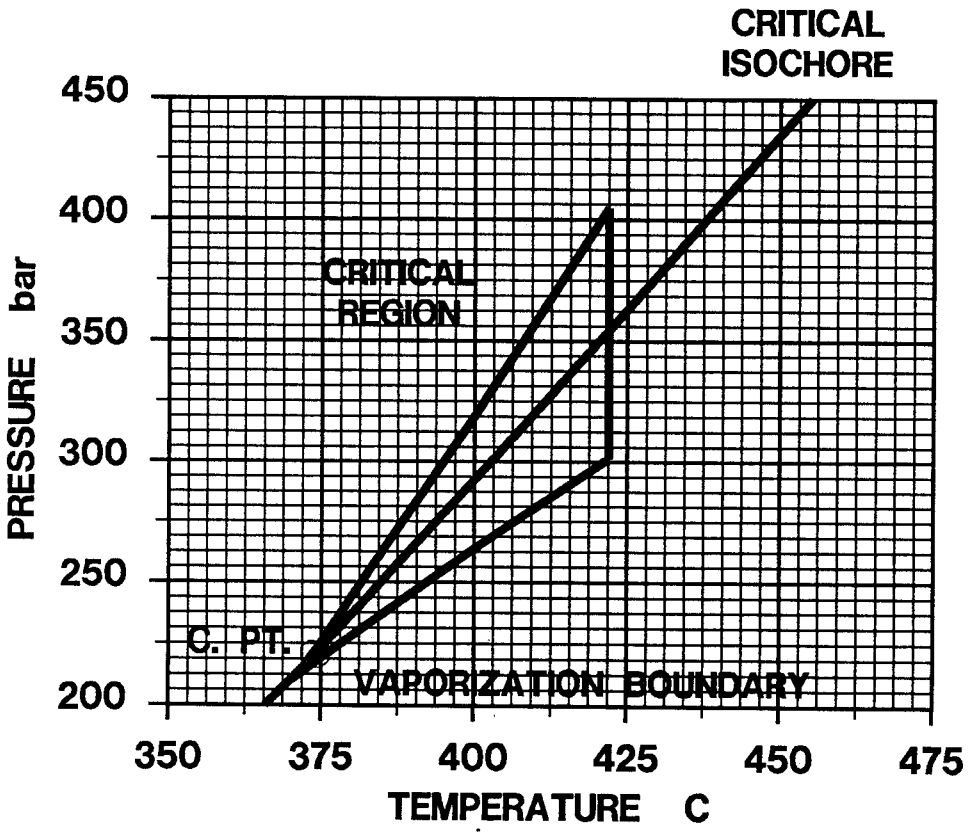

Fig. 7. The $P-T$ grid used for computation and projection of H_2O properties in the present study. Note axis dimensions (350°–475°*C* and 200–450 *bars*) and granularities (3.125°*C* and 6.25 *bars*) as well as locations of the critical region (bound by the 421.85°*C* isotherm and 0.20 and 0.42 g/cm^3 isochores), critical isohcore (0.322778 g/cm^3), critical point (373.917°*C*, 220.46 *bars*), and vaporization boundary.

each property is referenced to its three-dimensional projection over this grid, isobaric and isothermal cross sections of this surface (boldface gridlines in fig. 7), and 25-element skeleton tables containing computed values at intersection points of the cross sections. Approx 20 percent of the grid is enclosed within the critical region, as defined by the validity boundary of the LS equation of state: the 421.85°*C* isotherm, 0.20 and 0.42 g/cm^3 isochores, and vaporization-boundary segment that bridges these isochores. The critical region, vaporization boundary, critical point (647.067°*K* = 373.917°*C*, 220.46 *bars*), and critical isochore (0.322778 g/cm^3) are all illustrated in figure 7.

Within the critical region, all property values are computed with reference to the LS equation; elsewhere, the HGK equation is used. In lieu of an alternative, computationally convenient approach (see above),

transition between these two formulations is accomplished by a simple switch function along the validity perimeter of the LS equation. This algorithm necessarily imposes discontinuities of property-dependent magnitude across the critical region boundary. As discussed above, these discrepancies are inconsequential except for three higher-order differentiates of the fundamental equations: namely, c_v, $(\partial\alpha/\partial T)_p$, and X. Accordingly, these minor discontinuities are not explicitly illustrated in the property surfaces and cross sections presented below; rather, all adjacent datum, including those bridging the critical-region boundary, are connected in the same point-to-point fashion. This graphical convention facilitates appreciation of the discontinuities' inconspicuous nature, even at the granularity of the isothermal (2 *bars*) and isobaric (1°C) sections. However, the relatively large and potentially significant boundary discontinuities in c_v, $(\partial\alpha/\partial T)_p$, and X are explicitly depicted and discussed.

In the following property descriptions, five pressure-temperature regions of fluid H_2O stability are distinguished by location with respect to the vaporization boundary and critical point (fig. 8). The *liquid* region

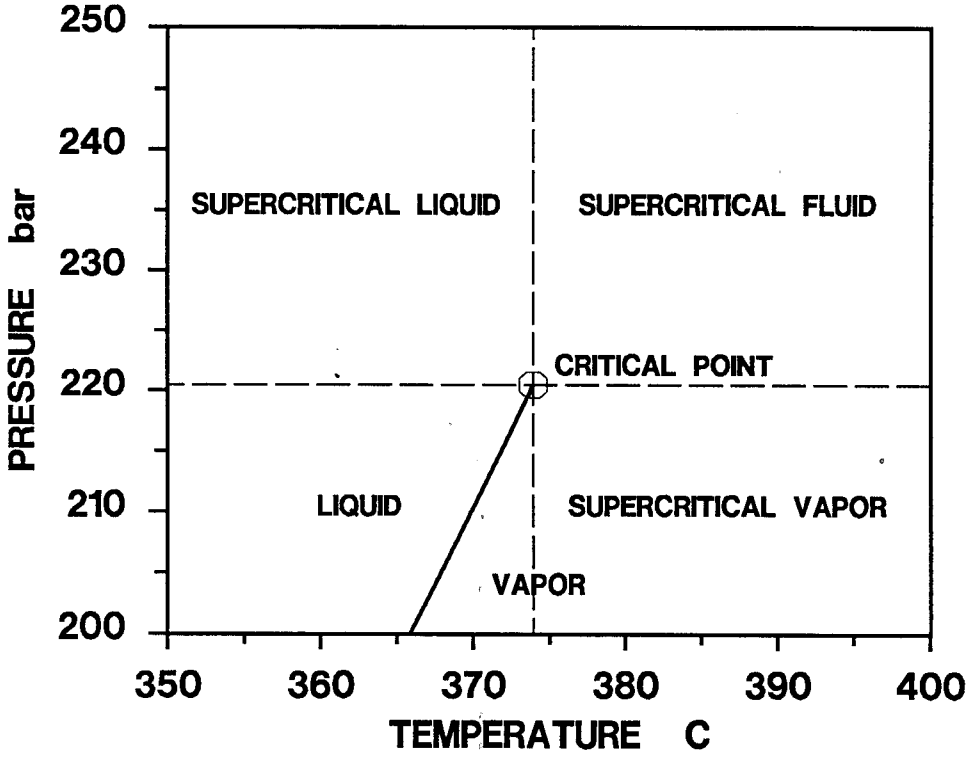

Fig. 8. $P-T$ regions of fluid H_2O stability: liquid, vapor, and supercritical liquid, vapor, and fluid; see text.

falls between the vaporization boundary and critical isobar; the *vapor* region falls between the vaporization boundary and critical isotherm. The *supercritical liquid* region is constrained to supercritical pressures and subcritical temperatures; the *supercritical vapor* region is constrained to supercritical temperatures and subcritical pressures. Finally, the *supercritical fluid* region encompasses all conditions of supercritical temperature *and* pressure. Of course, only three fluid *phases* of H_2O are actually distinguished: liquid, vapor, and supercritical fluid, the latter of which in this context encompasses supercritical liquid, vapor, and fluid as defined above.

STATE PROPERTIES

As described above, the fundamental thermodynamic functions, $\tilde{P}(\tilde{T}, \tilde{\mu})$ in the critical region, eq (37), and $A_m(T, \rho)$ in the global region, eq (33), were initially obtained from integration of the corresponding equations of state: $\tilde{\rho}(\tilde{T}, \tilde{\mu})$ and $P(T, \rho)$, respectively. As a result, these state functions and their derivative properties are now cast as first- and higher-order partial derivatives of the fundamental equations.

Equations of state.—The equation of state in the critical region is given by

$$\rho = \rho_c \left(\frac{\partial \tilde{P}}{\partial} \right)_{\tilde{T}}; \tag{48}$$

the analogous expression for the global region is

$$P = \frac{\rho^2}{CM} \left(\frac{\partial A_m}{\partial \rho} \right)_T. \tag{49}$$

Eqs (48) and (49) and requisite derivatives of (33) and (37) were used to compute the $\rho(P, T)$ surface, $\rho(T)$-isobars, and $\rho(P)$-isotherms illustrated in figure 9, and the $\rho(P, T)$ values listed in table 7.

Over the range of state conditions considered in this study, $\rho(P)_T$ and $-\rho(T)_P$ are monotone, increasing functions characterized by pronounced sigmoid behavior in the near-critical region that dampens with temperature and pressure (fig. 9). This dampening sigmoidicity, a mathematical consequence of critical-point singularity in the equation of state, produces local extrema in first- and second-order derivative properties that diverge to $\pm\infty$ with approach to criticality. This asymptotic behavior of equation-of-state derivatives is responsible for all near-critical anomalies in the thermodynamic, transport, and electrostatic properties of H_2O. Consequently, accurate prediction of such anomalous behavior is essentially dependent upon development of an extremely precise equation of state.

Levelt Sengers and others (1983) report that eq (48) represents the experimental $P(T, \rho)$ data of Rivkin and Akhundov (1962, 1963, 1966) to within their estimated accuracy. This excellent correspondence is ex-

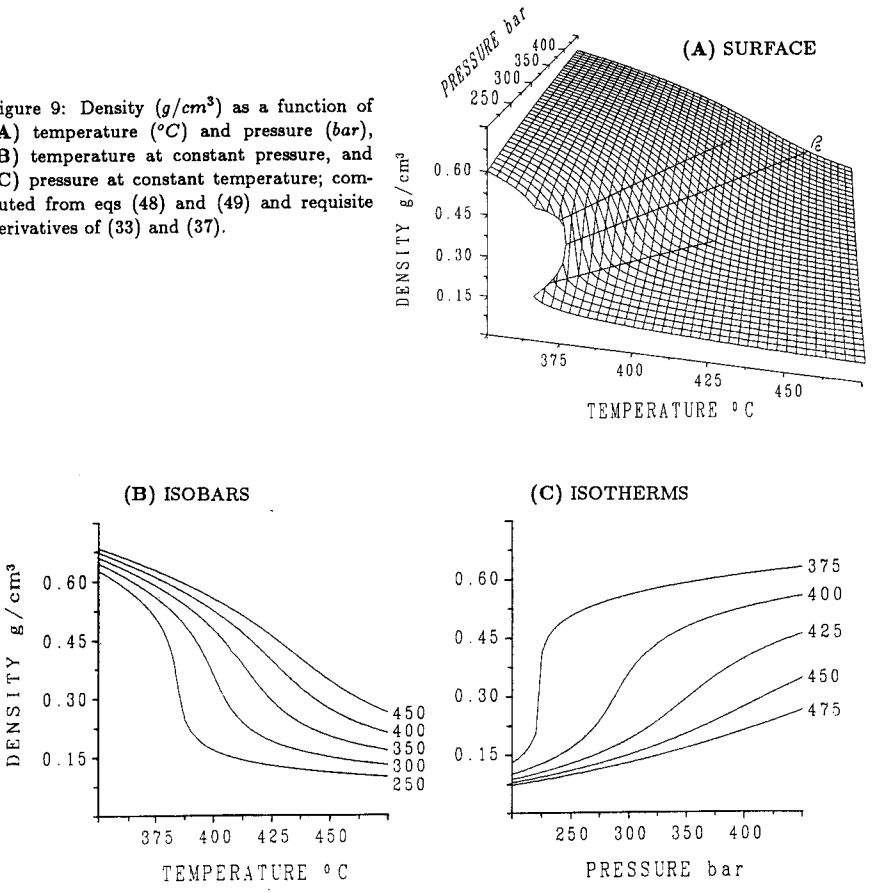

Figure 9: Density (g/cm^3) as a function of **(A)** temperature ($°C$) and pressure (bar), **(B)** temperature at constant pressure, and **(C)** pressure at constant temperature; computed from eqs (48) and (49) and requisite derivatives of (33) and (37).

TABLE 7

Density (g/cm^3) *as a function of pressure* (bars) *and temperature* (°C)*; computed from eqs (48), (49), and requisite derivatives of (33) and (37). The exponentiation is shorthand for* $\times 10^{-1}$

$P \backslash T$	375	400	425	450	475
250	0.50521	0.16663	0.12682	0.10909	0.97935^{-1}
300	0.55825	0.35838	0.18866	0.14845	0.12829
350	0.58798	0.47489	0.29194	0.20163	0.16519
400	0.60956	0.52367	0.39456	0.27091	0.20998
450	0.62680	0.55478	0.45749	0.34337	0.26170

pected, of course, because these data were used in the regression analysis from which several adjustable constants inherent to the equation were obtained. However, comparison (this study) of eq (48) with high-quality critical-region measurements (Hanafusa and others, 1983) *not* used in this fitting procedure reveals average discrepancy of less than two parts per ten thousand between calculated and experimental $P(T, \rho)$. This agreement is superior to that achieved using eq (49). Outside the critical region, Haar, Gallagher, and Kell (1984) report that eq (49) represents experimental $\rho(T, P)$ excluded from their regression analysis to within, in general, a few parts per thousand.

Compressibility and expansivity.—The coefficient of isothermal compressibility is defined as

$$\beta \equiv \frac{1}{\rho}\left(\frac{\partial \rho}{\partial P}\right)_T \equiv -\frac{1}{V}\left(\frac{\partial V}{\partial P}\right)_T . \tag{50}$$

Within the critical region, this coefficient is expressed as

$$\beta = -\frac{\tilde{T}}{\tilde{\rho}^2 P_c}\left(\frac{\partial^2 \Delta \tilde{P}}{\partial \Delta \tilde{\mu}^2}\right)_{\Delta \tilde{T}} ; \tag{51}$$

in the global region, isothermal compressibility is given by

$$\beta = CM\left\{2\rho^2\left(\frac{\partial A_m}{\partial \rho}\right)_T + \rho^3\left(\frac{\partial^2 A_m}{\partial \rho^2}\right)_T\right\}^{-1} . \tag{52}$$

Eqs (48), (49), (51), (52), and requisite derivatives of (33) and (37) were used to compute the $\beta(P, T)$ surface, $\beta(T)$-isobars, and $\beta(P)$-isotherms illustrated in figure 10, and the $\beta(P, T)$-values listed in table 8.

Isothermal compressibility diverges sharply from background values of $\approx 10^{-3}$ *bar*$^{-1}$ to ∞ at the critical point (fig. 10A). The relatively strong character of this divergence, that is, the relatively large magnitude of its governing exponent ($\gamma_{c_\xi} = 1.241$ in eq 16), results from the functional dependence of β on second-order *isothermal* differentiation of eqs (37) and (33), a direction that *intersects* the *P–T* vaporization boundary and confluent critical isochore (Griffiths and Wheeler, 1970; Levelt Sengers, 1982). Note that β divergence is sharpest when criticality is approached *along* the critical isochore (or vaporization boundary) — which is therefore coincident with the near-critical locus of maxima in $\beta(T)$-isobars and $\beta(P)$-isotherms — and less pronounced along any other approach path in the *P–T* plane (Griffiths and Wheeler, 1970; Levelt Sengers, 1982). With increasing pressure and temperature, however, these two maxima depart unequally from the critical isochore toward subcritical densities. As a result, the $\beta(P, T)$ surface is folded upward into a *P–T* crease that is sharpest at its critical-point origin, then flattens as it gradually departs

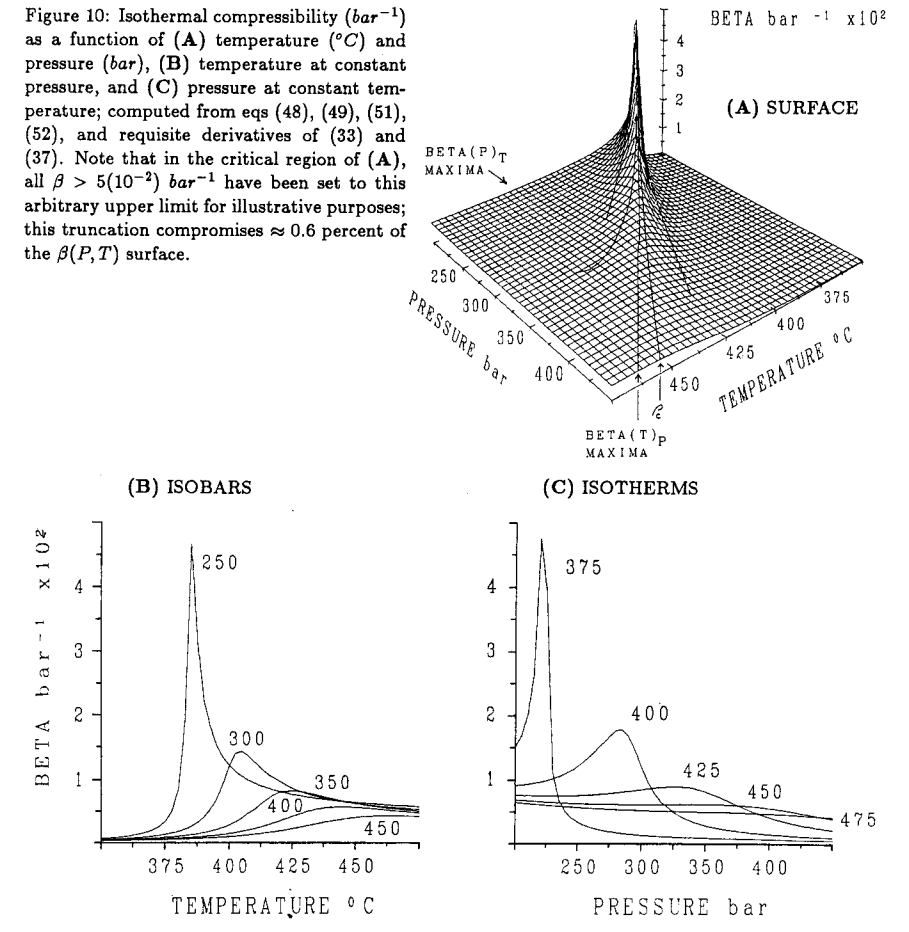

Figure 10: Isothermal compressibility (bar^{-1}) as a function of **(A)** temperature ($°C$) and pressure (bar), **(B)** temperature at constant pressure, and **(C)** pressure at constant temperature; computed from eqs (48), (49), (51), (52), and requisite derivatives of (33) and (37). Note that in the critical region of **(A)**, all $\beta > 5(10^{-2})\ bar^{-1}$ have been set to this arbitrary upper limit for illustrative purposes; this truncation compromises ≈ 0.6 percent of the $\beta(P,T)$ surface.

TABLE 8

Isothermal compressibility (bar^{-1}) *as a function of pressure* (bars) *and temperature* (°C)*; computed from eqs (48), (49), (51), (52), and requisite derivatives of (33) and (37). Exponentiations are shorthand for* $\times 10^{[-1,-2,-3]}$

$P \backslash T$	375	400	425	450	475
250	0.33310^{-2}	0.12095^{-1}	0.75424^{-2}	0.62678^{-2}	0.56422^{-2}
300	0.13097^{-2}	0.11996^{-1}	0.85019^{-2}	0.61119^{-2}	0.51992^{-2}
350	0.83914^{-3}	0.27715^{-2}	0.81093^{-2}	0.61192^{-2}	0.49296^{-2}
400	0.62480^{-3}	0.14225^{-2}	0.40864^{-2}	0.55020^{-2}	0.46433^{-2}
450	0.50103^{-3}	0.94939^{-3}	0.21459^{-2}	0.39090^{-2}	0.41082^{-2}

from subcritical densities beyond the critical region, where the surface is relatively flat (fig. 10A).

Unequal departure of $\beta(T)_P$ and $\beta(P)_T$ maxima from the critical isochore in the P–T plane subdivides the $\beta(P, T)$ surface into three major regions of specific partial derivative variation: (1) a region that includes the entire low-density side of $\beta(T)_P$ maxima at temperatures $\geq 450°C$ (where $\beta(P)_T$ becomes monotonic) but is confined between the two maxima at lower temperatures — in this region β decreases with both pressure and temperature; (2) a region to the low-density side of the $\beta(P)_T$ maxima where β increases with pressure and decreases with temperature; and (3) a region to the high-density side of the $\beta(T)_P$ maxima where β decreases with pressure and increases with temperature. Isothermal compressibilities of low-density ($\ll \rho_c$) supercritical fluid are typically several times larger than those of high-density ($\gg \rho_c$) supercritical fluid.

The coefficient of isobaric expansivity is defined as

$$\alpha \equiv -\frac{1}{\rho}\left(\frac{\partial \rho}{\partial T}\right)_P \equiv \frac{1}{V}\left(\frac{\partial V}{\partial T}\right)_P. \tag{53}$$

Within the critical region, this coefficient is expressed as

$$\alpha = \frac{\tilde{T}}{\tilde{\rho}\tilde{T}}\left\{\tilde{P}_{11} + \left(\frac{\partial^2 \Delta \tilde{P}}{\partial \Delta \tilde{\mu} \partial \Delta \tilde{T}}\right)_{\Delta \tilde{T}, P}\right\},$$

or, equivalently

$$= -\frac{\tilde{T}}{\tilde{\rho}^2 T_c}\left(\frac{\partial^2 \Delta \tilde{P}}{\partial \Delta \tilde{\mu}^2}\right)_{\Delta \tilde{T}}\left\{\tilde{P} + \tilde{T}\left(\frac{\partial \tilde{P}}{\partial \tilde{T}}\right)_{\tilde{\rho}}\right\} \tag{54}$$

where the latter equality, of greater convenience than the former in the context of evaluating $(\partial\alpha/\partial T)_\rho$, follows from combination of eq (51) with $(\partial P/\partial T)_\rho = \alpha/\beta$. In the global region, isobaric expansivity is given by

$$\alpha = \left(\frac{\partial^2 A_m}{\partial \rho \partial T}\right)_{T,\rho}\left\{2\left(\frac{\partial A_m}{\partial \rho}\right)_T + \rho\left(\frac{\partial^2 A_m}{\partial \rho^2}\right)_T\right\}^{-1}. \tag{55}$$

Eqs (37), (48), (49), (54), (55), and requisite derivatives of (33) and (37) were used to compute the $\alpha(P, T)$ surface, $\alpha(T)$-isobars, and $\alpha(P)$-isotherms illustrated in figure 11, and the $\alpha(P, T)$ values listed in table 9.

Comparison of the $\alpha(P, T)$ and $\beta(P, T)$ surfaces reveals striking similarity in their functional form. In particular, isobaric expansivity asymptotically decreases from ∞ at the critical point toward background values ($10^{-3} - 10^{-2}\,°K^{-1}$; fig. 11A) in the same manner as described above for isothermal compressibility (Sengers and Levelt Sengers, 1978; Levelt Sengers, Morrison, and Chang, 1983). This close functional correspon-

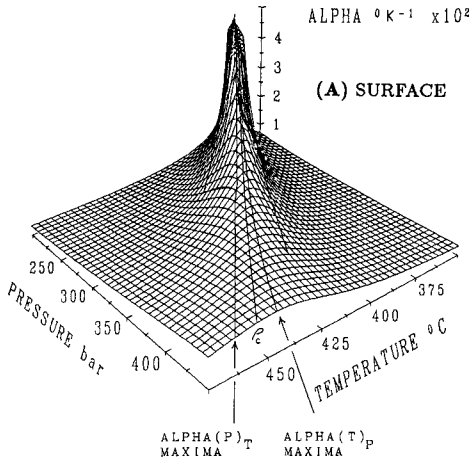

Figure 11: Isobaric expansivity ($^{\circ}K^{-1}$) as a function of (**A**) temperature ($^{\circ}C$) and pressure (bar), (**B**) temperature at constant pressure, and (**C**) pressure at constant temperature; computed from eqs (37), (48), (49), (54), (55), and requisite derivatives of (33) and (37). Note that in the critical region of (**A**), all $\alpha > 5(10^{-2})\ ^{\circ}K^{-1}$ have been set to this arbitrary upper limit for illustrative purposes; this truncation compromises ≈ 2.1 percent of the $\alpha(P,T)$ surface.

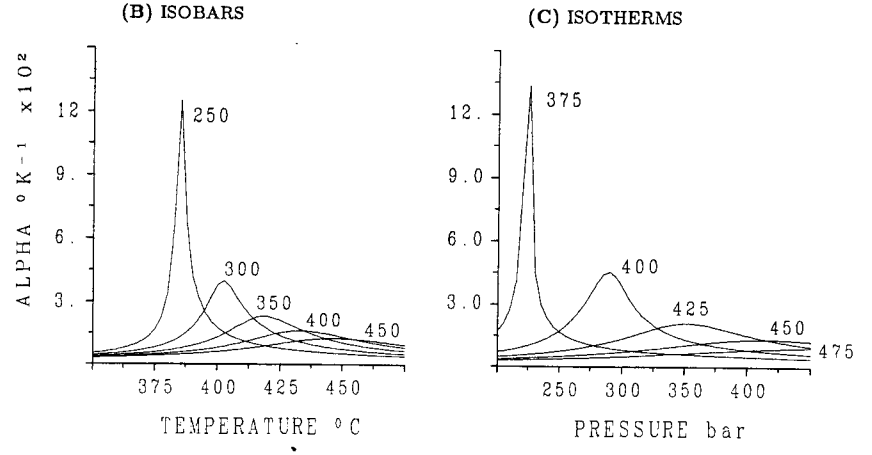

TABLE 9

Isobaric expansivity ($^{\circ}K^{-1}$) *as a function of pressure* (bars) *and temperature* ($^{\circ}C$)*; computed from eqs (48), (49), (54), (55), and requisite derivatives of (33) and (37). Exponentiations are shorthand for* $\times 10^{[-1,-2]}$

$P \backslash T$	375	400	425	450	475
250	0.16539^{-1}	0.17301^{-1}	0.74655^{-2}	0.49601^{-2}	0.37902^{-2}
300	0.80443^{-2}	0.37789^{-1}	0.13504^{-1}	0.70818^{-2}	0.48880^{-2}
350	0.57986^{-2}	0.12957^{-1}	0.20761^{-1}	0.10224^{-1}	0.63297^{-2}
400	0.46932^{-2}	0.79718^{-2}	0.14958^{-1}	0.12932^{-1}	0.79750^{-2}
450	0.40164^{-2}	0.59774^{-2}	0.97763^{-2}	0.12177^{-1}	0.91929^{-2}

dence reflects the dependence of α, like β, on second-order differentiation of eqs (37) and (33) in a P–T direction oblique to that of phase transition and the confluent critical isochore (Griffiths and Wheeler, 1970; Levelt Sengers, 1982). Hence, the divergent character of α is also fundamentally strong and sharpest when criticality is approached along the critical isochore or vaporization boundary.

Relative maxima in $\alpha(T)_P$ and $\alpha(P)_T$ occur at larger densities than their β counterparts. This density shift has two noteworthy consequences. First, the restricted region where α decreases both with temperature and pressure, confined between the two maxima projections, is approximately centered on the critical isochore (fig. 11A); the corresponding region for β is located to the high-temperature side of the critical isochore (fig. 10A). Second, this near-symmetric relationship of $\alpha(T)_P$ and $\alpha(P)_T$ maxima with respect to the critical isochore results in a lack of significant discrepancy between expansivities of supercritical liquid and vapor; the corresponding β extrema both follow subcritical paths which results in such discrepancy as noted above.

Expansivity and compressibility also differ slightly in magnitude. Within the critical region, $\alpha(P, T)$ $°K^{-1}$ is typically several times larger than $\beta(P, T)$ bar^{-1}; in the near-critical region, this difference approaches an order of magnitude. Hence, $\rho(T, P)$ will decrease more for an isobaric $1°K$ temperature increase than it will for an isothermal 1 *bar* pressure drop, significantly more so in the critical region.

Isobaric temperature derivative of expansivity.—Equations used to predict standard partial molal heat capacities of aqueous species in the context of electrostatic models of ion solvation (Helgeson, Kirkham, and Flowers, 1981; Tanger and Helgeson, 1988) require values for $(\partial\alpha/\partial T)_P$. As a result, requisite higher-order derivatives of eqs (37) and (33) were generated in the course of the present study, and accuracy of the computed analytic $(\partial\alpha/\partial T)_P$ was verified by comparison with its finite difference counterparts.

The isobaric temperature derivative of the isobaric expansivity coefficient is defined by

$$\left(\frac{\partial\alpha}{\partial T}\right)_P \equiv \alpha^2 - \frac{1}{\rho}\left(\frac{\partial^2\rho}{\partial T^2}\right)_P . \tag{56}$$

Within the critical region, this derivative can be expressed as

$$\left(\frac{\partial\alpha}{\partial T}\right)_P = \frac{\tilde{T}^2}{\tilde{\rho}^2 T_c}\left\{\left[\frac{P}{P_c} + \left(\frac{\partial\tilde{P}}{\partial\tilde{T}}\right)_{\tilde{\rho}}\right]\left\{2\left(\frac{\partial^2\Delta\tilde{P}}{\partial\Delta\tilde{\mu}^2}\right)_{\Delta\tilde{T}}\left\{\alpha - \frac{1}{\tilde{T}}\right\} - \frac{\tilde{T}}{\tilde{T}}\left(\frac{\partial^3\Delta\tilde{P}}{\partial\Delta\tilde{\mu}^2\partial\Delta\tilde{T}}\right)_{\Delta\tilde{T},\Delta\tilde{T},P}\right\} - \frac{\tilde{T}}{\tilde{T}}\left(\frac{\partial^2\Delta\tilde{P}}{\partial\Delta\tilde{\mu}^2}\right)_{\Delta\tilde{T}}\left(\frac{\partial^2\tilde{P}}{\partial\tilde{T}^2}\right)_{\tilde{\rho},P}\right\}; \tag{57}$$

in the global region, $(\partial\alpha/\partial T)_P$ is given by

$$\left(\frac{\partial\alpha}{\partial T}\right)_P = \alpha\left(\frac{\partial^2 A_m}{\partial\rho\partial T}\right)_{T,\rho}^{-1}\left\{\left(\frac{\partial^3 A_m}{\partial\rho\partial T^2}\right)_{T,\rho,P} - \alpha\left[2\left(\frac{\partial^2 A_m}{\partial\rho\partial T}\right)_{T,P} + \rho\left(\frac{\partial^3 A_m}{\partial\rho^2\partial T}\right)_{T,T,P} - \rho\alpha\left(\frac{\partial^2 A_m}{\partial\rho^2}\right)_T\right]\right\}. \quad (58)$$

Eqs (48), (49), (54), (55), (57), (58) and requisite derivatives of (33) and (37) were used to compute the $(\partial\alpha/\partial T)_P$ (P, T) surface, $(\partial\alpha/\partial T)_P$ (T)-isobars, and $(\partial\alpha/\partial T)_P$ (P)-isotherms illustrated in figure 12, and the $(\partial\alpha/\partial T)_P$ (P, T) values listed in table 10.

The $(\partial\alpha/\partial T)_P$ surface, isobars, and isotherms can be visualized as discontinuity-smoothed, spliced versions of their $\alpha_{\rho>\rho_c}$ and $-\alpha_{\rho<\rho_c}$ counterparts (figs. 11 and 12). More precisely, all $(\partial\alpha/\partial T)_P(T)_{P>P_c}$ and $(\partial\alpha/\partial T)_P \cdot (P)_{T>T_c}$ isopleths display local negative minima *and* positive maxima, at sub- and supercritical densities, respectively, that asymptotically increase in absolute magnitude and converge toward the critical isochore with approach to criticality —hence, $(\partial\alpha/\partial T)_P$ diverges to ∞ when approached from $\rho > \rho_c$ but to $-\infty$ when approached from $\rho < \rho_c$. The pressure-temperature loci of these four extrema straddle the associated locus of $(\partial\alpha/\partial T)_P = 0$ (which is identical, of course, to that of $\alpha(T)_P$ maxima), itself near-coincident with ρ_c (fig. 13). Because these extrema and the zero-point projection all converge to ρ_c with approach to criticality, all five occur within a few degrees and bars of one another in the near-critical region. As a result, small variations in near-critical temperature or pressure may cause sign-reversal and/or large fluctuations in the absolute magnitude of $(\partial\alpha/\partial T)_P$.

Cursory inspection of figures 12B, C, and 13 reveals seemingly non-trivial discontinuity between the HGK and LS equations along the critical-region boundary. In general, these discrepancies amount to less than 6 and 15 percent,along, respectively, the 0.42 and 0.2 isochores, varying between these limits along the 421.85°C isotherm, except in the vicinity of its intersection with the $(\partial\alpha/\partial T)_P = 0$ projection, where on a percentage basis they are, of course, relatively large. The occurrence of such discontinuity reflects the dependence of $(\partial\alpha/\partial T)_P$ on third-order differentiation of eqs (33) and (37), which expectedly magnifies analogous, albeit inconspicuous, discrepancies present in properties solely dependent on lower-order derivatives. This magnification principle can be seen in figure 13, where several extrema projections evidence pressure discontinuities along the 421.85°C isotherm. Such discontinuities in $(\partial\alpha/\partial T)_P$ minima and maxima span 3.5 to 4.0 *bars;* analogous offsets in $\alpha(T)_P$ maxima — dependent only on second-order differentiation — measure $\approx$ 0.5 *bars;* and that in the critical isochore — a function of first-order partials — less than 0.2 *bars*. As implied, first- and second-derivative properties of eqs (33) and (37) can, in general, be considered continuous (with the exception of c_v as discussed below). Boundary discrepancies in third-derivative parameters, although significantly larger,

Figure 12: $(\partial\alpha/\partial T)_P$ $(°K^{-2})$ as a function of **(A)** temperature $(°C)$ and pressure (bar), **(B)** temperature at constant pressure, and **(C)** pressure at constant temperature; computed from eqs (48), (49), (54), (55), (57), (58), and requisite derivatives of (33) and (37). Note that in the critical region of **(A)**, all $-5(10^{-3}) \geq (\partial\alpha/\partial T)_P \geq 5(10^{-3})$ have been set to these arbitrary lower and upper limits for illustrative purposes; these truncations compromise ≈ 10.2 percent of the overall surface.

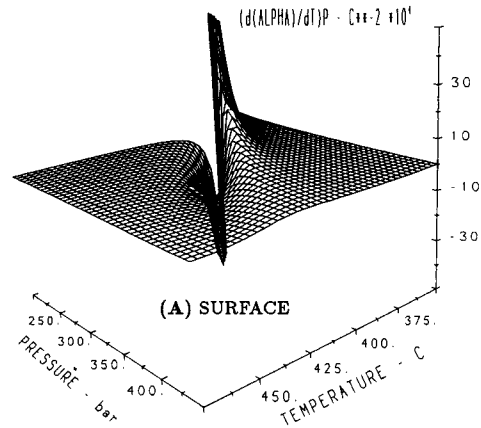

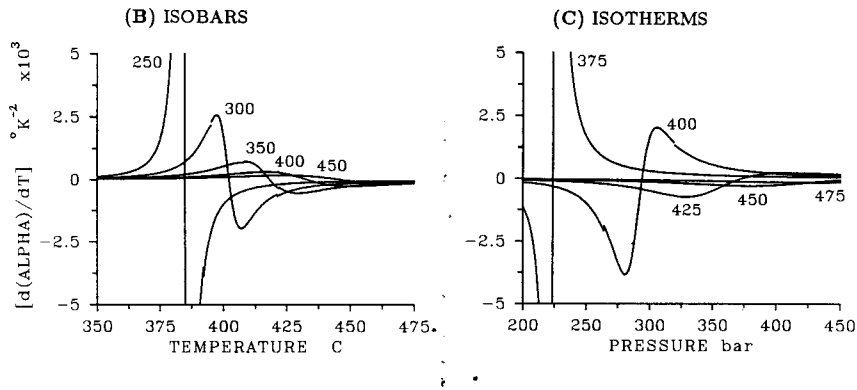

TABLE 10

$(\partial\alpha/\partial T)_P$ $(°K^{-2})$ as a function of pressure (bars) and temperature (°C); computed from eqs (48), (49), (54), (55), (57), (58), and requisite derivatives of (33) and (37). Exponentiations are shorthand for $\times 10^{[-2,-3]}$

$P \backslash T$	375	400	425	450	475
250	0.16554^{-2}	-0.99384^{-3}	-0.15844^{-3}	-0.63640^{-4}	-0.34466^{-4}
300	0.29730^{-3}	0.17054^{-2}	-0.49736^{-3}	-0.13113^{-3}	-0.58724^{-4}
350	0.13432^{-3}	0.54605^{-3}	-0.47789^{-3}	-0.24739^{-3}	-0.96304^{-4}
400	0.80029^{-4}	0.20573^{-3}	0.22875^{-3}	-0.25222^{-3}	-0.13688^{-3}
450	0.54549^{-4}	0.11003^{-3}	0.18103^{-3}	-0.43483^{-4}	-0.13692^{-3}

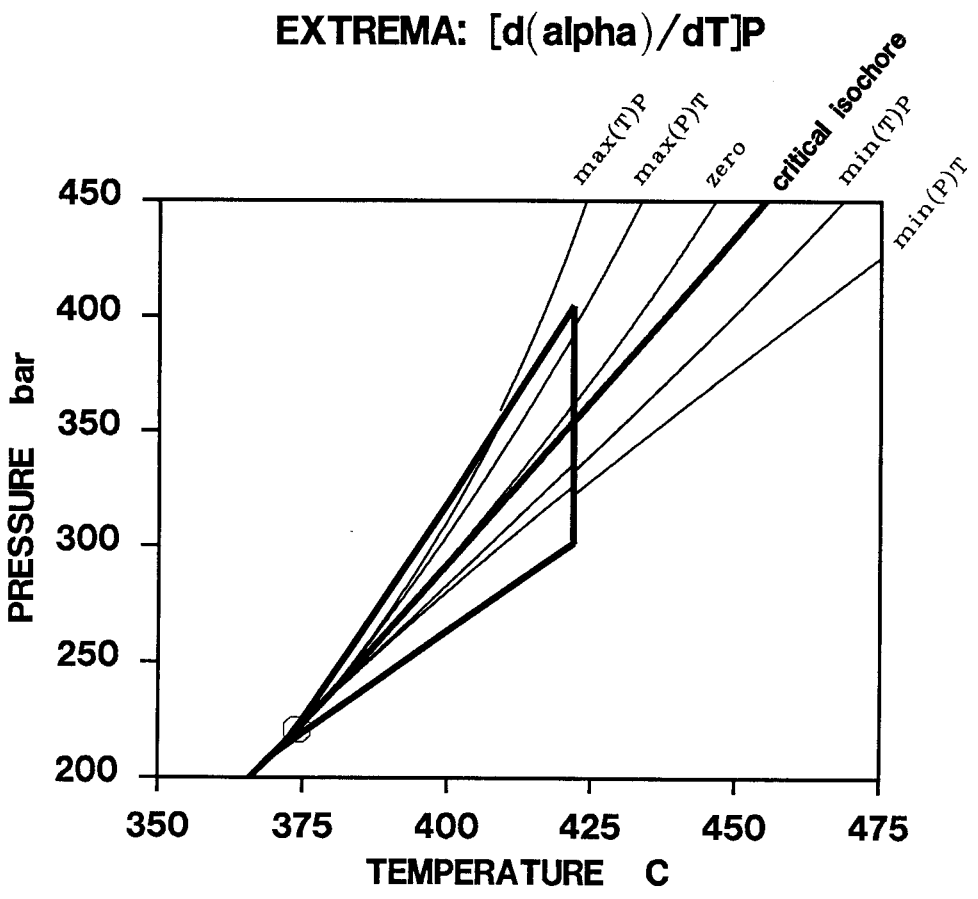

Fig. 13. P–T projections of $(\partial\alpha/\partial T)_\rho$ extrema computed from eqs (48) and (49), (54) and (55), (57) and (58), and the requisite derivatives of eqs (33) and (37). Also included, for reference, are the critical isochore, critical-region outline, and the zero contour for $(\partial\alpha/\partial T)_\rho$.

are not sufficiently so to be problematic in most applications; moreover, given the complexity of and theoretical differences between the two expressions, the magnitude of such discrepancies is remarkably small.

THERMODYNAMIC PROPERTIES

All thermodynamic properties are obtained from appropriate differentiation of the two fundamental functions, $\tilde{P}(\tilde{T}, \tilde{\mu})$ in the critical region, eq (37), and $A_m(T, \rho)$ elsewhere, eq (33), in accord with the first and second laws of thermodynamics. These properties are presented and analyzed below in terms of their P–T projections, calculated using the specified derivatives and equations-of-state (48) and (49).

Helmholtz and Gibbs free energies.—The Helmholtz free energy, A, is defined as

$$dA \equiv d(U - TS) \equiv -SdT - PdV. \tag{59}$$

Within the critical region, Helmholtz free energy per mole is expressed as

$$A_m = \frac{CMP_c}{\rho_c}\left(\frac{1}{\tilde{T}}\right)\left\{\tilde{P}\left(\frac{\partial\tilde{P}}{\partial\tilde{\mu}}\right)_{\tilde{T}}^{-1} - \tilde{\mu}\right\}; \tag{60}$$

over the global region, this property is the fundamental thermodynamic function itself, eq (33). Eqs (33), (37), (47) through (49), (60), and the requisite derivative of (37) were used to compute the $\Delta A_m(P, T)$ surface, $\Delta A_m(T)$-isobars, and $\Delta A_m(P)$-isotherms illustrated in figure 14, and the $\Delta A_m(P, T)$ values listed in table 11.

The apparent molal Helmholtz free energy, ΔA_m, decreases with temperature at constant pressure and increases with pressure at constant temperature. Outside the near-critical region, $\Delta A_m(T)_P$ and $\Delta A_m(P)_T$ are both close to linear, and the absolute magnitude of $(\partial\Delta A_m/\partial T)_P$ is several times larger than that of $(\partial\Delta A_m/\partial P)_T$ (fig. 14B and C). As a result, the global region of the $\Delta A_m(P, T)$ surface is essentially planar, tilting slightly upward with pressure, more distinctly downward with temperature (fig. 14A).

In the near-critical region, however, $-(\partial\Delta A_m/\partial T)_P$ and $(\partial\Delta A_m/\partial P)_T$ develop distinguishable local maxima; both partials diverge to ∞ at the critical point. These local maxima cause a slight warping of the $\Delta A_m(P, T)$ surface (fig. 14A) and impose a subtle sigmoid form on $\Delta A_m(T)$-isobars and $\Delta A_m(P)$-isotherms (fig. 14B and C). Such near-critical anomalies in ΔA_m have the same geometric basis as similar features in density (fig. 9A and C): unique equality of coexisting liquid and vapor properties at the critical point. However, these anomalies are much less pronounced in ΔA_m than in density because the parabolic $\Delta A_m(T)$ vaporization boundary has a much smaller radius of curvature at its critical-point vertex than does the $\rho(T)$ coexistence curve (compare figs. 14A and 9A).

The Gibbs free energy, G, is defined as

$$dG \equiv d(U - TS + PV) \equiv -SdT + VdP. \tag{61}$$

Within the critical region, Gibbs free energy is given by

$$G_m = \frac{CMP_c}{\rho_c}\left(\frac{\partial\tilde{P}}{\partial\tilde{\mu}}\right)_{\tilde{T}}^{-1}\left\{\left(\frac{1}{\tilde{T}} + 1\right)\tilde{P} - (\tilde{T} + 1)\left(\frac{\partial\tilde{P}}{\partial\tilde{T}}\right)_{\tilde{\mu}} - \left(\frac{\tilde{\mu}}{\tilde{T}}\right)\left(\frac{\partial\tilde{P}}{\partial\tilde{\mu}}\right)_{\tilde{T}}\right\}; \tag{62}$$

the corresponding expression for the global region is

$$G_m = A_m + \rho\left(\frac{\partial A_m}{\partial\rho}\right)_T. \tag{63}$$

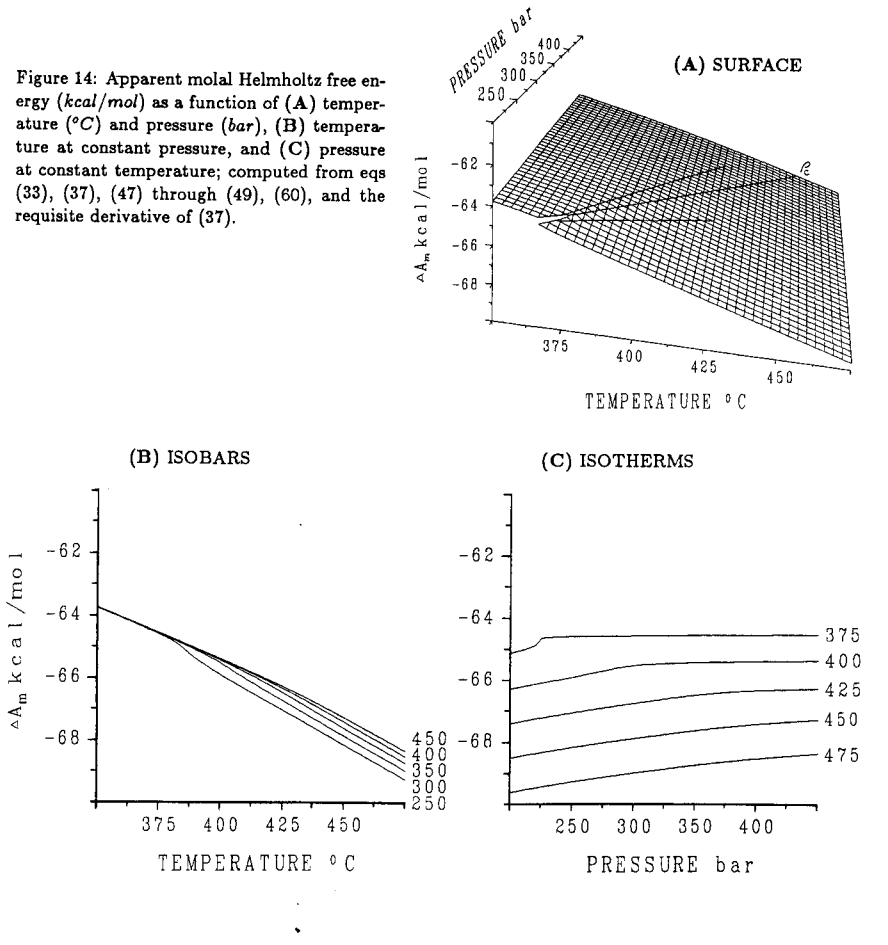

Figure 14: Apparent molal Helmholtz free energy (*kcal/mol*) as a function of (**A**) temperature (°*C*) and pressure (*bar*), (**B**) temperature at constant pressure, and (**C**) pressure at constant temperature; computed from eqs (33), (37), (47) through (49), (60), and the requisite derivative of (37).

TABLE 11

Apparent molal Helmholtz free energy (kcal/mol) *as a function of pressure* (bars) *and temperature* (°C)*; computed from eqs (33), (37), (47) through (49), (60), and the requisite derivative of (37)*

$P \backslash T$	375	400	425	450	475
250	−64.599	−65.908	−67.063	−68.179	−69.290
300	−64.577	−65.531	−66.758	−67.893	−69.005
350	−64.564	−65.438	−66.497	−67.645	−68.762
400	−64.555	−65.406	−66.355	−67.441	−68.555
450	−64.546	−65.387	−66.291	−67.300	−68.383

Eqs (33), (37), (47) through (49), (62), (63), and requisite derivatives of (33) and (37) were used to compute the $\Delta G_m(P, T)$ surface, $\Delta G_m(T)$-isobars, and $\Delta G_m(P)$-isotherms illustrated in figure 15, and the $\Delta G_m(P, T)$ values listed in table 12.

Excluding the near-critical region, the functional form of apparent molal Gibbs free energy, ΔG_m, is nearly identical to that of apparent molal Helmholtz free energy (compare figs. 15 and 14). However, because ΔG_m of coexisting liquid and vapor are equivalent along the entire vaporization boundary, $(\partial \Delta G_m/\partial T)_P$ and $(\partial \Delta G_m/\partial P)_T$ do not diverge to $\pm\infty$ at the critical point, in contrast to their ΔA_m analogs.

Internal energy and enthalpy.—The differential expression for internal energy is given by the Clausius equation:

$$dE \equiv TdS - PdV. \tag{64}$$

Within the critical region, internal energy per mole is given by

$$E_m = \frac{CMP_c}{\rho_c}\left(\frac{\partial \tilde{P}}{\partial \tilde{\mu}}\right)_{\tilde{T}}^{-1}\left(\frac{\partial \tilde{P}}{\partial \tilde{T}}\right)_{\tilde{\mu}}; \tag{65}$$

the corresponding expression for the global region is

$$E_m = A_m - T\left(\frac{\partial A_m}{\partial T}\right)_{\rho}. \tag{66}$$

Eqs (33), (47) through (49), (65), (66), and requisite derivatives of (33) and (37) were used to compute the $\Delta E_m(P, T)$ surface, $\Delta E_m(T)$-isobars, and $\Delta E_m(P)$-isotherms illustrated in figure 16, and the $\Delta E_m(P, T)$ values listed in table 13.

In contrast to ΔA_m and ΔG_m, apparent molal internal energy, ΔE_m, *increases* with temperature at constant pressure and *decreases* with pressure at constant temperature. In further contrast, distinguishable local maxima in $(\partial \Delta E_m/\partial T)_P$ and minima in $(\partial \Delta E_m/\partial P)_T$ are not constrained to the near-critical region; these extrema are clearly evident throughout the critical region as they asymptotically approach $\pm\infty$ at the critical point (fig. 16B and C). Consequently, the $\Delta E_m(P, T)$ surface, $\Delta E_m(T)$-isobars, and $\Delta E_m(P)$-isotherms all have distinguishable sigmoid form throughout the critical region that sharpens with proximity to the critical point (fig. 16). These functional anomalies have the same geometric basis as those noted above for density and ΔA_m. Moreover, because the parabolic $\Delta E_m(T)$ and $\rho(T)$ vaporization boundaries have similar radius of curvature at their critical-point vertices, the functional form of $\Delta E_m(P, T)$ and its first- and higher-order derivatives mirrors that of $\rho(P, T)$ and its derivatives (compare figs. 16 and 9).

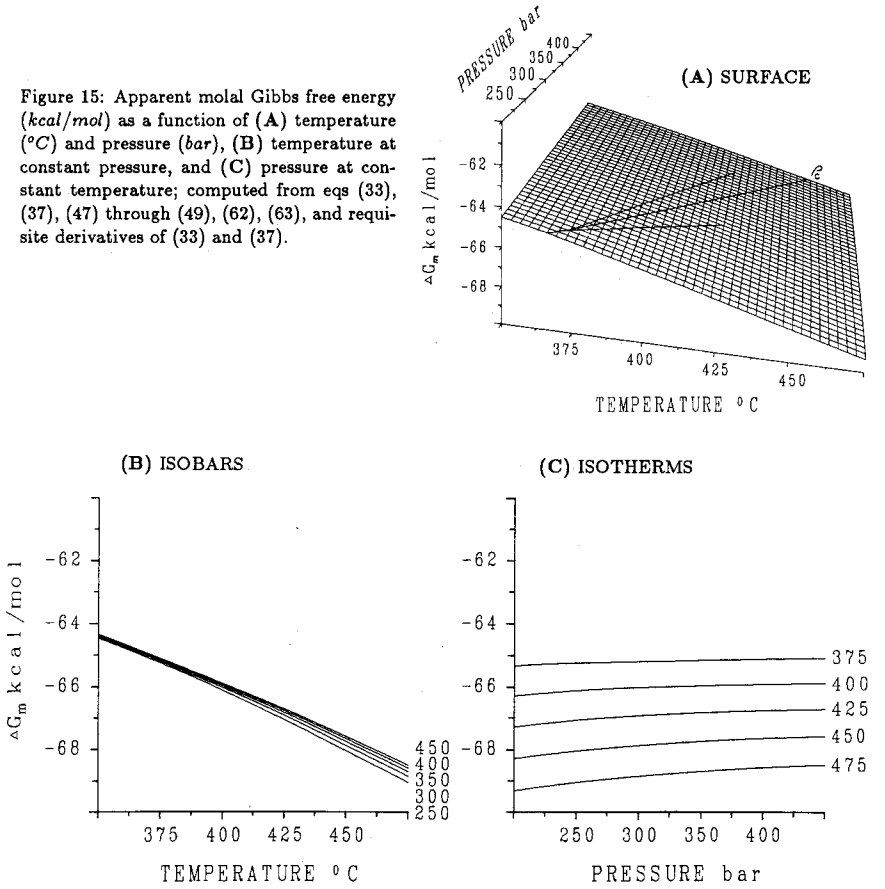

Figure 15: Apparent molal Gibbs free energy (*kcal/mol*) as a function of (**A**) temperature (*°C*) and pressure (*bar*), (**B**) temperature at constant pressure, and (**C**) pressure at constant temperature; computed from eqs (33), (37), (47) through (49), (62), (63), and requisite derivatives of (33) and (37).

TABLE 12

Apparent molal Gibbs free energy (kcal/mol) *as a function of pressure* (bars) *and temperature* (°C)*; computed from eqs (33), (37), (47) through (49), (62), (63), and requisite derivatives of (33) and (37)*

$P \setminus T$	375	400	425	450	475
250	–65.260	–66.136	–67.088	–68.067	–69.065
300	–65.220	–66.045	–66.947	–67.897	–68.872
350	–65.182	–65.994	–66.855	–67.772	–68.724
400	–65.146	–65.951	–66.792	–67.680	–68.608
450	–65.111	–65.912	–66.742	–67.610	–68.517

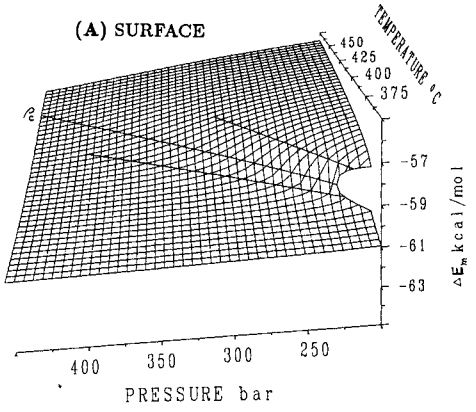

Figure 16: Apparent molal internal energy (*kcal/mol*) as a function of (**A**) temperature (*°C*) and pressure (*bar*), (**B**) temperature at constant pressure, and (**C**) pressure at constant temperature; computed from eqs (33), (47) through (49), (65), (66), and requisite derivatives of (33) and (37).

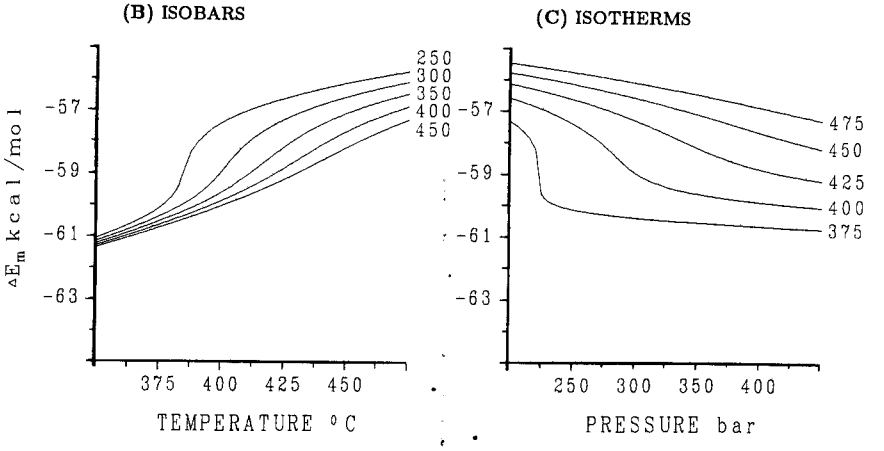

TABLE 13

Apparent molal internal energy (kcal/mol) *as a function of pressure* (bars) *and temperature* (°C)*; computed from eqs (33), (47) through (49), (65), (66), and requisite derivatives of (33) and (37)*

$P \backslash T$	375	400	425	450	475
250	−60.136	−57.431	−56.653	−56.167	−55.786
300	−60.403	−58.978	−57.319	−56.604	−56.118
350	−60.555	−59.642	−58.189	−57.124	−56.491
400	−60.667	−59.901	−58.858	−57.700	−56.899
450	−60.756	−60.065	−59.221	−58.212	−57.321

The differential expression for enthalpy, H, is given by

$$dH \equiv d(U + PV) = TdS + VdP. \tag{67}$$

Within the critical region, enthalpy per mole is computed from

$$H_m = \frac{CMP_c}{\rho_c}\left(\frac{\partial\tilde{P}}{\partial\tilde{\mu}}\right)_{\tilde{T}}^{-1}\left\{\tilde{P} - \tilde{T}\left(\frac{\partial\tilde{P}}{\partial\tilde{T}}\right)_{\tilde{\mu}}\right\}; \tag{68}$$

the corresponding expression for the global region is

$$H_m = A_m - T\left(\frac{\partial A_m}{\partial T}\right)_\rho + \rho\left(\frac{\partial A_m}{\partial \rho}\right)_T. \tag{69}$$

Eqs (33), (37), (47) through (49), (68), (69), and requisite derivatives of (33) and (37) were used to compute the $\Delta H_m(P, T)$ surface, $\Delta H_m(T)$-isobars, and $\Delta H_m(P)$-isotherms illustrated in figure 17, and the $\Delta H_m(P, T)$ values listed in table 14.

The functional form of apparent molal enthalpy, ΔH_m, corresponds closely to that of ΔE_m (compare figs. 17 and 16). Consequently, at the critical point $-(\partial\Delta H_m/\partial P)_T = (\partial\Delta H_m/\partial T)_P = \infty$; the latter leads to the divergence of c_p to ∞ at criticality. Because of geometric similarity between vaporization boundaries, the functional form of $\Delta H_m(P, T)$ and its first- and higher-order derivatives mirrors that of $\rho(P, T)$ and its derivatives (compare figs. 17 and 9).

Entropy.—Within the critical region, third-law molal entropy values are given by

$$S_m = \frac{CMP_c}{T_c\rho_c}\left(\frac{\partial\tilde{P}}{\partial\tilde{\mu}}\right)_{\tilde{T}}^{-1}\left\{\tilde{P} - \tilde{T}\left(\frac{\partial\tilde{P}}{\partial\tilde{T}}\right)_{\tilde{\mu}} - \left(\frac{\partial\tilde{P}}{\partial\tilde{\mu}}\right)_{\tilde{T}}\right\}; \tag{70}$$

the corresponding expression for the global region is

$$S_m = -\left(\frac{\partial A_m}{\partial T}\right)_\rho. \tag{71}$$

Eqs (37), (47) through (49), (70), (71), and requisite derivatives of (33) and (37) were used to compute the $S_{m,tl}(P, T)$ surface, $S_{m,tl}(T)$-isobars, and $S_{m,tl}(P)$-isotherms illustrated in figure 18, and the $S_{m,tl}(P, T)$ values listed in table 15.

The functional form of third-law molal entropy within and near the critical region is nearly identical to that of ΔE_m and ΔH_m (compare figs. 18, 16, and 17). Consequently, at the critical point where $S_{m,tl}$ converges to a finite value, $-(\partial\Delta S_{m,tl}/\partial P)_T = (\partial\Delta S_{m,tl}/\partial T)_P = \infty$; the latter definition, in equivalent fashion to its ΔH_m analog, leads to the divergence of c_p to ∞ with approach to criticality. In addition, as noted above for ΔE_m and ΔH_m, the functional form of $S_{m,tl}(P, T)$ and its derivatives mirrors that of $\rho(P, T)$ and its derivatives (compare figs. 18 and 9).

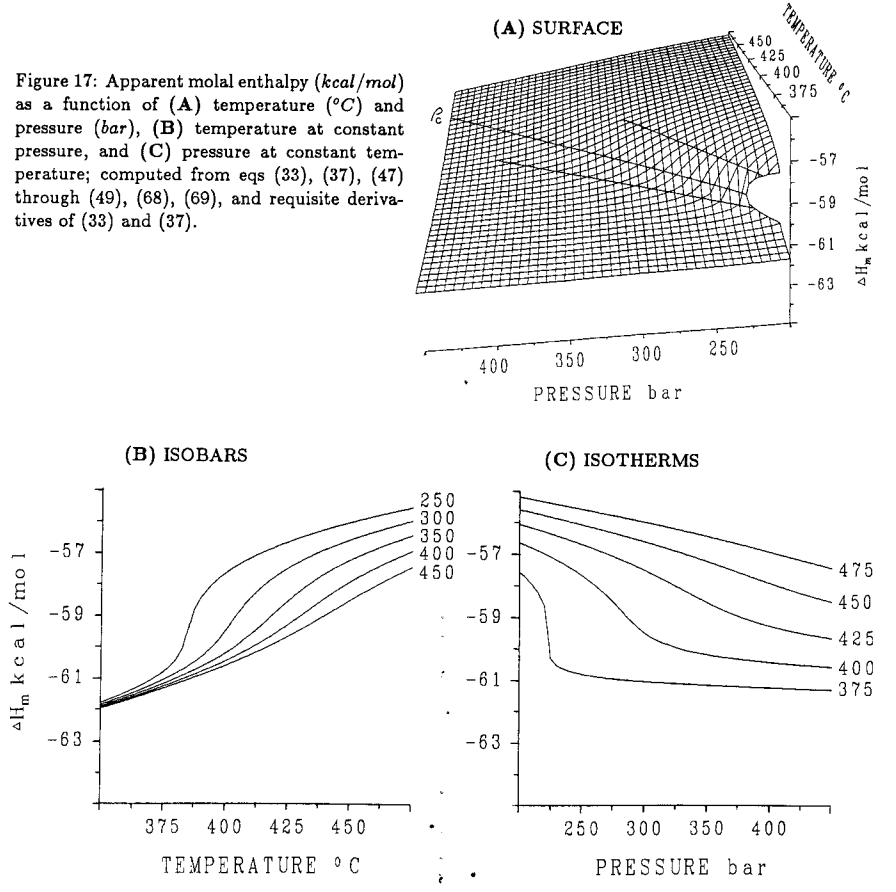

Figure 17: Apparent molal enthalpy (*kcal/mol*) as a function of (**A**) temperature (°*C*) and pressure (*bar*), (**B**) temperature at constant pressure, and (**C**) pressure at constant temperature; computed from eqs (33), (37), (47) through (49), (68), (69), and requisite derivatives of (33) and (37).

TABLE 14

Apparent molal enthalpy (kcal/mol) *as a function of pressure* (bars) *and temperature* (°C)*; computed from eqs (33), (37), (47) through (49), (68), (69), and requisite derivatives of (33) and (37)*

$P \setminus T$	375	400	425	450	475
250	−60.805	−57.667	−56.687	−56.063	−55.570
300	−61.055	−59.500	−57.517	−56.616	−55.994
350	−61.182	−60.207	−58.555	−57.259	−56.461
400	−61.267	−60.454	−59.304	−57.947	−56.962
450	−61.330	−60.599	−59.680	−58.530	−57.463

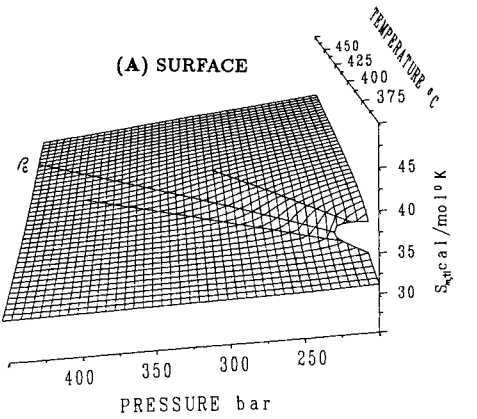

Figure 18: Third law molal entropy ($cal/mol°K$) as a function of (A) temperature ($°C$) and pressure (bar), (B) temperature at constant pressure, and (C) pressure at constant temperature; computed from eqs (37), (47) through (49), (70), (71), and requisite derivatives of (33) and (37).

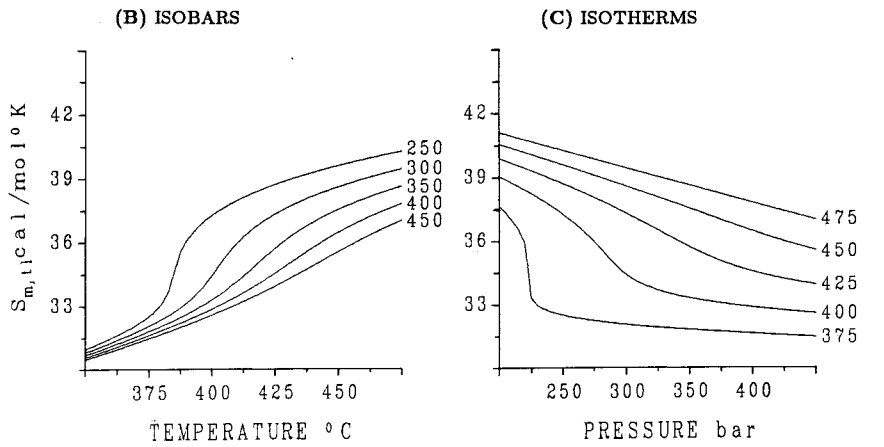

TABLE 15

Third law molal entropy (cal/mol°K) *as a function of pressure* (bars) *and temperature* (°C)*; computed from eqs (37), (47) through (49), (70), (71), and requisite derivatives of (33) and (37)*

$P \backslash T$	375	400	425	450	475
250	32.502	37.259	38.692	39.570	40.242
300	32.056	34.400	37.301	38.571	39.417
350	31.802	33.275	35.682	37.509	38.595
400	31.615	32.844	34.520	36.430	37.771
450	31.464	32.570	33.909	35.526	36.978

Heat capacity.—Isochoric heat capacity is defined by

$$c_v \equiv \left(\frac{\partial \Delta U}{\partial T}\right)_V \equiv \left(\frac{\partial U}{\partial T}\right)_V \equiv T\left(\frac{\partial S}{\partial T}\right)_V . \tag{72}$$

Within the critical region, c_v is given by

$$c_v = \frac{CMP_c}{T_c \rho_c} \tilde{T}^2 \left(\frac{\partial \tilde{P}}{\partial \tilde{\mu}}\right)_{\tilde{T}}^{-1} \left\{ \left(\frac{\partial^2 \tilde{P}}{\partial \tilde{T}^2}\right)_{\tilde{\mu}} - \left(\frac{\partial^2 \tilde{P}}{\partial \tilde{\mu}^2}\right)_{\tilde{T}}^{-1} \left(\frac{\partial^2 \tilde{P}}{\partial \tilde{T} \partial \tilde{\mu}}\right)_{\tilde{\mu},\tilde{T}} \right\}; \tag{73}$$

the corresponding expression for the global region is

$$c_v = -T\left(\frac{\partial^2 A_m}{\partial T^2}\right)_\rho . \tag{74}$$

Eqs (48), (49), (73), (74), and requisite derivatives of (33) and (37) were used to compute the $c_v(P, T)$ surface, $c_v(T)$-isobars, and $c_v(P)$-isotherms illustrated in figure 19, and the $c_v(P, T)$ values listed in table 16. Note that boundary discontinuities between eqs (73) and (74) (see below) are explicitly illustrated in the cross-sectional plots.

Isochoric heat capacity, like isothermal compressibility and isobaric expansivity, diverges from background values ($\approx$ 10 to 15 cal/mol°K) to ∞ at the critical point. In contrast to the strong divergence of α and β, however, the divergent character of c_v is relatively weak, that is, governed by an exponent of relatively small magnitude ($\alpha_{ce} = 0.11$ in eq 17). This distinction reflects the functional dependence of c_v on second-order *isochoric* (or, analogously, constant chemical potential) differentiation of eqs (33) and (37), which is directionally *equivalent* to the confluent critical isochore and vaporization boundaries (Griffiths and Wheeler, 1970; Levelt Sengers, 1982). Although one cannot clearly differentiate between strong (α, β) and weak (c_v) divergence from comparison of figures 10A, 11A, and 19A (owing to the scale-dependency of such asymptotic behavior), the weak nature of c_v divergence is readily appreciated by examination of the critical isochore on the $\Delta E_m(P, T)$ and $S_{m,ll}(P, T)$ surfaces (figs. 16A and 18A). The isobaric temperature derivative along this path is infinite *at the critical point,* but clearly finite and small in the near-critical region. Consequently, only the infinite c_v at critically required truncation in figure 19A.

Although fundamentally weak, the near-critical asymptotic behavior of c_v is otherwise similar to that of α and β. As noted above, divergence of all such properties is relatively sharpest with approach to criticality along the vaporization boundary or critical isochore (Griffiths and Wheeler, 1970; Levelt Sengers, 1982). Hence, the locus of relative maxima in $c_v(T)$-isobars and $c_v(P)$-isotherms (fig. 19) coincides with ρ_c in the near-critical region. These two P–T projections then depart unequally from that of ρ_c with increasing temperature and pressure. Initially, supercritical maxima in $c_v(T)_P$ and $c_v(P)_T$ follow paths of decreasing density; however, these trends reverse in the critical region at approx 230 to 240 *bars* for $c_v(T)_P$ and 415° to 420°C for $c_v(P)_T$. These reversals ultimately

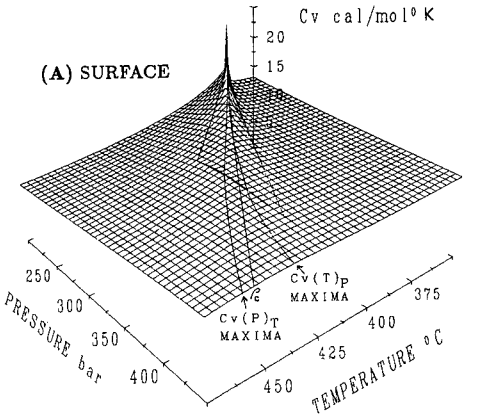

Figure 19: Isochoric heat capacity ($cal/mol°K$) as a function of (**A**) temperature ($°C$) and pressure (bar), (**B**) temperature at constant pressure, and (**C**) pressure at constant temperature; computed from eqs (48), (49), (73), (74), and requisite derivatives of (33) and (37). Note that in (**A**), the infinite critical-point value has been artificially set to 25 $cal/mol°K$ for illustrative purposes.

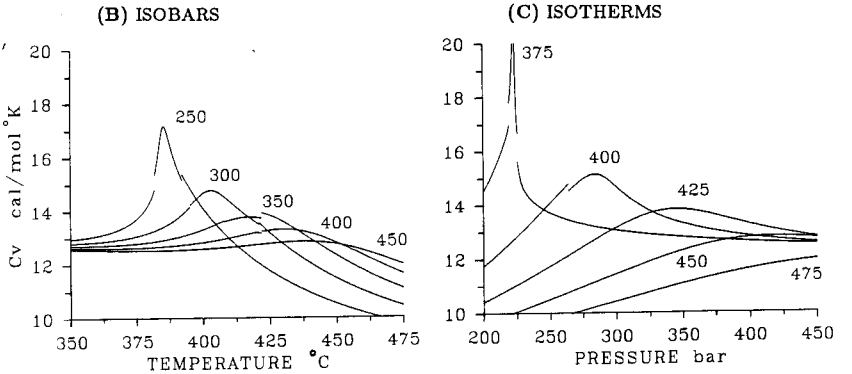

TABLE 16

Isochoric heat capacity (cal/mol°K) *as a function of pressure* (bars) *and temperature* (°C)*; computed from eqs (48), (49), (73), (74), and requisite derivatives of (33) and (37). Exponentiations are shorthand for* $\times 10^{[1,2]}$

$P \backslash T$	375	400	425	450	475
250	0.13705^2	0.14086^2	0.11741^2	0.10512^2	0.97739^1
300	0.13052^2	0.14651^2	0.13157^2	0.11445^2	0.10430^2
350	0.12774^2	0.13287^2	0.13812^2	0.12295^2	0.11070^2
400	0.12612^2	0.12805^2	0.13252^2	0.12764^2	0.11612^2
450	0.12504^2	0.12558^2	0.12759^2	0.12720^2	0.11956^2

cause both projections to cross the critical isochore, at approx 300 to 310 *bars* for $c_v(T)_P$ maxima and 475° to 480°*C* for $c_v(P)_T$ maxima.

Because $c_v(T)_P$ and $c_v(P)_T$ maxima depart unequally from the critical isochore in the supercritical *P–T* plane, the $c_v(P, T)$ surface, like that of α and β, is subdivided into three regions of specific partial derivative variation: (1) a region confined between the two maxima where c_v decreases with both pressure and temperature; (2) a region to the low-density side of $c_v(P)_T$ maxima where c_v increases with pressure and decreases with temperature; and (3) a region to the high-density side of the $c_v(T)_P$ maxima where c_v decreases with pressure and increases with temperature. At pressures < 300 *bars* and temperatures < 400°*C*, the $c_v(P, T)$ surface corresponds most closely to the $\beta(P, T)$ because their isothermal and isobaric maxima projections are nearly coincident. At higher pressures and temperatures, up to approx 450 *bars* and 475°*C*, the functional form of $c_v(P, T)$ is most comparable to that of $\alpha(P, T)$, because in this region c_v maxima projections are near-coincident with those of α.

Boundary discrepancies between c_v predictions of the LS and HGK equations are the largest of any second-derivative property considered in this study. For this reason, these discontinuities were explicitly illustrated in figure 19B and C. Because of their critical-point proximity, intersections of the 0.20 and 0.42 g/cm^3 isochores with the 375°*C* isotherm are characterized by relatively large c_v discontinuities: 6.8 and 4.9 percent, respectively. All other such discontinuities with the exception of that at 250 *bars*, 0.42 g/cm^3 (here, 3.7 percent) span less than 2 percent of the lower value. Moreover, the 375°*C*-isotherm discrepancies, although conspicuous in figure 19B and C, are essentially indistinguishable when connected point-to-point, owing to the near-vertical slope of $c_v(T \approx T_c)_{P \approx P_c}$. This connectivity algorithm was employed in the analogous α and β cross sections to bridge similar discontinuities, albeit of lesser magnitude. In summary, boundary discontinuities in first- and second-derivative properties of the fundamental equations are, in general, of insufficient magnitude to adversely affect most applications.

Isobaric heat capacity is defined by

$$c_p \equiv \left(\frac{\partial \Delta H}{\partial T}\right)_P \equiv \left(\frac{\partial H}{\partial T}\right)_P = T\left(\frac{\partial S}{\partial T}\right)_P, \tag{75}$$

and related to c_v by first derivative properties of the equation of state:

$$c_p = c_v + CM\left(\frac{T\alpha^2}{\rho\beta}\right). \tag{76}$$

Within the critical region, this property is obtained from

$$c_p = c_v + \frac{CMP_c}{T_c\rho_c}\left(\frac{\partial \tilde{P}}{\partial \tilde{\mu}}\right)_{\tilde{T}}^{-1}\left\{\left(\frac{\partial^2 \tilde{P}}{\partial \tilde{\mu}^2}\right)_{\tilde{T}}\left(\frac{\partial \tilde{P}}{\partial \tilde{\mu}}\right)_{\tilde{T}}^{-2}\left[\tilde{P} - \tilde{T}\left(\frac{\partial \tilde{P}}{\partial \tilde{T}}\right)_{\tilde{\mu}}\right]^2\right\}; \tag{77}$$

the corresponding expression for the global region is

$$c_p = c_v + T\rho^2\left(\frac{\partial^2 A_m}{\partial\rho\partial T}\right)^2_{T,\rho}\left\{2\rho\left(\frac{\partial A_m}{\partial\rho}\right)_T + \rho^2\left(\frac{\partial^2 A_m}{\partial\rho^2}\right)_T\right\}^{-1}. \quad (78)$$

Eqs (37), (48), (49), (73), (74), (77), (78), and requisite derivatives of (33) and (37) were used to compute the $c_p(P, T)$ surface, $c_p(T)$-isobars, and $c_p(P)$-isotherms illustrated in figure 20, and the $c_p(P, T)$ values listed in table 17.

Isobaric heat capacity, like c_v, diverges from background values ($\approx$20–40 *cal/mol°K*) to ∞ at the critical point. Unlike c_v, however, but in analogy with β and α, c_p is strongly divergent as a consequence of its functional dependency on second-order *isothermal* differentiation of eqs (33) and (37) (Griffiths and Wheeler, 1970; Levelt Sengers, 1982). The functional form of c_p is thus similar to those of c_v, β, and α; in detail, however, it corresponds most closely to that of α (compare figs. 11 and 20). In the context of eq (75), this close correspondence reflects the mirror relationship of $\Delta H_m(T)$- and $S_{m,tl}(T)$-isobars to $\rho(T)$-isobars noted above and the convention of positive expansivity, eq (53).

The striking functional similarity between $c_p(P, T)$ and $\alpha(P, T)$ also follows from eq (76). This equation expresses c_p as the sum of weakly-divergent c_v and a second term whose behavior in the critical region is dominated by strongly-divergent α. This sharp divergence of α effectively controls the functional form of c_p, as indicated by the near-coincidence of α and c_p extrema projections. The presence of temperature as a multiplicative factor in (76) causes c_p background values to be several times larger than those of c_v; in the near-critical region this discrepancy exceeds an order of magnitude.

In the critical region, experimental maxima in $c_p(T)_P$ reported by Sirota and Mal'tsev (1962) agree with those predicted by eq (77) to within accuracy estimates for the measurements (Levelt Sengers and others, 1983). In the global region, similar agreement is obtained between experimental data and eq (78) (Haar, Gallagher, and Kell, 1984).

ELECTROSTATIC PROPERTIES

The negative reciprocal of the H_2O dielectric constant ($-1/\epsilon$) and its partial derivatives with respect to temperature and pressure, collectively referred to below as Born functions (Helgeson and Kirkham, 1974a; Helgeson, Kirkham, and Flowers, 1981), define electrostatic properties of the solvent that strongly influence the thermodynamic behavior of solute species at high temperatures and pressures, and control this behavior in the critical region (Johnson, 1987; Helgeson, 1991). This functional dependence is quantified by equations derived from electrostatic ion-solvation theory (Born, 1920; Bjerrum, 1929; Helgeson and Kirkham, 1974b, 1976; Helgeson, Kirkham, and Flowers, 1981; Tanger and Helgeson, 1988; Shock and Helgeson, 1988; Shock and others, ms) that represent solvation contributions to the standard partial molal properties of aqueous solutes in terms of the H_2O Born functions. As a

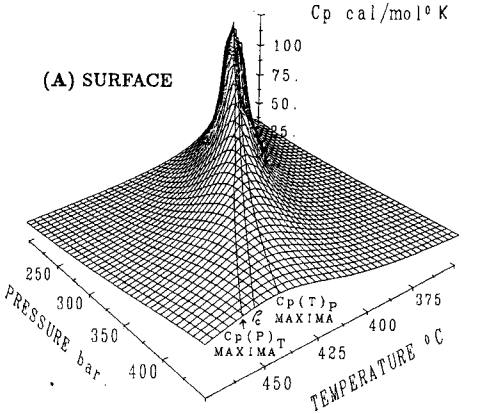

Figure 20: Isobaric heat capacity ($cal/mol°K$) as a function of **(A)** temperature ($°C$) and pressure (bar), **(B)** temperature at constant pressure, and **(C)** pressure at constant temperature; computed from eqs (37), (48), (49), (73), (74), (77), (78), and requisite derivatives of (33) and (37). Note that in the critical region of **(A)**, all $c_p > 125$ $cal/mol°K$ have been set to this arbitrary upper limit for illustrative purposes; this truncation compromises ≈ 2.6 percent of the $c_p(P,T)$ surface.

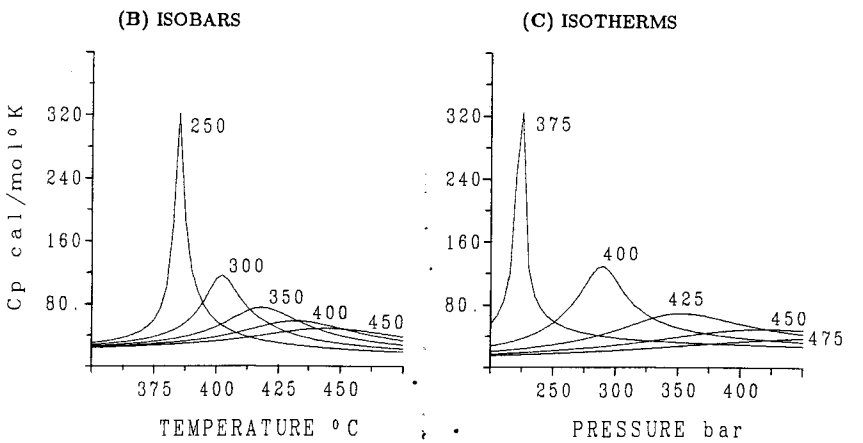

TABLE 17

Isobaric heat capacity (cal/mol°K) *as a function of pressure* (bars) *and temperature* (°C)*; computed from eqs (37), (48), (49), (73), (74), (77), (78), and requisite derivatives of (33) and (37). Exponentiations are shorthand for* $\times 10^{[2,3]}$

$P \setminus T$	375	400	425	450	475
250	0.59070^2	0.57137^2	0.29256^2	0.21716^2	0.18149^2
300	0.37753^2	0.11093^3	0.47332^2	0.28657^2	0.21969^2
350	0.31793^2	0.50255^2	0.68540^2	0.38676^2	0.26919^2
400	0.28752^2	0.37532^2	0.54966^2	0.47699^2	0.32626^2
450	0.26839^2	0.32220^2	0.42025^2	0.47120^2	0.37278^2

result, accurate representation of the H_2O dielectric constant at elevated temperatures and pressures is of fundamental importance to predictive solution chemistry.

Numerous expressions representing $\epsilon(T, \rho)$ have been proposed during the past half-century (Kirkwood, 1939; Oster and Kirkwood, 1943; Franck, 1956; Quist and Marshall, 1965; Helgeson and Kirkham, 1974a; Bradley and Pitzer, 1979; Silvester and Pitzer, 1977; Uematsu and Franck, 1980; Pitzer, 1983; McKenzie and Helgeson, 1984); unfortunately, none of these satisfies both essential requirements of high-temperature geochemical calculations: (1) representation of experimental $\epsilon(T, P)$ values (Oshry, ms; Owen and others, 1961; Heger, ms; Heger, Uematsu, and Franck, 1980) to within measurement uncertainty over their aggregate temperature-pressure range (0–550°C, 1–5000 *bars*), and (2) theoretically sound, predictive extrapolation to conditions beyond these present-day experimental limits. Each of the proposed equations do, however, accurately represent a unique subset of the experimental database. The empirical Helgeson-Kirkham (1974a) and Uematsu-Franck (1980) expressions are of greatest use in this regard, providing close approximation of these data over virtually their entire temperature-pressure range. Similarly, certain of the proposed equations are of functional form that permits useful extrapolation to higher temperatures. Outstanding examples in this category are the Pitzer (1983) equation, which provides theoretically-sound, elevated-temperature predictions (as well as close approximation of experimental values at $T > 325°C$), and again the Uematsu-Franck (1980) equation, which permits smooth, albeit theoretically-unconstrained, extrapolation to both high temperatures and pressures.

In the present study, predictions from the purely empirical fit given by Helgeson and Kirkham (1974a) for low-intermediate temperatures and the semi-empirical expression proposed by Pitzer (1983) for intermediate-high temperatures have been merged into a single representative equation. Specifically, we adopt the function proposed by Uematsu and Franck (1980) but refine its adjustable coefficients to obtain accurate representation of the Helgeson-Kirkham (1974a) and Pitzer (1983) formulations within their respective regions of applicability. The Helgeson-Kirkham (1974a), Pitzer (1983), and modified Uematsu-Franck (1980) expressions are described below.

The Helgeson-Kirkham (1974a) equation.—The Helgeson-Kirkham (1974a) equation represents $\epsilon(T, \rho(T, P))$ as an empirical fourth-order power function:

$$\epsilon = \sum_{i=0}^{4} \sum_{j=0}^{4-i} e_{i,j}\, T^i\, \rho^j, \tag{79}$$

whose adjustable coefficients, $e_{i,j}$ (table 18), were obtained from a regression fit of experimental $\epsilon(T, P)$ measurements (Oshry, ms; Owen and others, 1961; Heger, ms), converted a priori to $\epsilon(T, \rho)$ using the equation of state given by Keenan and others (1969) at $P \leq 1000$ *bars*, and that

TABLE 18

Coefficients $e_{i,j}$ ($T^{-i}\rho^{-j}$) for eq (79). Modified from Helgeson and Kirkham (1974a, table 14)

i	j	$e_{i,j}$	i	j	$e_{i,j}$
0	0	$4.39109592(10^{2})$	1	3	$-6.13941874(10^{-2})$
0	1	$-2.18995148(10^{2})$	2	0	$4.61662109(10^{-3})$
0	2	$1.82898246(10^{1})$	2	1	$-1.35650709(10^{-3})$
0	3	$1.54886800(10^{2})$	2	2	$1.60491325(10^{-4})$
0	4	$-6.13542375(10^{1})$	3	0	$-4.03643333(10^{-6})$
1	0	$-2.33277456(10^{0})$	3	1	$5.94046919(10^{-7})$
1	1	$1.00498361(10^{0})$	4	0	$1.31604037(10^{-9})$
1	2	$-2.08896146(10^{-1})$			

proposed by Helgeson and Kirkham (1974a) for $1000 \leq P \leq 5000$ *bars*. Eq (79) reproduces these experimental data from 100° to 500°*C* and 250 to 5000 *bars* within 1 percent except for vapor-saturated liquid near the critical point (here, within 5 percent), a precision that agrees favorably with the reported experimental tolerances (Helgeson and Kirkham, 1974a). It can be argued that none of the aforementioned equations provides superior representation of experimental data over this range of state conditions, acknowledging that the Uematsu-Franck (1980) expression yields similarly close approximation.

Because of its accurate representation of measured values, the Helgeson-Kirkham (1974a) equation has been used in an integrated series of recent publications that present an equation of state for aqueous ions and electrolytes (Helgeson, Kirkham, and Flowers, 1981; Tanger and Helgeson, 1988; Shock and others, 1991), correlation algorithms for predicting equation-of-state parameters from experimental data (Shock and Helgeson, 1988), and specific parameter values for a large number of aqueous ions and 1:1/1:2 electrolytes (Tanger and Helgeson, 1988), inorganic neutral aqueous species (Shock, Helgeson, and Sverjensky, 1989), organic species (Shock and Helgeson, 1990), and inorganic metal complexes (Sverjensky, Shock, and Helgeson, ms). Equations that relate these parameters to experimental standard partial molal volume, heat capacity, and Gibbs free energy data are sensitive functions of H_2O dielectric properties. Hence, in developing a more versatile dielectric expression, it is highly desirable to retain predictions consistent with eq (79) over the temperature-pressure range of its applicability.

In general, however, polynomial representations such as the Helgeson-Kirkham (1974a) expression cannot be reliably extrapolated beyond the state-condition range of experimental $\epsilon(T, P)$ measurements used to obtain their adjustable coefficients. In the particular, yet typical, case of eq (79), extrapolation to higher temperatures (especially above 600°*C*) produces highly unrealistic results (Helgeson and Kirkham, 1974a).

Even in situations where extrapolation of such an equation yields satisfactory functional behavior, as does the Uematsu-Franck (1980) expression (see below), it is of obvious advantage to refine details of this behavior in the context of theoretical considerations. At $T > 550°C$, for example, predictions of $\epsilon(T, P)$ that closely mimic those of the Uematsu-Franck (1980) equation can also be obtained from the Pitzer (1983) formulation, which is consistent with well-established polarization-field theory.

The Pitzer (1983) equation.—The $\epsilon(T, \rho)$ expression proposed by Pitzer (1983) represents one of several attempts (others include Franck, 1956; Quist and Marshall, 1965; Helgeson and Kirkham, 1974a; Heger, Uematsu, and Franck, 1980) to reconcile empirically the theoretically-attractive Kirkwood equation (Kirkwood, 1939; Oster and Kirkwood, 1943) with experimental data. Derived from Onsager's (1936) theoretical analysis of local polarization fields in liquids, the Kirkwood equation can be expressed as

$$\frac{(\epsilon - 1)(2\epsilon + 1)}{9\epsilon} = \frac{4\pi N_A}{3V_m}\left(\alpha_k + \frac{u^2 g_K}{3k_B T}\right), \tag{80}$$

where the right-hand side of eq (80) represents the V_m-normalized local polarization field, N_A refers to Avogadro's number ($6.02252(10^{23})$ mol^{-1}), k_B stands for Boltzmanns constant ($1.38054(10^{-16})$ $erg/°K$), α_k denotes molecular polarizability ($1.444(10^{-23})$ cm^3/mol), u signifies the molecular dipole moment ($1.84(10^{-18})$ esu), and g_K, the Kirkwood coefficient, accounts for molecular orientation. In practice, (for example, Franck, 1956; Quist and Marshall, 1965; Heger, Uematsu, and Franck, 1980; Pitzer, 1983), g_K must be determined empirically. From a computational standpoint, it is convenient to rearrange eq (80) to read

$$\epsilon = \frac{\Phi + \sqrt{\Phi^2 + 8}}{4},$$

where

$$\Phi = 1 + C_{K,1}\,\rho + C_{K,2}\,g^*,$$

$$g^* = \frac{\rho\, g_K}{T},$$

$$C_{K,1} = \frac{12\pi N_A \alpha_k}{M},$$

and

$$C_{K,2} = \frac{4\pi N_A u^2}{k_B M}. \tag{81}$$

Pitzer (1983) used eq (80) together with dielectric constants measured at intermediate-high temperatures ($350 \leq T \leq 550°C$) by Heger (ms) and Heger, Uematsu, and Franck (1980) and predicted at high

densities ($0.6 \leq \rho \leq 1.0\ g/cm^3$) by Uematsu and Franck (1980) to obtain a series of $g_K(T, \rho)$ values he found could be accurately represented with an empirical T–ρ polynomial of minimal T-dependence:

$$g_K = 1 + 2.68\rho + 6.69\rho^5\left(\left(\frac{565}{T}\right)^{0.3} - 1\right). \tag{82}$$

Eqs (81) and (82) reproduce the Heger (ms) and Heger, Uematsu, and Franck (1980) measurements to 1000 *bars* with an average residual of 2.2 percent (Pitzer, 1983), a tolerance commensurate with experimental uncertainty limits. Moreover, the functional dependencies of eq (81) on g_K and of eq (82) on T led Pitzer (1983) to estimate that this formulation will be correct to within 5 percent for $T < 823°C$ and $\rho \leq 0.7\ g/cm^3$ and to within 15 percent for "very high" temperature and $\rho \leq 0.5\ g/cm^3$.

Although Pitzer's (1983) fit of the Kirkwood equation provides theoretically-sound estimates of the dielectric constant from 550° to at least 1000°C and yields close representation of the high-temperature experimental data, it does not provide sufficiently close approximation of lower temperature ($< 350°C$) measurements to be quantitatively useful in this range. Hence, the present goal is to develop a single continuous equation that represents predictions from the Helgeson-Kirkham (1974a) and Uematsu-Franck (1980) expressions at low temperatures and those given by Pitzer's (1983) formulation at high temperatures.

The modified Uematsu-Franck (1980) equation.—The Uematsu-Franck (1980) equation, like the earlier Helgeson-Kirkham (1974a) formulation, represents the dielectric constant as a fourth-order power function in temperature and density:

$$\epsilon = \sum_{i=0}^{4} k_i(\hat{T})\hat{\rho}^i, \tag{83}$$

where $\hat{T} = T/(298.15°K)$, $\hat{\rho} = \rho/(1\ g/cm^3)$, and the $k_i(\hat{T})$ are given by

$$k_0(\hat{T}) = 1,$$
$$k_1(\hat{T}) = e_1\hat{T}^{-1},$$
$$k_2(\hat{T}) = e_2\hat{T}^{-1} + e_3 + e_4\hat{T},$$
$$k_3(\hat{T}) = e_5\hat{T}^{-1} + e_6\hat{T} + e_7\hat{T}^2,$$

and

$$k_4(\hat{T}) = e_8\hat{T}^{-2} + e_9\hat{T}^{-1} + e_{10}. \tag{84}$$

Coefficients $e_{1\ldots10}$ (column 1, table 19) were obtained from a global least-squares fit of 892 accuracy-weighted $\epsilon(T, P)$ measurements to 550°C and 5000 *bars* (sources listed in table 2, Uematsu and Franck, 1980), which were converted to $\epsilon(T, \rho)$ using equations of state given by Vukalovich and others (1967) for $P \leq 1000$ *bars* and Juza (1968) for $P > 1000$

TABLE 19

Original (Uematsu and Franck, 1980, table 3) and revised (this study, see text) coefficients e_i for eqs (83) and (84)

i	e_i (original)	e_i (revised)
1	$0.762571(10^1)$	$0.1470333593(10^2)$
2	$0.244003(10^3)$	$0.2128462733(10^3)$
3	$-0.140569(10^3)$	$-0.1154445173(10^3)$
4	$0.277841(10^2)$	$0.1955210915(10^2)$
5	$-0.962805(10^2)$	$-0.8330347980(10^2)$
6	$0.277841(10^2)$	$0.3213240048(10^2)$
7	$-0.102099(10^2)$	$-0.6694098645(10^1)$
8	$-0.452059(10^2)$	$-0.3786202045(10^2)$
9	$0.846395(10^2)$	$0.6887359646(10^2)$
10	$-0.358644(10^2)$	$-0.2729401652(10^2)$

bars. Eqs (83) and (84) represent these control data to within 0.5 percent for $T \leq 100°C$; 1.0 percent for $100° < T \leq 250°C$; 2.5 percent for $250 < T \leq 550°C$ where $\rho \geq 0.3\ g/cm^3$; and 5 percent for $0.12 \leq \rho \leq 0.3\ g/cm^3$ where $\epsilon < 5$ (Uematsu and Franck, 1980). These uncertainties compare favorably with corresponding experimental tolerances (Oshry, ms; Owen and others, 1961; Heger, ms; Heger, Uematsu, and Franck, 1980).

In addition, the behavior of eqs (83) and (84) closely mimics that of the Helgeson-Kirkham (1974a) expression over this range of state conditions; particularly so for $\rho > 0.4$ where the two equations provide equally close representation of experimental measurements (Uematsu and Franck, 1980). Moreover, extrapolation of eqs (83) and (84) to higher temperatures also mimics the behavior of Pitzer's (1983) expression. This functional bridging of predictions from the Helgeson-Kirkham (1974a) and Pitzer (1983) equations by the Uematsu-Franck (1980) expression is illustrated in figure 21, which demonstrates that the three equations yield nearly identical behavior within the intermediate temperature range 350°to 550°C over a wide range of pressure. Because the functional form of eqs (83) and (84) smoothly meshes that of eq (79) and eqs (81) and (82) at low and high temperatures, respectively, predictions of the former expression can be brought into very close agreement with those of the latter two by appropriate refinement of coefficients. $e_{1...10}$.

This refinement can be achieved using the following four-step procedure: (1) define a practical transition boundary between the validity regions of eq (79) and eqs (81) and (82); (2) generate a set of T–ρ coordinates (spanning both validity regions) over which $\epsilon(T, \rho)$ are to be evaluated; (3) calculate these $\epsilon(T, \rho)$ using eq (79) and eqs (81) and (82)

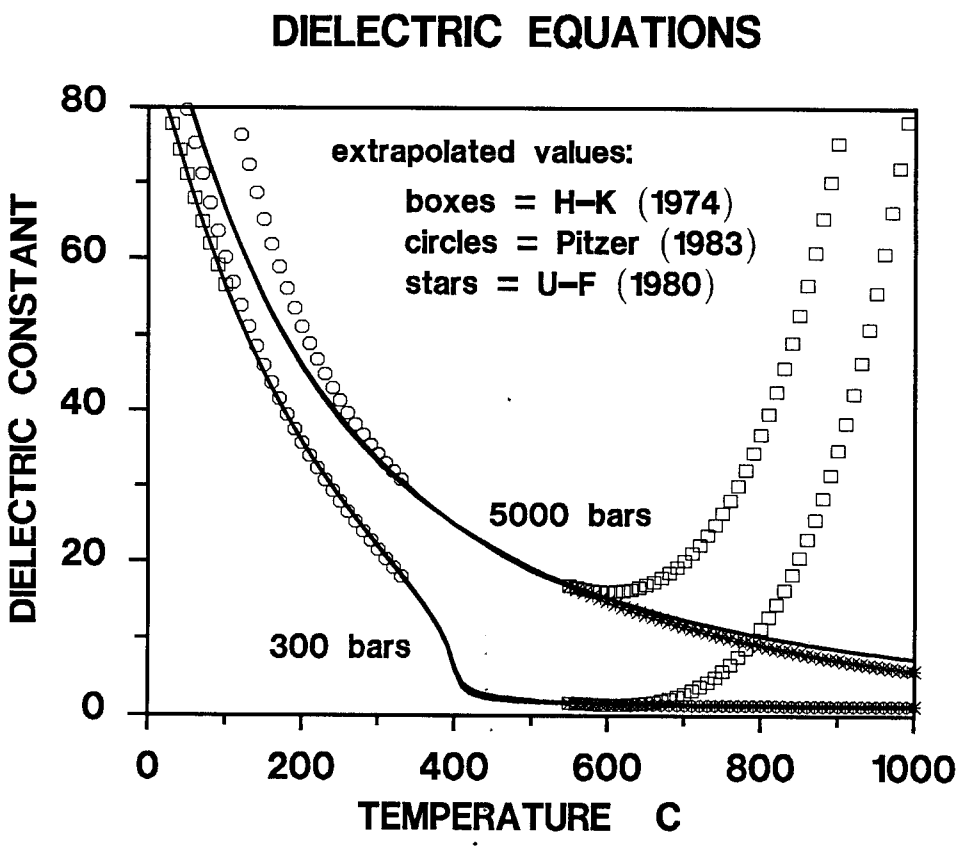

Fig. 21. The dielectric constant (*dimensionless*) as a function of temperature (0°–1000°*C*) at constant pressure (300 and 5000 *bars*), computed from eqs (48) and (49), (79), and (81) through (84) together with adjustable coefficients given in table 18 and column one of table 19. Extrapolated values refer to calculations beyond the recognized temperature limits of eqs (79) (Helgeson and Kirkham, 1974a), (81) and (82) (Pitzer, 1983), and (83) and (84) (Uematsu and Franck, 1980). Note close correspondence between predictions from the Helgeson-Kirkham (1974a) and Uematsu-Franck (1980) expressions for $T \leq 550°C$; those of Uematsu-Franck (1980) and Pitzer (1983) for $T \geq 325°C$; and among all three equations at $325° \leq T \leq 550°C$.

together with supporting equations-of-state (33) and (37); and (4) perform a nonlinear least-squares regression of these data with eq (83), thereby obtaining new $e_{1...10}$ values. In practice, steps (2) to (4) must be iterated until a satisfactory fit is realized.

The transition boundary is defined as the T–ρ projection along which dielectric constants computed using eq (79) and eqs (81) and (82) are equivalent. Control points along this projection were calculated using a modified golden section search algorithm (Miller, 1984; Gill, Murray, and Wright, 1981), then fit by a standard, two-dimensional cubic spline

interpolator (deBoor, 1978). Given this switch function and a reliable software implementation (James, ms) of the requisite nonlinear least-squares algorithm (Draper and Smith, 1981), success of this approach is largely dependent upon design of the dataset.

Of particular importance are dimensions, granularity, and weighting factors characterizing the $\epsilon(T, \rho)$ grid. In lieu of more direct means, a series of Monte Carlo experiments were performed in which these parameters (alone and in combination) were systematically varied in order to generate an optimal model grid. The best results were obtained for a dataset composed of 493 $\epsilon(T, \rho)$ values calculated (1) across an orthogonal T–ρ grid having uniform 25°*C* and 0.05 g/cm^3 increments, but truncated by the liquid-vapor dome, fusion boundaries, 1000°*C* isotherm, 5000 *bar* isobar, and 0.05 and 1.10 g/cm^3 isochores; (2) along both branches of the liquid-vapor dome itself, from the triple point to 370°*C* at 10°*C* increments (also including 25°*C*) — but again truncated by the 0.05 g/cm^3 isochore, and (3) at 25°*C*, 0.99706 g/cm^3 (1 *bar*). The T–ρ domain that defines this dataset is illustrated in figure 22.

Nonlinear least-squares regression of these data with eqs (83) and (84), using as initial coefficient estimates those given in column one of table 19, reproduced the control values with an average residual of 0.12. Revised coefficients generated by the least-squares algorithm are given in column two of table 19. Even after account of uncertainties associated with this fit-to-fit approach, the predicted values still fall within experimental uncertainties (Heger, ms; Heger, Uematsu, and Franck, 1980). This close representation reflects the minimal residuals associated with regression of data that implicitly define a smooth function (in this case, two separate functions) with another similar function. In summary, eqs (83) and (84), when used with the $e_{1...10}$ values given in column two of table 19 and equations-of-state (33) and (37), provide close representation of experimental dielectric measurements, their approximation using the Helgeson-Kirkham (1974a) expression at low-intermediate temperatures, and both their approximation and extrapolative prediction using Pitzer's (1983) modified Kirkwood equation at intermediate-high temperatures.

Equation-of-state considerations.—In principal, it is important to emphasize that representation of experimental $\epsilon_1(T_1, P_1)$ data as $\epsilon_1(T_1, \rho_1(T_1, P_1))$ in fit equations such as eqs (79) and (81) through (84) necessitates employment of an equation of state, $\rho_1(T_1, P_1)$ prior to regression analysis of the adjustable coefficients. Thus, strictly speaking, the proposed dielectric equation will accurately reproduce these data only if supported by the same equation of state. If a different state function, $\rho_2(T_1, P_1)$, is used and T and P are independent, $\epsilon_2(T_1, \rho_2(T_1, P_1)) \neq \epsilon_1(T_1, \rho_1(T_1, P_1))$; if T and ρ are independent, then $P_2(T_1, \rho_2(T_1, P_1)) \neq P_1(T_1, \rho_1)$.

In practice, however, such calculational discrepancies are rarely of quantitative concern. Consider, as a typical example, use of the Helgeson-Kirkham (1974a) formulation in the context of several different supporting equations of state, where the independent variables are T and P.

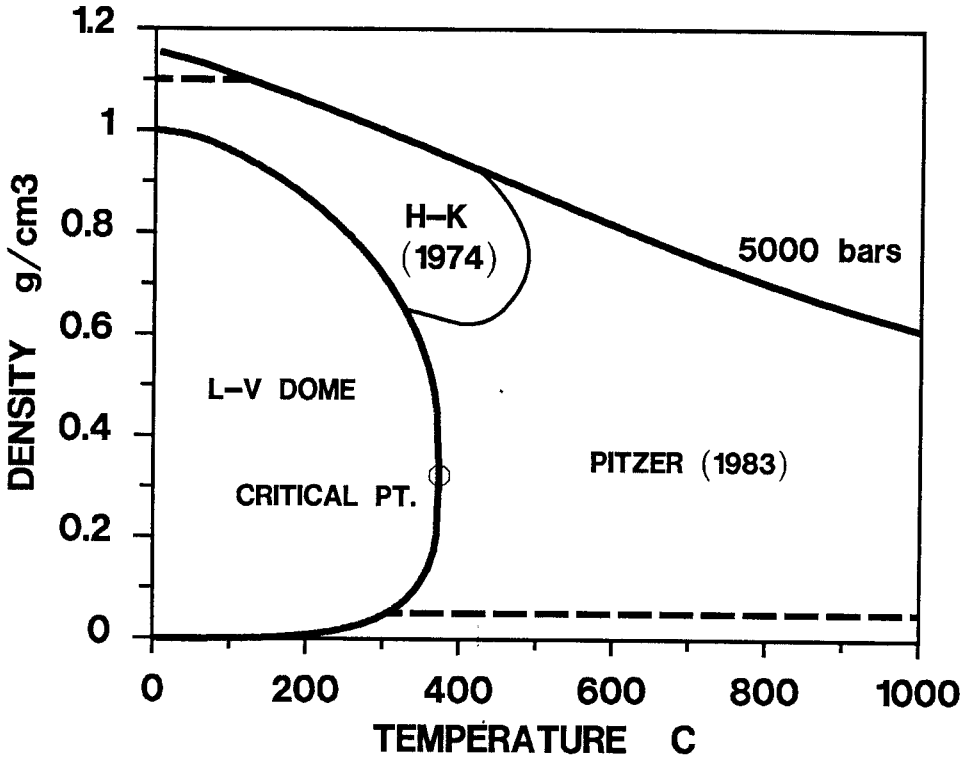

Fig. 22. The $T-\rho$ domain of dielectric-constant data used to revise the adjustable coefficients of eqs (83) and (84) (table 19); see text. Values were computed using eqs (48) and (49), (79), and (81) and (82) and restricted to the region delineated by the liquid-vapor dome, fusion boundaries, 1000°C isotherm, 5000 *bar* isobar, and 0.05 and 1.10 g/cm^3 isochores. Subdomains where data were calculated using the Helgeson-Kirkham (1974a) and Pitzer (1983) equations are separated by the unique $T-\rho$ projection that defines equality of the two equations.

Recall that for $P \leq 1000$ *bars*, adjustable coefficients for the Helgeson-Kirkham (1974a) expression were calculated with reference to the equation of state given by Keenan and others (1969). At 400°C, 300 *bars*, this latter formulation returns a density of 0.35846 g/cm^3 and the dependent Helgeson-Kirkham (1974a) expression, a value of 6.2006 for the dielectric constant. Analogous calculations, supported instead by the HGK and LS equations of state, return 0.35805 g/cm^3, 6.1924 and 0.35838 g/cm^3, 6.1991, respectively. Hence, evaluation of a given dielectric equation, even in the critical region, is relatively insensitive to the supporting equation of state, *provided this state function is sufficiently similar to the dielectric expression's implicit equation of state,* that proposed by Keenan and others (1969) in this case. Moreover, note that all three values are in good agreement with their experimental counterpart: 6.0 ± 0.35 (Heger,

Uematsu, and Franck, 1980). In the near-critical region, where experimental data are as yet unavilable, this relative insensitivity of dielectric predictions to supporting state function still holds. At 375°*C*, 223.5 *bars*, for instance, the Helgeson-Kirkham (1974a) equation predicts dielectric constant values of 6.27, 6.32, and 6.18 in the context of the equation of state given by Keenan and others (1969), the HGK equation, and the LS equation, respectively.

Because of their functional dependence on isothermal compressibility and isobaric expansivity, first-order partial derivatives of the dielectric constant with respect to pressure and temperature are more sensitive to the supporting equation of state than the dielectric constant itself. Continuing the previous examples, corresponding values of $(\partial\epsilon/\partial P)_T$, for instance, at 400°*C*, 300 *bars* are $0.893(10^{-1})$, $0.877(10^{-1})$, and $0.900(10^{-1})$ bar^{-1}; however, at 375°*C*, 223.5 *bars*, the analogous values are 1.87, 2.48, and 3.23 bar^{-1}. Hence, dependency of $(\partial\epsilon/\partial P)_T$ on the supporting state function is insignificant outside the near-critical region but potentially significant very near the critical point. Similar relationships hold for $(\partial\epsilon/\partial T)_P$, but higher-order derivatives will display increased sensitivity to the supporting equation of state. However, keep in mind that dielectric equations such as the Helgeson-Kirkham (1974a), Uematsu-Franck (1980), and Pitzer (1983) formulations represent fits to the dielectric constant itself, not its partial derivatives. Hence, so long as these fit equations represent the data to within experimental tolerance, and similar correspondence is maintained between their analytic derivatives and the associated, experimental finite difference derivatives, use of these equations with various, sufficiently-similar equations of state is, from a pragmatic viewpoint, acceptable.

The preceding discussion supports the following conclusion with regard to development of our modified Uematsu-Franck equation: given (1) accurate representation of experimental dielectric measurements by the Helgeson-Krikham (1974a) and Pitzer (1983) expressions and their implicit equations of state, (2) close correlation between these state functions and the HGK and LS equations of state, and (3) accurate representation of dielectric predictions from the Helgeson-Kirkham (1974a) and Pitzer (1983) expressions by our modified Uematsu-Franck (1980) equation, this revised formulation can be employed with confidence until improved alternatives become available.

Functional behavior of the dielectric constant and Born functions within and near the critical region is described below in the context of eqs (83) and (84), implemented using the revised adjustable coefficients given in table 19.

Dielectric constant.—Eqs (48), (49), (83), (84), requisite derivatives of (33) and (37), and the revised coefficients of table 19 were used to compute the $\epsilon(P, T)$ surface, $\epsilon(T)$-isobars, and $\epsilon(P)$-isotherms illustrated in figure 23, and the $\epsilon(P, T)$ values listed in table 20.

The dielectric constant increases with pressure at constant temperature and decreases with temperature at constant pressure. Although

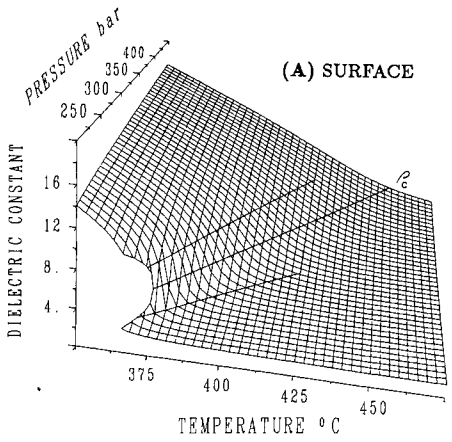

Figure 23: Dielectric constant (*dimensionless*) as a function of (**A**) temperature (°*C*) and pressure (*bar*), (**B**) temperature at constant pressure, and (**C**) pressure at constant temperature; computed from eqs (48), (49), (83), (84), requisite derivatives of (33) and (37), and coefficients given in column two of table 19.

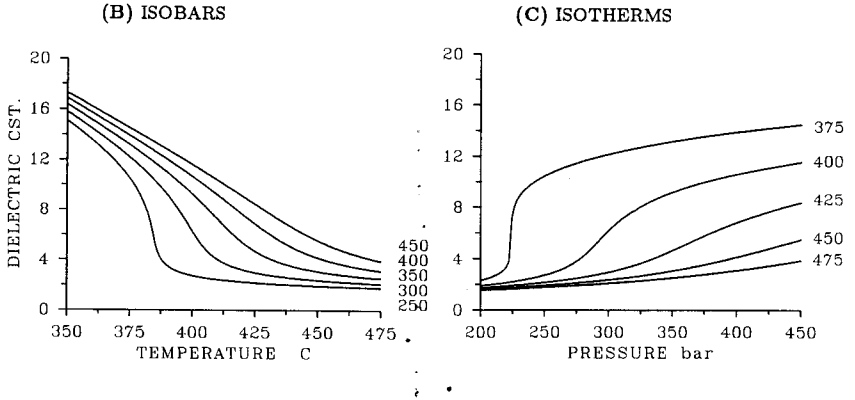

TABLE 20

Dielectric constant (dimensionless) *as a function of pressure* (bars) *and temperature* (°C)*; computed from eqs (48), (49), (83), (84), requisite derivatives of (33) and (37), and the revised coefficients of table 19. Exponentiations are shorthand for* $\times 10^{[1,2]}$

$P \setminus T$	375	400	425	450	475
250	0.10541^{2}	0.27268^{1}	0.21427^{1}	0.19009^{1}	0.17551^{1}
300	0.12188^{2}	0.62851^{1}	0.29543^{1}	0.23460^{1}	0.20648^{1}
350	0.13155^{2}	0.92227^{1}	0.46821^{1}	0.30502^{1}	0.24906^{1}
400	0.13877^{2}	0.10612^{2}	0.68494^{1}	0.41456^{1}	0.30809^{1}
450	0.14465^{2}	0.11545^{2}	0.83912^{1}	0.55045^{1}	0.38635^{1}

$\epsilon(P)_T$ and $\epsilon(T)_P$ are monotonic, their partial derivatives display local maxima in the critical region. These maxima increase exponentially through the near-critical region and at the critical point $(\partial\epsilon/\partial P)_T = -(\partial\epsilon/\partial T)_P = \infty$. Consequently, the $\epsilon(P, T)$ surface, $\epsilon(T)$-isobars, and $\epsilon(P)$-isotherms all display a sharp sigmoid form in the near-critical region that dampens with temperature and pressure (fig. 23). The functional form of the dielectric constant is thus very similar to that of density (compare figs. 9 and 23); however, $\epsilon(P, T)$ exceeds $\rho(P, T)$ (g/cm^3) by an order of magnitude.

Born functions.—The Z Born function is defined (Helgeson, Kirkham, and Flowers, 1981) as

$$Z = -\frac{1}{\epsilon}. \tag{85}$$

Eqs (48), (49), (79), (83) through (85), requisite derivatives of (33) and (37), and the revised coefficients of table 19 were used to compute the $Z(P, T)$ surface, $Z(T)$-isobars, and $Z(P)$-isotherms illustrated in figure 24, and the $Z(P, T)$ values listed in table 21.

The Z Born function, like ϵ, has a functional form that corresponds closely to that of density. In addition, $Z(P, T)$ and $\rho(P, T)$ (g/cm^3), unlike $\epsilon(P, T)$ and $\rho(P, T)$ (g/cm^3), are of nearly equivalent magnitude, albeit opposite sign (compare figs. 9 and 24). Other than this sign conflict, Z and ρ differ only in the magnitude of their partial derivatives outside the critical region. Specifically, isothermal pressure and isobaric temperature derivatives of Z exceed those of ρ for low-density supercritical vapor and are smaller than those of ρ for high-density supercritical liquid. *In the critical region, however,* $(\partial Z/\partial P)_T \approx (\partial\rho/\partial P)_T$ *and* $(\partial Z/\partial T)_P \approx (\partial\rho/\partial T)_P$ (compare figs. 9B and 24B and figs. 9C and 24C).

The isothermal pressure derivative of Z defines the Q Born function (Helgeson and Kirkham, 1974a):

$$Q \equiv \left(\frac{\partial Z}{\partial P}\right)_T \equiv \frac{1}{\epsilon^2}\left(\frac{\partial\epsilon}{\partial P}\right)_T, \tag{86}$$

where in the context of eq (83)

$$\left(\frac{\partial\epsilon}{\partial P}\right)_T = \beta \sum_{i=0}^{4} i\, k_i(\hat{T})\, \hat{\rho}^i. \tag{87}$$

Eqs (48), (49), (51), (52), (83), (84), (86), (87), requisite derivatives of (33) and (37), and the revised coefficients of table 19 were used to compute the $Q(P, T)$ surface, $Q(T)$-isobars, and $Q(P)$-isotherms illustrated in figure 25, and the $Q(P, T)$ values listed in table 22.

The Q Born function diverges from background values of $\approx 10^{-3}$ bar^{-1} outside the critical region to ∞ at the critical point. Owing to its functional dependence on β, the near-critical divergent character of Q is strong and sharpest with critical-point approach along the vaporization

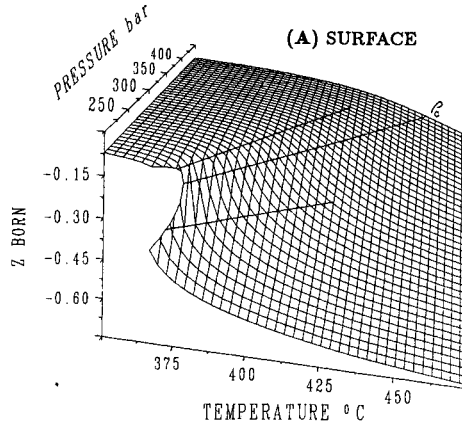

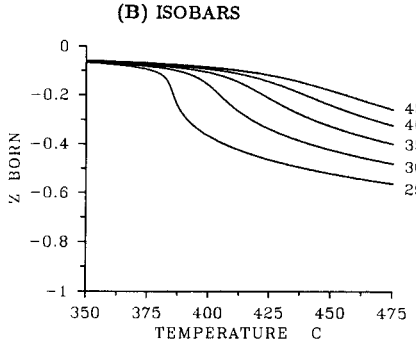

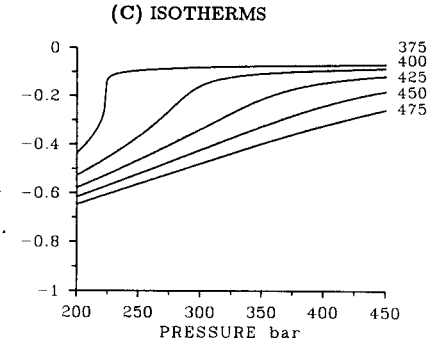

Figure 24: *Z* Born function (*dimensionless*) as a function of (**A**) temperature (°*C*) and pressure (*bar*), (**B**) temperature at constant pressure, and (**C**) pressure at constant temperature; computed from eqs (48), (49), (83) through (85), requisite derivatives of (33) and (37), and coefficients given in column two of table 19.

TABLE 21

The Z Born function (dimensionless) *as a function of pressure* (bars) *and temperature* (°C)*; computed from eqs (48), (49), (83) through (85), requisite derivatives of (33) and (37), and the revised coefficients of table 19. Exponentiations are shorthand for* $\times 10^{[-1,0]}$

$P \setminus T$	375	400	425	450	475
250	-0.94870^{-1}	-0.36673^{0}	-0.46670^{0}	-0.52607^{0}	-0.56976^{0}
300	-0.82050^{-1}	-0.15911^{0}	-0.33849^{0}	-0.42626^{0}	-0.48432^{0}
350	-0.76015^{-1}	-0.10843^{0}	-0.21358^{0}	-0.32785^{0}	-0.40151^{0}
400	-0.72062^{-1}	-0.94230^{-1}	-0.14600^{0}	-0.24122^{0}	-0.32458^{0}
450	-0.69132^{-1}	-0.86617^{-1}	-0.11917^{0}	-0.18167^{0}	-0.25883^{0}

Figure 25: Q Born function (bar^{-1}) as a function of **(A)** temperature ($^{\circ}C$) and pressure (bar), **(B)** temperature at constant pressure, and **(C)** pressure at constant temperature; computed from eqs (48), (49), (51), (52), (83), (84), (86), (87), requisite derivatives of (33) and (37), and coefficients given in column two of table 19. Note that in the critical region of **(A)**, all $Q > 2(10^{-2})$ bar^{-1} have been set to this arbitrary upper limit for illustrative purposes; this truncation compromises ≈ 1.2 percent of the $Q(P,T)$ surface.

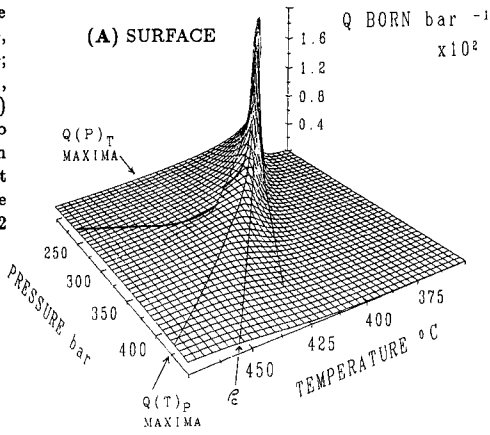

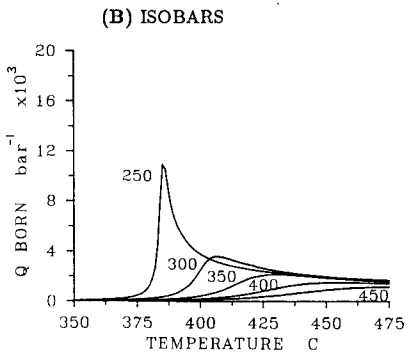

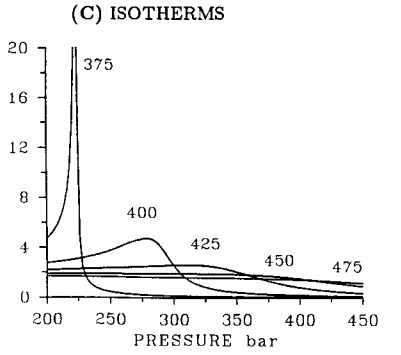

TABLE 22

The Q Born function (bar^{-1}) *as a function of pressure* (bars) *and temperature* ($^{\circ}$C)*; computed from eqs (48), (49), (51), (52), (83), (84), (86), (87), requisite derivatives of (33) and (37), and the revised coefficients of table 19. Exponentiations are shorthand for* $\times 10^{[-4,-3,-2]}$

$P \backslash T$	375	400	425	450	475
250	0.45508^{-3}	0.38536^{-2}	0.24521^{-2}	0.19851^{-2}	0.17222^{-2}
300	0.15763^{-3}	0.24803^{-2}	0.26610^{-2}	0.19996^{-2}	0.16900^{-2}
350	0.94292^{-4}	0.42644^{-3}	0.20476^{-2}	0.19041^{-2}	0.16119^{-2}
400	0.66862^{-4}	0.19452^{-3}	0.79885^{-3}	0.14967^{-2}	0.14468^{-2}
450	0.51595^{-4}	0.12066^{-3}	0.35883^{-3}	0.89658^{-3}	0.11651^{-2}.

boundary or confluent critical isochore. As a result, the locus of maxima in $Q(T)$-isobars and $Q(P)$-isotherms (fig. 25B and C) are coincident with ρ_c in the near-critical region. With increasing pressure and temperature, however, these two maxima depart unequally in the P–T plane from the critical isochore toward subcritical densities. The $Q(P, T)$ surface is therefore folded upward along a P–T crease that is sharpest at its critical point origin, then flattens as it migrates toward subcritical densities in the critical region; the surface is relatively flat in the global region (fig. 25A).

Because $Q(T)_P$ and $Q(P)_T$ maxima depart unequally from the critical isochore in the supercritical P–T plane, the $Q(P, T)$ surface is subdivided into three regions of specific partial derivative variation: (1) a region confined between the two maxima where Q decreases with both pressure and temperature, (2) a region to the low-density side of the $Q(P)_T$ maxima where Q increases with pressure and decreases with temperature, and (3) a region to the high-density side of the $Q(T)_P$ maxima where Q decreases with pressure and increases with temperature.

The unsmoothed, readily apparent discontinuity imposed upon the $Q(P)_T$ maxima projection by equation-of-state crossover is unique among Born functions considered in this study. Its atypically large magnitude reflects the presence of a highly equation-of-state-sensitive, second-order extremum (specifically, $(\partial^2 Q/(\partial P \partial T))_{T,P} = 0$), also characteristic of β (fig. 10A), that in this case (unlike β) occurs in the immediate vicinity of the critical-region boundary (fig. 25A). Note that discontinuities in the $Q(P, T)$ surface itself are similar in magnitude to those of other properties dependent on second-order differentiation of eqs (33) and (37); that is, relatively insignificant, as evidenced by inspection of figure 25.

As implied above, the functional form of $Q(P, T)$ is controlled by that of $\beta(P, T)$ (compare figs. 10 and 25). For example, note close correspondence between their isobaric temperature and isothermal pressure maxima. As a result of this correspondence, Q values of supercritical vapor typically exceed those of supercritical liquid, as is also the case for β values. However, because projections of Q maxima occur to the low-density side of their β counterparts, this difference in supercritical vapor and liquid values is even larger in Q than in β.

The control of $\beta(P, T)$ on $Q(P, T)$ is most striking in the critical region where $(\partial Z/\partial P)_T\ bar^{-1} \approx (\partial \rho/\partial P)_T\ g\ cm^{-3}\ bar^{-1}$ and $\rho^{-1} \approx 2.4 - 5.0\ cm^3/g$. As a result of this correlation between Z and ρ derivatives, the discrepancy in magnitude between Q and β is almost entirely accountable to normalization of $(\partial \rho/\partial P)_T$ by ρ to obtain β, eq (50). Consequently, *to a first approximation in the critical region,* $Q \approx \hat{\rho}\beta$, where $\hat{\rho}$ represents dimensionless density (normalized by $1\ g/cm^3$).

The isobaric temperature derivative of Z defines the Y Born function (Helgeson and Kirkham, 1974a):

$$Y \equiv \left(\frac{\partial Z}{\partial T}\right)_P \equiv \frac{1}{\epsilon^2}\left(\frac{\partial \epsilon}{\partial T}\right)_P, \tag{88}$$

where from differentiation of eq (83)

$$\left(\frac{\partial \epsilon}{\partial T}\right)_P = \sum_{i=0}^{4} \hat{\rho}^i \left\{\left(\frac{\partial k_i(\hat{T})}{\partial T}\right)_P - i\,\alpha\, k_i(\hat{T})\right\}. \tag{89}$$

Eqs (37), (48), (49), (54), (55), (83), (84), (88), (89), requisite derivatives of (33), (37), and (84), and the revised coefficients of table 19 were used to compute the $Y(P, T)$ surface, $Y(T)$-isobars, and $Y(P)$-isotherms illustrated in figure 26, and the $Y(P, T)$ values listed in table 23.

The Y Born function diverges from background values of $\approx 10^{-3}\,°K^{-1}$ outside the critical region to $-\infty$ at the critical point. Like $Q(\beta)$, the functional dependence of Y on $-\alpha$ leads to strong divergence, again sharpest with approach to criticality along the vaporization boundary or critical isochore. Hence, the locus of near-critical *minima* in $Y(T)$-isobars and $Y(P)$-isotherms (fig. 26B and C) are mutually coincident with ρ_c. With increasing temperature and pressure, however, these two projections depart unequally from ρ_c in the P–T plane toward subcritical densities. As a result, the $Y(P, T)$ surface is folded *downward* along a P–T crease that is sharpest at criticality, then flattens with migration to subcritical densities in the critical region; the surface is relatively flat in the global region (fig. 26A).

Unequal departure of $Y(T)_P$ and $Y(P)_T$ minima from the critical isochore subdivides the $Q(P, T)$ surface into three regions of specific partial derivative variation: (1) a region confined between the two minima where Y increases with both pressure and temperature, (2) a region to the low-density side of the $Y(P)_T$ minima where Y decreases with pressure and increases with temperature, and (3) a region to the high-density side of the $Y(T)_P$ minima where Y increases with pressure and decreases with temperature.

The functional form of $Y(P, T)$ is controlled by that of $-\alpha(P, T)$ as was $Q(P, T)$ by $\beta(P, T)$ (compare figs. 11 and 26). Extrema projections for Y occur to the low-density side of their α counterparts in analogy to the corresponding relationship between Q and β. However, in this case the density shift is sufficient to translate the $Y(T)_P$ minima from the sub- to supercritical density side of the critical isochore. As a result, Y values of supercritical fluid typically exceed those of supercritical vapor, in contrast to the $\alpha(P, T)$ surface.

Again in analogy to the $\beta(P, T)$, $Q(P, T)$ relationship, the control of $-\alpha(P, T)$ on $Y(P, T)$ is most striking in the critical region. The corresponding partial derivative approximation is given by $(\partial Z/\partial T)_P\,°K^{-1} \approx -(\partial \rho/\partial T)_P$ *g cm*$^{-3}$ $°K^{-1}$, and the difference between Y and α corresponds closely to normalization of $(\partial \rho/\partial T)_P$ by $-\rho$ to obtain α, eq (53). As a result, *to a first approximation in the critical region,* $Y \approx -\hat{\rho}\alpha$.

The isobaric temperature derivative of Y defines the X Born function (Helgeson and Kirkham, 1974a):

$$X \equiv \left(\frac{\partial Y}{\partial T}\right)_P \equiv \left(\frac{\partial^2 Z}{\partial T^2}\right)_P \equiv \frac{1}{\epsilon^2}\left(\frac{\partial^2 \epsilon}{\partial T^2}\right)_P - 2\,\epsilon\, Y^2, \tag{90}$$

Figure 26: Y Born function ($^\circ K^{-1}$) as a function of (**A**) temperature ($^\circ C$) and pressure (*bar*), (**B**) temperature at constant pressure, and (**C**) pressure at constant temperature; computed from eqs (37), (48), (49), (54), (55), (83), (84), (88), (89), requisite derivatives of (33) and (37), and coefficients given in column two of table 19. Note that in the critical region of (**A**), all $Y < -2(10^{-2})\ ^\circ K^{-1}$ have been set to this arbitrary lower limit for illustrative purposes; this truncation compromises ≈ 4.0 percent of the $Y(P,T)$ surface.

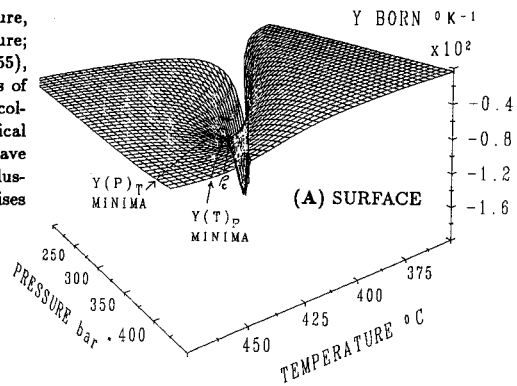

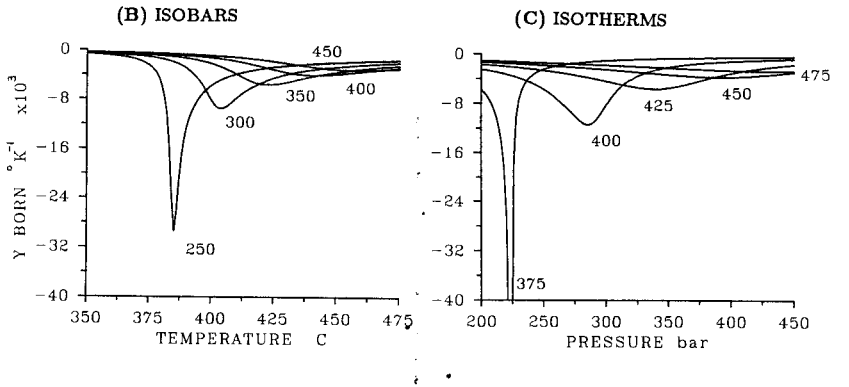

TABLE 23

The Y Born function ($^\circ K^{-1}$) *as a function of pressure* (bars) *and temperature* ($^\circ C$)*; computed from eqs (37), (48), (49), (54), (55), (83), (84), and (88), (89), requisite derivatives of (33) and (37), and the revised coefficients of table 19. Exponentiations are shorthand for* $\times 10^{[-3,-2]}$

$P \backslash T$	375	400	425	450	475
250	-0.24371^{-2}	-0.59716^{-2}	-0.28794^{-2}	-0.19919^{-2}	-0.15433^{-2}
300	-0.11214^{-2}	-0.80815^{-2}	-0.46465^{-2}	-0.27407^{-2}	-0.19908^{-2}
350	-0.79310^{-3}	-0.21818^{-2}	-0.55596^{-2}	-0.35698^{-2}	-0.24624^{-2}
400	-0.63604^{-3}	-0.12538^{-2}	-0.31555^{-2}	-0.38413^{-2}	-0.28459^{-2}
450	-0.54165^{-3}	-0.91001^{-3}	-0.18263^{-2}	-0.30530^{-2}	-0.29229^{-2}

where from differentiation of eq (83)

$$\left(\frac{\partial^2 \epsilon}{\partial T^2}\right)_P \equiv \sum_{i=0}^{4} \hat{\rho}^i \left\{\left(\frac{\partial^2 k_i(\hat{T})}{\partial T^2}\right)_P - i\left[\alpha\left(\frac{\partial k_i(\hat{T})}{\partial T}\right)_P + k_i(\hat{T})\left(\frac{\partial \alpha}{\partial T}\right)_P\right] - i\alpha\left[\left(\frac{\partial k_i(\hat{T})}{\partial T}\right)_P - i\alpha\, k_i(\hat{T})\right]\right\}. \quad (91)$$

Eqs (37), (48), (49), (54), (55), (57), (58), (83), (84), (88) through (91), requisite derivatives of (33), (37), and (84), and the revised coefficients of table 19 were used to compute the $X(P, T)$ surface, $X(T)$-isobars, and $X(P)$-isotherms illustrated in figure 27, and the $X(P, T)$ values listed in table 24.

The functional form of $X(P, T)$ is predominantly controlled by that of $-(\partial\alpha/\partial T)_P$ (compare figs. 12 and 27). As a result, $X(T)_{P>P_c}$ and $X(P)_{T>T_c}$ isopleths exhibit local negative minima *and* positive maxima, at *super-* and *sub*critical densities, respectively, that asymptotically increase in absolute magnitude and converge toward the critical isochore with approach to criticality — hence, X Born diverges to $-\infty$ when the critical point is approached from $\rho > \rho_c$ but to ∞ when the approach path is from $\rho < \rho_c$. The pressure-temperature loci of the four local extrema straddle the associated locus of $X = 0$ (which is identical to that of $Y(T)_P$ minima), itself near-coincident with ρ_c (fig. 28). Because these four extrema and the zero-point projection all converge to ρ_c at criticality, all five occur within a few degrees and bars of one another in the near-critical region. As a result, small variations in near-critical temperature or pressure may cause sign reversal and/or large fluctuations in the absolute magnitude of the X Born function.

The dependence of X Born on $(\partial\alpha/\partial T)_P$, and thus on third-order differentiation of fundamental eqs (33) and (37), leads to potentially significant discontinuities between predictions based on the HGK and LS equations of state along the critical-region boundary (figs. 27B and C). These discrepancies are similar in magnitude to those reported above for $(\partial\alpha/\partial T)_P$. In general, they amount to less than 6 and 15 percent along, respectively, the 0.42 and 0.2 isochores and vary between these limits along the 421.85°C isotherm, except in the vicinity of its intersection with the $X = 0$ projection, where on a percentage basis they are relatively large. Associated discontinuities in X Born function extrema projections (fig. 28) are also similar in magnitude to their $(\partial\alpha/\partial T)_P$ counterparts, spanning 3.5 to 4.0 bars along the 421.85°C isotherm. Taken as a whole, X Born function discontinuities along the critical-region perimeter, although large relative to their Z, Q, and Y counterparts, are not sufficiently so to be problematic in most applications. In this regard it bears repeating that, given the complexity of and theoretical differences between the HGK and LS equations of state, the magnitude of these discrepancies is remarkably small.

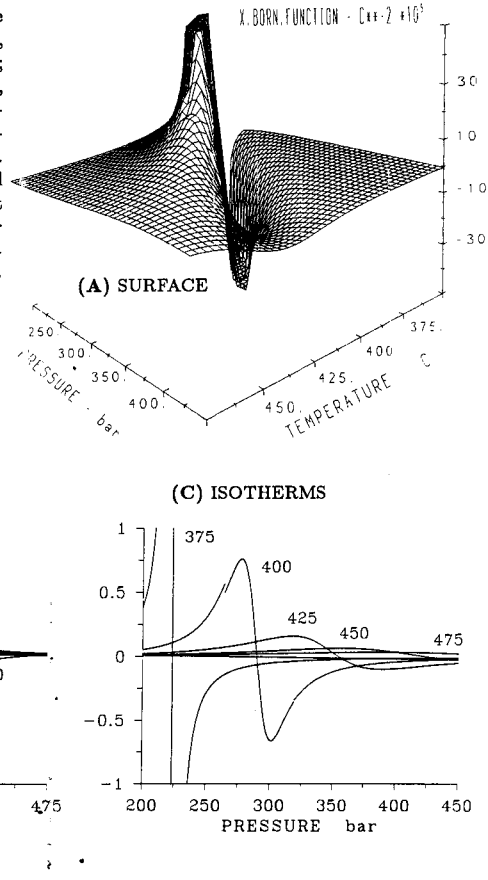

Figure 27: X Born function ($°K^{-2}$) as a function of **(A)** temperature ($°C$) and pressure (bar), **(B)** temperature at constant pressure, and **(C)** pressure at constant temperature; computed from eqs (37), (48), (49), (54), (55), (57), (58), (83), (84), (88) through (91), requisite derivatives of (33) and (37), and coefficients given in column two of table 19. Note that in the critical region of **(A)**, all $-5(10^{-4}) \geq X \geq 5(10^{-4})\ °K^{-2}$ have been set to these arbitrary lower and upper limits for illustrative purposes; these truncations compromise $\approx$ 14.0 percent of the $X(P,T)$ surface.

TABLE 24

The X Born function ($°K^{-2}$) *as a function of pressure* (bars) *and temperature* (°C)*; computed from eqs (37), (48), (49), (54), (55), (57), (58), (83), (84), (88) through (91), requisite derivatives of (33) and (37), and the revised coefficients of table 19. Exponentiations are shorthand for* $\times 10^{[-3,-2]}$

$P \backslash T$	375	400	425	450	475
250	-0.28048^{-3}	0.29417^{-3}	0.54020^{-4}	0.23621^{-4}	0.13720^{-4}
300	-0.49519^{-4}	-0.64866^{-3}	0.13608^{-3}	0.42733^{-4}	0.21217^{-4}
350	-0.22555^{-4}	-0.12071^{-3}	0.32679^{-4}	0.64149^{-4}	0.30173^{-4}
400	-0.13617^{-4}	-0.42576^{-4}	-0.96022^{-4}	0.35239^{-4}	0.34396^{-4}
450	-0.94162^{-5}	-0.22362^{-4}	-0.52942^{-4}	-0.24675^{-4}	0.22331^{-4}

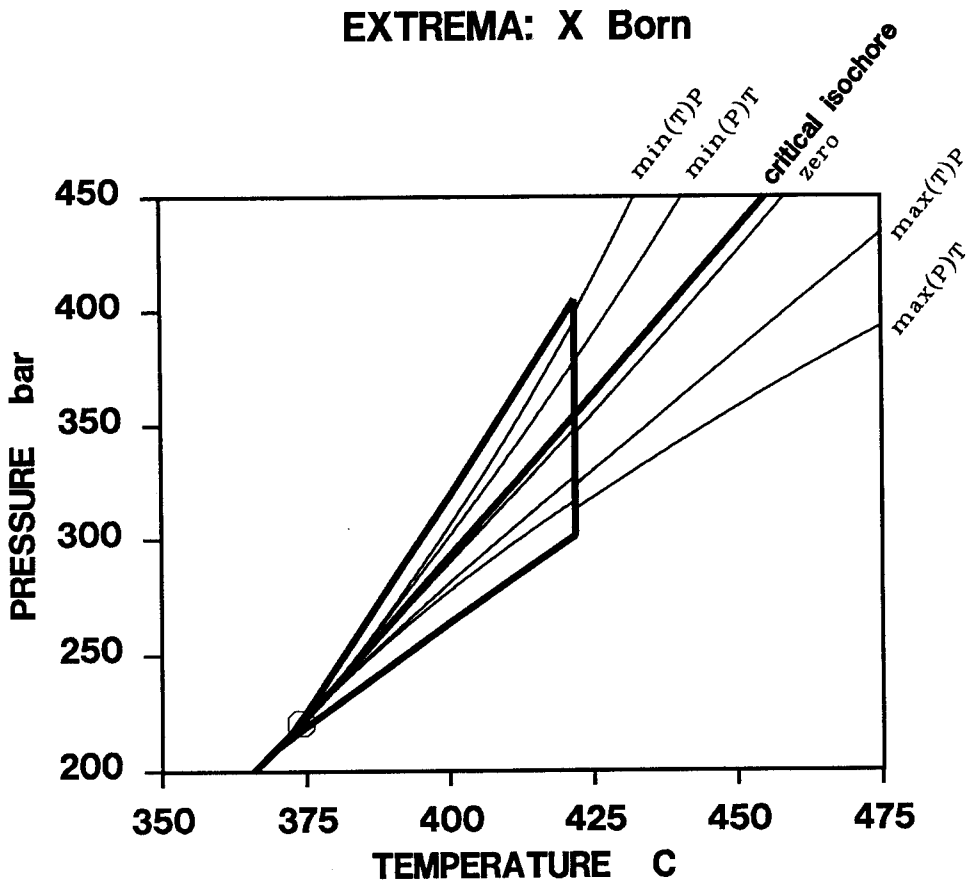

Fig. 28. $P-T$ projections of X Born function extrema computed from eqs (37), (48), (49), (54), (55), (57), (58), (83), (84), (88) through (91), requisite derivatives of eqs (33) and (37), and the revised adjustable coefficients of table 19. Also included, for reference, are the critical isochore, critical-region outline, and the zero contour for the X Born function.

Solvation contributions to several standard partial molal properties of aqueous ions, complexes, and electrolytes are dependent on the divergent H_2O Born functions described above. Specifically, standard partial molal enthalpies and entropies associated with the solvation process are functions of Y, corresponding volumes are dependent on Q, and heat capacities are functionally tied to both Y and X (Helgeson, Kirkham, and Flowers, 1981; Tanger and Helgeson, 1988). In the critical region, these dependencies so enhance the solvation contributions that the combined effects of all other contributing processes become negligible. In the *near*-critical region, $Q(\beta)$-, $Y(\alpha)$-, and $X((\partial\alpha/\partial T)_P)$-dependent

solvation terms attain magnitudes that not only dominate aqueous species behavior but also overwhelm standard molal volumes, enthalpies, entropies, and heat capacities of minerals and, as a result, effectively define corresponding standard molal properties of fluid-mineral reactions. These near-critical reaction properties can be closely approximated by taking account only of contributions dependent on partial derivatives of the fluid H_2O equation of state (Johnson, 1987).

TRANSPORT PROPERTIES

Values for the dynamic viscosity, η, and thermal conductivity, λ, of fluid H_2O are required for numerical modeling of fluid mass and thermal energy transport in hydrothermal systems (Norton and Knight, 1977; Straus and Schubert, 1977; Norton and Cathles, 1979; Norton, 1984). Equations that accurately represent these transport properties within and near the critical region (Basu and Sengers, 1977; Watson, Basu, and Sengers 1980a, b; Basu, Sengers, and Watson, 1980; Sengers and Kamgar-Parsi, 1984; Sengers and others, 1984; Sengers and Watson, 1986) are presented and analyzed below in the context of the HGK and LS equations of state.

The dynamic viscosity and thermal conductivity equations, $\eta\ (\overline{T}, \overline{\rho})$ and $\lambda(\overline{T}, \overline{\rho})$, are defined as functions of the reduced, dimensionless quantities $\overline{T} = T/T_c^*$ and $\overline{\rho} = \rho/\rho_c^*$, where T_c^*, $= 647.27°K$ and $\rho_c^* = 317.763\ kg/m^3$ (Sengers and others, 1984). However, adjustable coefficients inherent to these equations were obtained by regression analysis of experimental $[\eta, \lambda]\ (P, T)$ measurements, which necessitates the apriori equation-of-state conversion $\rho(T, P)$. Hence, these coefficients are, in principal, functionally dependent on the employed equation of state as well as the experimental data. This situation is analogous to that described above for the dielectric constant: strictly speaking, the same equation of state used to compute $\rho(P, T)$ prior to regression fitting of $[\eta, \lambda]\ (T, \rho)$ should be used to compute $\rho(T, P)$ before subsequent implementation of $[\eta, \lambda]\ (T, \rho)$. However, again in analogy to the dielectric constant, use of the proposed $[\eta, \lambda]\ (P, T)$ equations together with the HGK and LS equations of state, which were not used for pre-regression $\rho(P, T)$ transformation, does not introduce discrepancies that exceed uncertainty estimates for the experimental data (Sengers and Kamgar-Parsi, 1984; Sengers and others, 1984).

Dynamic viscosity.—The equation currently adopted by the IAPS for computation of dynamic viscosity (Sengers and Kamgar-Parsi, 1984; see Sengers and Watson, 1986, for the dimensionless analog) can be expressed as

$$\eta = \eta_0(\overline{T})\ \eta_1(\overline{T}, \overline{\rho})\ \eta_2(\overline{T}, \overline{\rho}). \tag{92}$$

TABLE 25

Coefficients $a_{\eta,i}$ for eq (93). Modified from Aleksandrov, Ivanov, and Matveev (1975)

i	$a_{\eta,i}$
0	$1.81583(10^{-2})$
1	$1.77624(10^{-2})$
2	$1.05287(10^{-2})$
3	$-3.6744(10^{-3})$

The first term in the right-hand product is the ideal gas contribution representing η in the low density limit (Aleksandrov, Ivanov, and Matveev, 1975);

$$\eta_0(T) = k_\eta \overline{T}^{1/2} \left\{ \sum_{i=0}^{3} \left(\frac{a_{\eta,i}}{\overline{T}^i} \right) \right\}^{-1}, \tag{93}$$

where $k_\eta = 10^{-5}\ g\ cm^{-1}\ s^{-1}$, and the $a_{\eta,i}$ (table 25) are coefficients determined from numerical fitting of eq (93) to experimental data. The second right-hand term in eq (92) represents dynamic viscosity over the global region as a power series expansion in $\overline{T}, \overline{\rho}$ (Aleksandrov, Ivanov, and Matveev, 1975):

$$\eta_1(\overline{T}, \overline{\rho}) = exp \left\{ \overline{\rho} \sum_{i=0}^{i} \sum_{j=0}^{j} a_{\eta,i,j} (\overline{T}^{-1} - 1)^i (\overline{\rho} - 1)^j \right\}, \tag{94}$$

where the $a_{\eta,i,j}$ (table 26) again represent coefficients obtained from least-squares fitting to experimental data. The third right-hand term in eq (92), $\eta_2(\overline{T}, \overline{\rho})$, is unity in the context of the adopted IAPS formulation.

In the global region, eq (92) represents all available experimental data to within measurement accuracy (Sengers and Kamgar-Parsi, 1984). However, weak divergence of η to ∞ at the critical point, predicted by theory (Hohenberg and Halperin, 1977) and verified by experiment (Rivkin and others, 1975; Rivkin, Levin, and Izrailevsky, 1976; Oltermann, ms), cannot be accounted for by eq (92) as defined above. As a result, one must incorporate into the $\eta_2(\overline{T}, \overline{\rho})$ term a theoretically justifiable expression that represents this divergence in order to reconcile the equation with theory and experiment. Such an expression, predicted from both mode-coupling and dynamic renormalization group theory (Sengers, 1985), was implemented by Basu, Sengers, and Watson (1980) and Watson, Basu, and Sengers (1980a, b):

$$\eta_2(\overline{T}, \overline{\rho}) = (q\xi)^{\Phi ce} = \left\{ q\xi_o \left(\frac{\overline{\chi}_T}{\Gamma_{ca}} \right)^{\nu ce/\gamma ce} \right\}^{\Phi ce}, \tag{95}$$

TABLE 26

Non-zero coefficients $a_{\eta,i,j}$ for eq (94). Modified from Aleksandrov, Ivanov, and Matveev (1975)

i	j	$a_{\eta,i,j}$	i	j	$a_{\eta,i,j}$
0	0	$5.132047(10^{-1})$	2	1	$1.241044(10^{0})$
0	1	$2.151778(10^{-1})$	2	2	$-1.263184(10^{0})$
0	2	$-2.818107(10^{-1})$	2	3	$2.340379(10^{-1})$
0	3	$1.778064(10^{-1})$	3	1	$1.476783(10^{0})$
0	4	$-4.176610(10^{-2})$	3	3	$-4.924179(10^{-1})$
1	0	$3.205656(10^{-1})$	3	4	$1.600435(10^{-1})$
1	1	$7.317883(10^{-1})$	3	6	$-3.629481(10^{-3})$
1	2	$-1.070786(10^{0})$	4	0	$-7.782567(10^{-1})$
1	3	$4.605040(10^{-1})$	5	0	$1.885447(10^{-1})$
1	5	$-1.578386(10^{-2})$			

where q refers to a system-dependent wave parameter $(3.76(10^{8})\ m^{-1})$, ξ denotes a correlation length representing the range of near-critical density fluctuations, ξ_0 stands for a system-dependent amplitude $(1.31(10^{-10})\ m)$, ϕ_{ce}, ν_{ce}, and γ_{ce} represent universal critical exponents, Γ_{ca} specifies a universal critical amplitude, and $\bar{\chi}_T$ corresponds to reduced isothermal compressibility ($\bar{\chi}_T = \bar{\rho}^2\ P_c^*\beta$, where $P_c^* = 221.15$ *bars*). By combining constants, eq (95) can be simplified (Basu, Sengers, and Watson, 1980; Watson, Basu, and Sengers, 1980a, b) to

$$\eta_2(\bar{T}, \bar{\rho}) = 0.922\,\bar{\chi}_T^{0.0263} = 1.13\ (\rho^2\beta)^{0.0263}. \tag{96}$$

Dynamic viscosity values computed from eqs (92) through (94) and (96) begin to diverge toward ∞ with approach to criticality when eq (96) exceeds unity; this condition is specified by

$$\bar{\chi}_T > 22 \text{ or, equivalently,}$$
$$\rho^2\beta > 10^{-2}\ g^2\ cm^{-6}\ bar^{-1}, \tag{97}$$

which in turn defines the theoretical T–ρ region of this weak divergence (Watson, Basu, and Sengers, 1980a, b) as

$$372.15°C < T < 379.40°C; \qquad 0.24 < \rho < 0.41\ g/cm^3. \tag{98}$$

In practice (Sengers and Kamgar-Parsi, 1984), all contributions of eq (96) to eq (92) are appropriately restricted to conditions defined by eqs (97) and (98) by explicitly specifying $\eta_2(\bar{T}, \bar{\rho}) \equiv 1$ everywhere beyond

these limits. Both the weak character and T–ρ range of near-critical η divergence to ∞ predicted by eqs (95) through (98) are in close agreement with experimental observations (Basu, Sengers, and Watson, 1980; Watson, Basu, and Sengers, 1980a, b; Sengers and Kamgar-Parsi, 1984).

Eqs (48), (49), (51), (52), (92) through (94), (96), and requisite derivatives of (33) and (37) were used to compute the $\eta(P, T)$ surface, $\eta(T)$-isobars, and $\eta(P)$-isotherms illustrated in figure 29, and the $\eta(P, T)$ values listed in table 27.

Outside the near-critical region, dynamic viscosity increases with pressure at constant temperature but displays a subtle local *minimum* with temperature at constant pressure. In the critical region, $-(\partial\eta/\partial T)_P$ and $(\partial\eta/\partial P)_T$ display local *maxima* that increase exponentially through the near-critical region to within less than a degree of the critical point; at the critical point, however, these partial derivatives are zero. The $\eta(P, T)$ surface, $\eta(T)$-isobars, and $\eta(P)$-isotherms therefore display a sharp sigmoid form in the near-critical region that dampens with temperature and pressure (fig. 29). This general functional form is quite similar to that of density (compare figs. 9 and 29).

Weak divergence of η to ∞ at the critical point causes local *maxima* in $\eta(T)_P$ and $\eta(P)_T$. The exponent governing this divergence, obtained by incorporating eq (16) into eq (96), is exceedingly small (≈ 0.0326); hence, the divergence is sufficiently weak that these local maxima are not developed until within a fraction of a degree and/or bar from the critical point. As a result, they are not discernable in figure 29. In addition, note that although η is infinite at criticality, the critical-point value illustrated in figure 29A is finite. This seeming discrepancy reflects the extremely weak character of η divergence together with our adopted convention, for illustrative purposes, of approximating infinite critical parameters by their values at $T_c + 10^{-5}$ °C, $P_c + 10^{-5}$ *bar*.

Thermal conductivity.—The thermal conductivity equation currently recommended by the IAPS can be expressed (Sengers and others, 1984; Sengers and Watson, 1986) as

$$\lambda = \lambda_0(\overline{T})\,\lambda_1(\overline{T}, \overline{\rho}) + \lambda_2(\overline{T}, \overline{\rho}). \tag{99}$$

The ideal gas contribution to eq (99), $\lambda_0(\overline{T})$, is given by (Aleksandrov and Maltveev, 1978)

$$\lambda_0(\overline{T}) = k_\lambda \overline{T}^{1/2}\left\{\sum_{i=0}^{3}\left(\frac{a_{\lambda,i}}{\overline{T}^i}\right)\right\}^{-1}, \tag{100}$$

where $k_\lambda = 2.39(10^{-3})$ *cal* cm^{-1} s^{-1} K^{-1}, and the $a_{\lambda,i}$ (table 28) are coefficients determined from numerical fitting of eq (100) to experimental data. Note that the functional form of eq (100) is identical to that of its dynamic viscosity counterpart, eq (93). Variations in λ with T, ρ over the

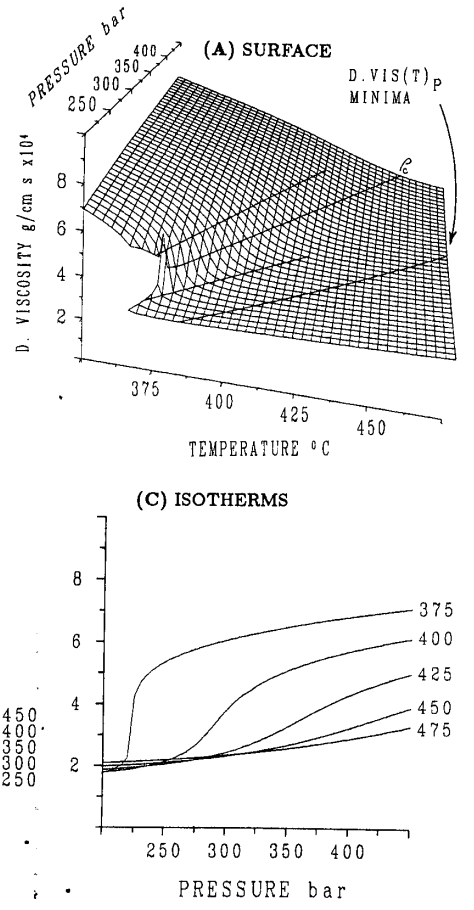

Figure 29: Dynamic viscosity ($g\,cm^{-1}\,s^{-1}$) as a function of (**A**) temperature ($°C$) and pressure (bar), (**B**) temperature at constant pressure, and (**C**) pressure at constant temperature; computed from eqs (48), (49), (51), (52), (92) through (96), and requisite derivatives of (33) and (37). Note that although dynamic viscosity is, in theory, infinite at the critical point, the critical value illustrated in (**A**) is finite (see text).

TABLE 27

Dynamic viscosity ($\times 10^3$ g cm^{-1} s^{-1}) as a function of pressure (bars) and temperature (°C); computed from eqs (48), (49), (51), (52), (92) through (96), and requisite derivatives of (33) and (37)

$P \backslash T$	375	400	425	450	475
250	0.58216	0.29176	0.28453	0.28957	0.29746
300	0.64570	0.44024	0.31861	0.30850	0.31104
350	0.68393	0.55783	0.39422	0.34026	0.33080
400	0.71309	0.61306	0.48612	0.39017	0.35883
450	0.73735	0.65068	0.54963	0.45055	0.39582

TABLE 28

Coefficients $a_{\lambda,i}$ for eq (100). Modified from Aleksandrov and Matveev (1978)

i	$a_{\lambda,i}$
0	$2.02223(10^0)$
1	$1.411166(10^1)$
2	$5.25597(10^0)$
3	$-2.01870(10^0)$

global region are represented by (Watson, 1977):

$$\lambda_1(\overline{T}, \overline{\rho}) = exp\left\{\overline{\rho} \sum_{i=0}^{i} \sum_{j=0}^{j} a_{\lambda,i,j}(\overline{T}^{-1} - 1)^i (\overline{\rho} - 1)^j\right\}, \qquad (101)$$

where the $a_{\lambda,i,j}$ (table 29) are coefficients obtained from least-squares fitting to experimental data. Again, the functional forms of $\lambda_1(\overline{T}, \overline{\rho})$ and $\eta_1(\overline{T}, \overline{\rho})$ are identical.

The final term in eq (99) accounts for the divergence of λ to ∞ at the critical point which is predicted by dynamic critical phenomena theory (Sengers, 1973; Basu and Sengers, 1977; Sengers and others, 1984) and has been verified experimentally (Le Neindre and others, 1973). The

TABLE 29

Coefficients $a_{\lambda,i,j}$ for eq (101). Modified from Watson (1977)

i	j	$a_{\lambda,i,j}$	i	j	$a_{\lambda,i,j}$
0	0	$1.3293046(10^0)$	2	0	$5.2246158(10^0)$
0	1	$-4.0452437(10^{-1})$	2	1	$-1.0124111(10^1)$
0	2	$2.4409490(10^{-1})$	2	2	$4.9874687(10^0)$
0	3	$1.8660751(10^{-2})$	2	3	$-2.7297694(10^{-1})$
0	4	$-1.2961068(10^{-1})$	2	4	$-4.3083393(10^{-1})$
0	5	$4.4809953(10^{-2})$	2	5	$1.3333849(10^{-1})$
1	0	$1.7018363(10^0)$	3	0	$8.7127675(10^0)$
1	1	$-2.2156845(10^0)$	3	1	$-9.5000611(10^0)$
1	2	$1.6511057(10^0)$	3	2	$4.3786606(10^0)$
1	3	$-7.6736002(10^{-1})$	3	3	$-9.1783782(10^{-1})$
1	4	$3.7283344(10^{-1})$	4	0	$-1.8525999(10^0)$
1	5	$-1.1203160(10^{-1})$	4	1	$9.3404690(10^{-1})$

theoretical expression for this term is given by (Basu and Sengers, 1977)

$$\lambda_2(\overline{T}, \overline{\rho}) = \frac{\Lambda k_B P_c^{*} \Gamma_{ca}^{\nu_{ce}/\gamma_{ce}}}{6\pi\xi_o} \left(\frac{\overline{T}}{\overline{P}}\right)^2 \left(\frac{\partial \overline{P}}{\partial \overline{T}}\right)_\rho^2 \frac{\overline{\chi}_T^{(\gamma_{ce}-\nu_{ce})/\gamma_{ce}}}{\eta_0(\overline{T})\, \eta_1(\overline{T}, \overline{\rho})}, \tag{102}$$

where Λ represents a dimensionless coefficient, k_B stands for Boltzmanns constant, Γ_{ca}, ν_{ce}, γ_{ce}, ξ_o, $\overline{\chi}_T$, $\eta_0(\overline{T})$, and $\eta_1(\overline{T}, \overline{\rho})$ are defined above, and $(\gamma_{ce} - \nu_{ce})/\gamma_{ce}) = 0.4678$.

The region where eq (102) contributes significantly to the functional form of eq (99) extends to temperatures approx 20 percent above critical (Basu and Sengers, 1977), a much wider range than the analogous limit of eq (98) for dynamic viscosity. These divergent contributions to λ are so-restricted in T–ρ space and smoothly meshed into those of eqs (100) and (101) by redefining $\lambda_2(\overline{T}, \overline{\rho})$ as the product of eq (102) and the crossover function specified by (Basu and Sengers, 1977)

$$f_{\lambda,co}(\overline{T}, \overline{\rho}) = \overline{\rho}^{1/2}\, exp\left[-18.66(\overline{T} - 1)^2 - (\overline{\rho} - 1)^4\right], \tag{103}$$

which smoothly converges from unity at the critical point to zero beyond the critical region. This redefinition of $\lambda_2(\overline{T}, \overline{\rho})$ transforms eq (102), after combining constants (Sengers and others, 1984) into

$$\lambda_2(\overline{T}, \overline{\rho}) = L f_{\lambda,co}(\overline{T}, \overline{\rho}) \left(\frac{\overline{T}}{\overline{P}}\right)^2 \left(\frac{\partial \overline{P}}{\partial \overline{T}}\right)_\rho^2 \frac{\overline{\chi}_T^{0.4678}}{\eta_0(\overline{T})\, \eta_1(\overline{T}, \overline{\rho})}, \tag{104}$$

where $L = 9.013(10^{-10})\, cal\, g\, cm^{-2}\, s^{-2}\, {}^{o}K^{-1}$. With the critical enhancement terms so-defined, eq (99) provides close representation of available experimental data both within and beyond the critical region (Sengers and others, 1984). Eqs (48), (49), (51), (52), (99) through (101), (103), (104), and requisite derivatives of (33) and (37) were used to compute the $\lambda(P, T)$ surface, $\lambda(T)$-isobars, and $\lambda(P)$-isotherms illustrated in figure 30, and the $\lambda(P, T)$ values listed in table 30.

The general functional form of thermal conductivity is similar to that of dynamic viscosity (compare figs. 29 and 30). There are, however, two significant differences. First, as implied above, the divergent character of λ is strong relative to that of η. This disparity reflects that between exponents that govern asymptotic behavior of the two properties. For λ, this exponent, obtained by incorporating eq (16) into eq (104), is ≈ 0.5805; the corresponding exponent for η is ≈ 0.0326, hence the relatively strong divergent behavior of λ. This sharp divergency causes local maxima in $\lambda(T)_P$ and $\lambda(P)_T$ to extend well beyond the near-critical region (fig. 30B and C). The second difference between $\lambda(P, T)$ and $\eta(P, T)$ is the lack of local minimum in $\lambda(T)_P$.

COMBINED PROPERTIES

Several ratios of state, thermodynamic, and transport properties presented above define additional fluid H_2O properties of practical

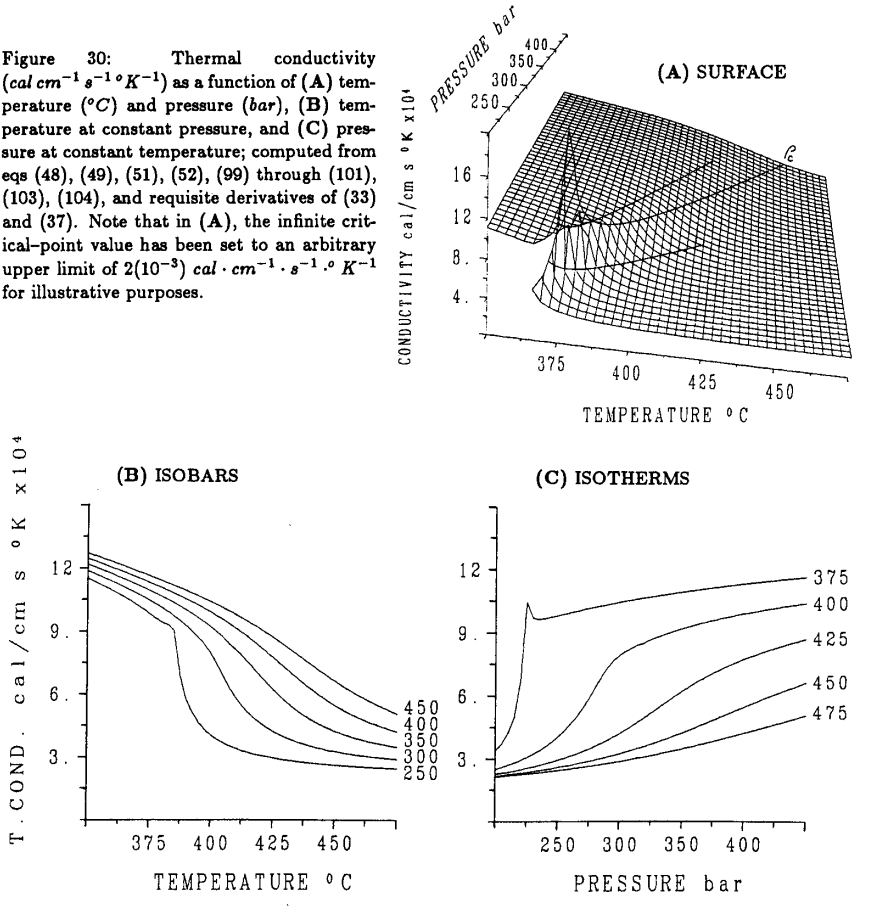

Figure 30: Thermal conductivity ($cal\,cm^{-1}\,s^{-1}\,{}^{o}K^{-1}$) as a function of **(A)** temperature (^{o}C) and pressure (bar), **(B)** temperature at constant pressure, and **(C)** pressure at constant temperature; computed from eqs (48), (49), (51), (52), (99) through (101), (103), (104), and requisite derivatives of (33) and (37). Note that in **(A)**, the infinite critical-point value has been set to an arbitrary upper limit of $2(10^{-3})$ $cal \cdot cm^{-1} \cdot s^{-1} \cdot {}^{o}K^{-1}$ for illustrative purposes.

TABLE 30

Thermal conductivity (cal cm^{-1} s^{-1} $°K^{-1}$) *as a function of pressure* (bars) *and temperature* (°C)*; computed from eqs (48), (49), (51), (52), (99) through (101), (103), (104), and requisite derivatives of (33) and (37). Exponentiations are shorthand for* $\times 10^{[-3,-2]}$

$P \backslash T$	375	400	425	450	475
250	0.98325^{-3}	0.40466^{-3}	0.29450^{-3}	0.26011^{-3}	0.24554^{-3}
300	0.10468^{-2}	0.79439^{-3}	0.42126^{-3}	0.32515^{-3}	0.28836^{-3}
350	0.10934^{-2}	0.91889^{-3}	0.62003^{-3}	0.42175^{-3}	0.34621^{-3}
400	0.11309^{-2}	0.98960^{-3}	0.77283^{-3}	0.54409^{-3}	0.42017^{-3}
450	0.11629^{-2}	0.10398^{-2}	0.86865^{-3}	0.66049^{-3}	0.50514^{-3}

importance in numerical modeling and analysis of heat and mass transfer processes in hydrothermal systems. Among the more important of these "combined" properties are kinematic viscosity, thermal diffusivity, the Prandtl number, and the isochoric expansivity-compressibility coefficient. These properties and sound velocity, which provides a valuable indicator of equation-of-state performance, are evaluated below.

Kinematic viscosity.—Kinematic viscosity is defined by the quotient of dynamic viscosity and density:

$$\nu = \frac{\eta}{\rho}\ (cm^2/s). \tag{105}$$

Eqs (48), (49), (51), (52), (92) through (96), (105), and requisite derivatives of (33) and (37) were used to compute the $\nu(P, T)$ surface, $\nu(T)$-isobars, and $\nu(P)$-isotherms illustrated in figure 31, and the $\nu(P, T)$ values listed in table 31.

The $\nu(P, T)$ surface displays subtle minima in $\nu(T)_P$ and $\nu(P)_T$ in the supercritical region. Between these two minima, ν increases slightly with pressure and temperature; to their high-density side, ν increases slightly with pressure and decreases slightly with temperature; and to their low-density side, ν decreases with pressure and increases with temperature — the magnitude of these derivatives in this latter region are large relative to the other two. In the critical region, both $(\partial\nu/\partial T)_P$ and $-(\partial\nu/\partial P)_T$ display local *maxima* that increase through the near-critical region to within the immediate vicinity of the critical point; at the critical point, however, these derivatives are zero. As a result, the $\nu(P, T)$ surface, $\nu(T)$-isobars, and $\nu(P)$-isotherms all display a gentle sigmoid form in the critical region which dampens with temperature and pressure (fig. 31).

In general, the functional form of kinematic viscosity is inversely related to that of dynamic viscosity and density. Although η and ρ are themselves functionally similar (compare figs. 9A and 29A), their difference in *magnitude* (ρ $[g/cm^3] \approx 10^2\eta$ $[g\ cm^{-1}\ s^{-1}]$) causes this mirror relationship relative to ν (cm^2/s). Functional similarity between ρ and η does, however, effectively dampen in kinematic viscosity the sigmoid character of isobaric and isothermal cross sections so pronounced in density and dynamic viscosity.

Kinematic viscosity displays the same weak divergence to ∞ at the critical point that characterizes dynamic viscosity (compare figs. 29A and 31A). Although this divergence causes local maxima in $\nu(T)_P$ and $\nu(P)_T$, its weak nature restricts the occurrence of these extrema to within a fraction of a degree and/or bar of criticality, hence they are not depicted in figure 31B and C. Note also that the critical-point ν value shown in figure 31A is rendered finite by the illustrative approximations discussed above for its η analog; the theoretical value is infinite.

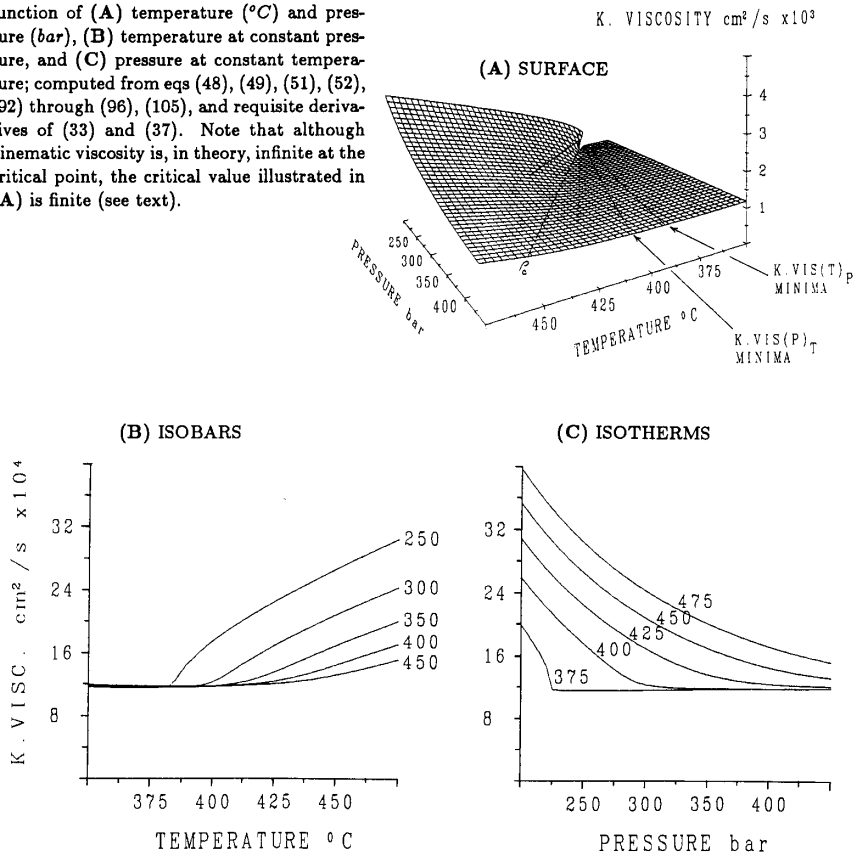

Figure 31: Kinematic viscosity (cm^2/s) as a function of (**A**) temperature ($°C$) and pressure (bar), (**B**) temperature at constant pressure, and (**C**) pressure at constant temperature; computed from eqs (48), (49), (51), (52), (92) through (96), (105), and requisite derivatives of (33) and (37). Note that although kinematic viscosity is, in theory, infinite at the critical point, the critical value illustrated in (**A**) is finite (see text).

TABLE 31

Kinematic viscosity ($\times 10^2$ cm^2/s) *as a function of pressure* (bars) *and temperature* (°C)*; computed from eqs (48), (49), (51), (52), (92) through (96), (105), and requisite derivatives of (33) and (37)*

$P \backslash T$	375	400	425	450	475
250	0.11523	0.17509	0.22436	0.26544	0.30374
300	0.11566	0.12284	0.16888	0.20782	0.24246
350	0.11632	0.11746	0.13503	0.16876	0.20025
400	0.11699	0.11707	0.12321	0.14402	0.17089
450	0.11764	0.11729	0.12014	0.13121	0.15125

Thermal diffusivity.—Thermal diffusivity is defined by the quotient of thermal conductivity and the density, isobaric heat capacity product:

$$\kappa = \frac{\lambda}{\rho\, c_p}\ (cm^2/s). \tag{106}$$

Eqs (37), (48), (49), (51), (52), (73), (74), (77), (78), (99) through (101), (103), (104), (106), and requisite derivatives of (33) and (37) were used to compute the $\kappa(P, T)$ surface, $\kappa(T)$-isobars, and $\kappa(P)$-isotherms illustrated in figure 32 and the $\kappa(P, T)$ values listed in table 32.

The $\kappa(P, T)$ surface is characterized by supercritical minima in both $\kappa(T)_P$ and $\kappa(P)_T$. Between these loci of $(\partial\kappa/\partial T)_P = 0$ and $(\partial\kappa/\partial P)_T = 0$, thermal diffusivity increases with both temperature and pressure; to their high-density side, κ increases with pressure but decreases with temperature; and to their low-density side, κ increases with temperature but decreases with pressure. With approach to criticality, the P–T projections of $\kappa(T)_P$ and $\kappa(P)_T$ minima converge unequally to that of the critical isochore as their decreasing magnitudes converge toward zero. This convergence follows from the functional dependence of thermal diffusivity on the ratio of moderately-strong and strong divergent properties (λ/c_p).

Prandtl number.—The Prandtl number is defined by the dimensionless ratio of kinematic viscosity to thermal diffusivity:

$$Pr = \frac{\nu}{\kappa} = \frac{\eta\, c_p}{\lambda}. \tag{107}$$

Eqs (37), (48), (49), (51), (52), (73), (74), (77), (78), (92) through (96), (99) through (101), (103), (104), (107), and requisite derivatives of (33) and (37) were used to compute the $Pr(P, T)$ surface, $Pr(T)$-isobars, and $Pr(P)$-isotherms illustrated in figure 33, and the $Pr(P, T)$ values listed in table 33.

The Prandtl number diverges from background values ($\approx$0.5–2.5) outside the critical region to ∞ at the critical point. This divergence is moderately strong owing to its functional dependence on strongly-divergent c_p and the reciprocal of, in a relative sense, weakly divergent λ. As with all aysmptotic properties, the divergence of Pr is sharpest when the critical point is approached along the vaporization boundary or confluent critical isochore. Hence, the loci of maxima in $Pr(T)$-isobars and $Pr(P)$-isotherms (fig. 33B and C) are coincident with ρ_c in the near-critical region. With increasing pressure and temperature, however, these two P–T extrema projections depart unequally from the critical isochore, toward subcritical densities in the case of $Pr(P)_T$ maxima, but supcritical values for $Pr(T)_P$. As a result, the $Pr(P, T)$ surface is subdivided into three regions of specific partial derivative variation: (1) a region confined between the two maxima where Pr decreases with both

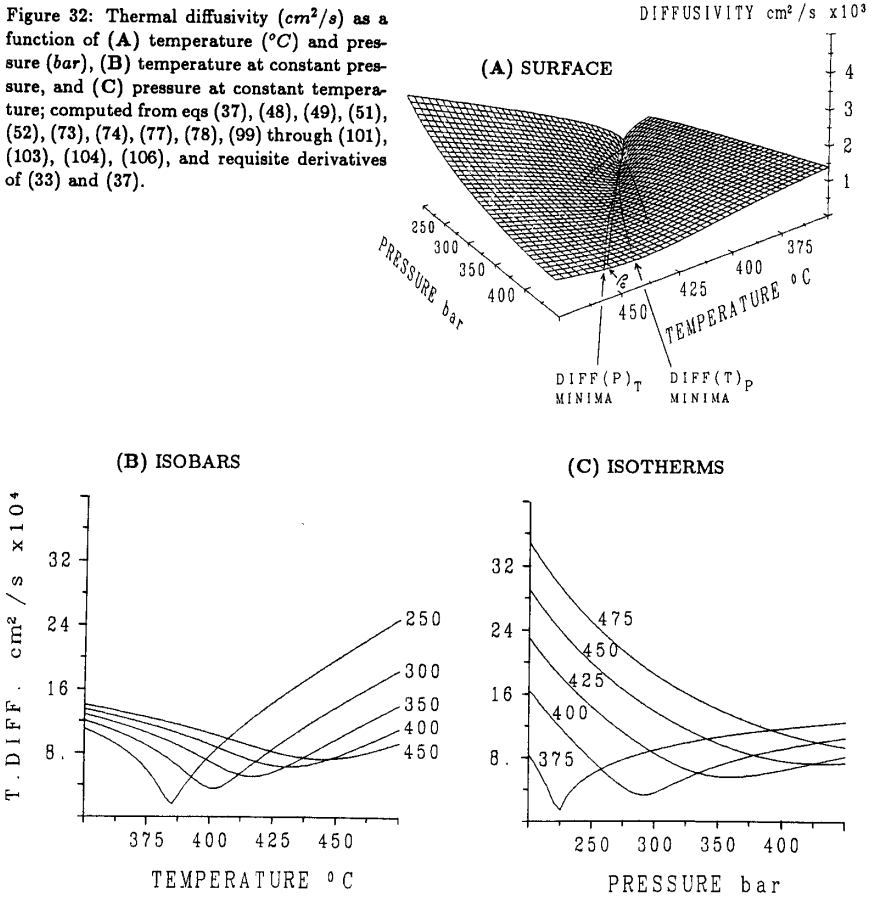

Figure 32: Thermal diffusivity (cm^2/s) as a function of **(A)** temperature ($°C$) and pressure (bar), **(B)** temperature at constant pressure, and **(C)** pressure at constant temperature; computed from eqs (37), (48), (49), (51), (52), (73), (74), (77), (78), (99) through (101), (103), (104), (106), and requisite derivatives of (33) and (37).

TABLE 32

Thermal diffusivity (cm^2/s) *as a function of pressure* (bars) *and temperature* (°C)*; computed from eqs (37), (48), (49), (51), (52), (73), (74), (77), (78), (99) through (101), (103), (104), (106), and requisite derivatives of (33) and (37). Exponentiations are shorthand for* $\times 10^{[-3,-2]}$

$P \backslash T$	375	400	425	450	475
250	0.59356^{-3}	0.76571^{-3}	0.14299^{-2}	0.19781^{-2}	0.24887^{-2}
300	0.89482^{-3}	0.36000^{-3}	0.84986^{-3}	0.13770^{-2}	0.18432^{-2}
350	0.10538^{-2}	0.69363^{-3}	0.55822^{-3}	0.97431^{-3}	0.14026^{-2}
400	0.11624^{-2}	0.90708^{-3}	0.64199^{-3}	0.75853^{-3}	0.11049^{-2}
450	0.12454^{-2}	0.10479^{-2}	0.81394^{-3}	0.73542^{-3}	0.93282^{-3}

Figure 33: Prandtl number (*dimensionless*) as a function of (**A**) temperature (°*C*) and pressure (*bar*), (**B**) temperature at constant pressure, and (**C**) pressure at constant temperature; computed from eqs (37), (48), (49), (51), (52), (73), (74), (77), (78), (92) through (96), (99) through (101), (103), (104), (107), and requisite derivatives of (33) and (37). Note that in the critical region of (**A**), all $Pr > 5$ have been set to this arbitrary upper limit for illustrative purposes; this truncation compromises ≈ 1.5 percent of the $Pr(P,T)$ surface.

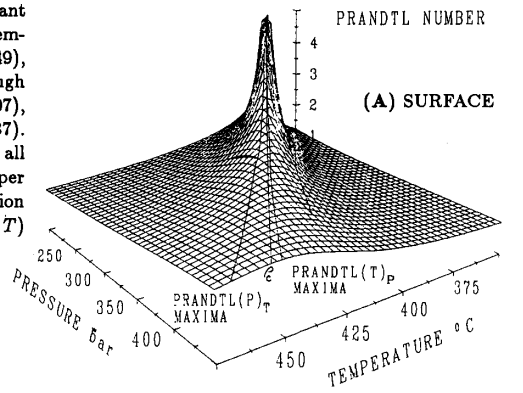

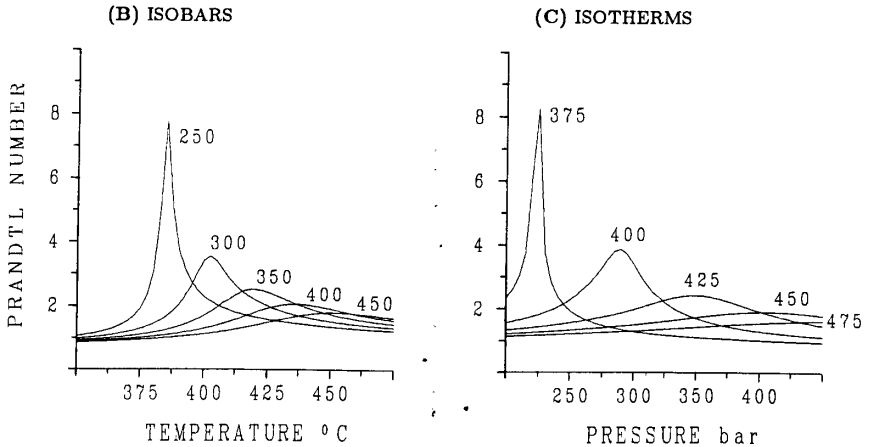

TABLE 33

The Prandtl number (dimensionless) *as a function of pressure* (bars) *and temperature* (°C)*; computed from eqs (37), (48), (49), (51), (52), (73), (74), (77), (78), (92) through (96), (99) through (101), (103), (104), (107), and requisite derivatives of (33) and (37). Exponentiations are shorthand for* $\times 10^{[0,1]}$

$P \setminus T$	375	400	425	450	475
250	0.19414^{1}	0.22867^{1}	0.15690^{1}	0.13419^{1}	0.12205^{1}
300	0.12926^{1}	0.34123^{1}	0.19872^{1}	0.15092^{1}	0.13154^{1}
350	0.11038^{1}	0.16935^{1}	0.24190^{1}	0.17321^{1}	0.14277^{1}
400	0.10064^{1}	0.12906^{1}	0.19191^{1}	0.18986^{1}	0.15466^{1}
450	0.94459^{0}	0.11192^{1}	0.14760^{1}	0.17842^{1}	0.16215^{1}

pressure and temperature, (2) a region to the low-density side of the $Pr(P)_T$ maxima where Pr increases with pressure and decreases with temperature, and (3) a region to the high-density side of the $Pr(T)_P$ maxima where Pr decreases with pressure and increases with temperature.

Isochoric expansivity-compressibility coefficient.—The isochoric expansivity-compressibility coefficient is defined as the ratio of isobaric expansivity and isothermal compressibility:

$$\frac{\alpha}{\beta} = \left(\frac{\partial P}{\partial T}\right)_{\rho} \ (bar/°K). \tag{108}$$

The isochoric expansivity-compressibility coefficient can be obtained directly from appropriate differentiation of the fundamental thermodynamic functions, eqs (22) and (37). Specifically, in the critical region

$$\frac{\alpha}{\beta} = \frac{P_c}{T_c}\left\{\tilde{P} - \tilde{T}\left(\frac{\partial \tilde{P}}{\partial \tilde{T}}\right)_{\tilde{\mu}}\right\}, \tag{109}$$

and in the global region

$$\frac{\alpha}{\beta} = \frac{\rho^2}{CM}\left(\frac{\partial^2 A_m}{\partial \rho \partial T}\right)_{T,\rho} \tag{110}$$

Eqs (37), (48), (49), (109), (110), and requisite derivatives of (33) and (37) were used to compute the $\alpha/\beta(P,T)$ surface $\alpha/\beta(T)$-isobars, and $\alpha/\beta(P)$-isotherms illustrated in figure 34, and the $\alpha/\beta(P,T)$ values listed in table 34.

The isochoric expansivity-compressibility surface maps $(\partial P/\partial T)_{\rho}$ for the $\rho(P, T)$ surface (fig. 9A). These isochoric slopes are steep for supercritical liquid, nearly flat for supercritical vapor, and in the critical region display smooth variation between these extremes. This variation is characterized by local maxima in $(\partial^2 P/\partial T^2)_{\rho}$ and $(\partial(\partial P/\partial T)_{\rho}/\partial P)_{\rho}$ that diverge to ∞ at the critical point. As a result, the function form of α/β for conditions of interest in this study corresponds closely to that of density (compare figs. 9 and 34). Note that although $\alpha = \beta = \infty$ at criticality, the associated α/β value is defined by the critical-point P–T slope (≈ 2.67 *bar*/°*K*) of the confluent vaporization boundary and critical isochore.

Sound velocity.—The speed of sound in fluid H_2O is defined by

$$\omega_s = \left\{\frac{\overline{C}\, c_p}{c_v}\left(\frac{\partial P}{\partial \rho}\right)_T\right\}^{1/2} = \left\{\frac{\overline{C}\, c_p}{c_v\, \rho\, \beta}\right\}^{1/2} \ (cm/s). \tag{111}$$

Eqs (37), (48), (49), (51), (52), (73), (74), (77), (78), (111), and requisite derivatives of (33) and (37) were used to compute the $\omega_s(P, T)$ surface,

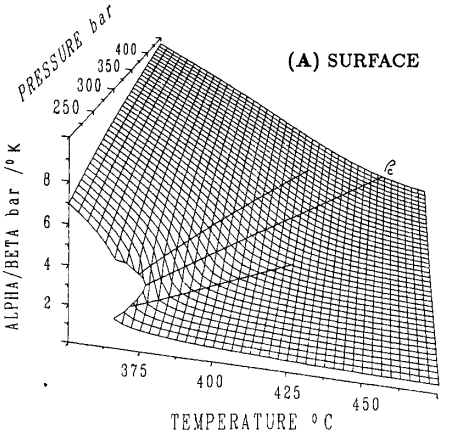

Figure 34: Isochoric expansivity compressibility ($bar/°K$) as a function of (**A**) temperature ($°C$) and pressure (bar), (**B**) temperature at constant pressure, and (**C**) pressure at constant temperature; computed from eqs (37), (48), (49), (109), (110), and requisite derivatives of (33) and (37).

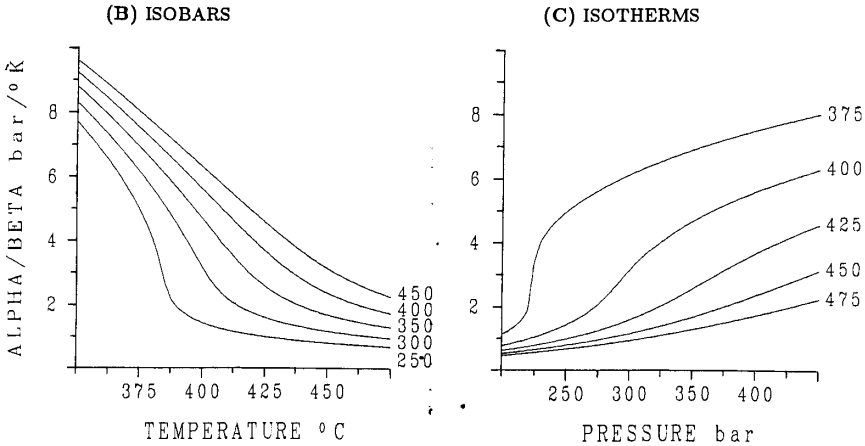

TABLE 34

Isochoric expansivity-compressibility (bars/°K) *as a function of pressure* (bars) *and temperature* (°C)*; computed from eqs (37), (48), (49), (109), (110), and requisite derivatives of (33) and (37). Exponentiations are shorthand for* $\times 10^{[0,1]}$

$P \backslash T$	375	400	425	450	475
250	0.49652^{1}	0.14305^{1}	0.98980^{0}	0.79136^{0}	0.67177^{0}
300	0.61423^{1}	0.31501^{1}	0.15883^{1}	0.11587^{1}	0.94015^{0}
350	0.69101^{1}	0.46749^{1}	0.25601^{1}	0.16708^{1}	0.12840^{1}
400	0.75115^{1}	0.56039^{1}	0.36603^{1}	0.23504^{1}	0.17175^{1}
450	0.80163^{1}	0.62961^{1}	0.45558^{1}	0.31152^{1}	0.22377^{1}

$\omega_s(T)$-isobars, and $\omega_s(P)$-isotherms illustrated in figure 35, and the $\omega_s(P, T)$ values listed in table 35.

The $\omega_s(P, T)$ surface is characterized by supercritical minima in both $\omega_s(T)_P$ and $\omega_s(P)_T$. Between P–T projections of these extrema, sound velocity increases with both temperature and pressure; to their high-density side, ω_s increases with pressure but decreases with temperature; and to their low-density side, ω_s increases with temperature but decreases with pressure. With approach to criticality, the P–T projections of $\omega_s(T)_P$ and $\omega_s(P)_T$ minima converge unequally to that of the critical isochore, as their decreasing magnitudes converge toward zero. This convergence follows from the functional dependence of sound velocity on a ratio of equally-strong divergent properties (c_p/β) and the reciprocal of a weakly divergent one (c_v).

Because sound velocity is defined by a ratio of three properties each obtained at the second level of differentiation of the fundamental surface, comparison of calculated values with those obtained experimentally provides an excellent benchmark of equation performance. In the critical region, eqs (48), (51), (73), (77), (111), and requisite derivatives of (37) provide accurate prediction of near-critical $\omega_s(P)_T$ minima determined experimentally by Erokhin and Kal'yanov (1979, 1980) (Levelt Sengers and others, 1983). The corresponding global-region eqs (49), (52), (74), (78), (111), and requisite derivatives of (33) represent all available data to within their reported measurement accuracy (Haar, Gallagher, and Kell, 1984). These findings represent strong evidence for both theoretical validity and practical utility of the LS and HGK equations of state.

SUMMARY

Transport and chemical processes in hydrothermal systems are to a large degree controlled by the properties of H_2O (Norton and Knight, 1977; Straus and Schubert, 1977; Norton and Cathles, 1979; Norton, 1984; Helgeson and Kirkham, 1974a, b, 1976; Helgeson, Kirkham, and Flowers, 1981; Johnson and Norton, 1986; Johnson, 1987; Tanger and Helgeson, 1988; Shock and others, ms; Helgeson, 1991). Thermodynamic, electrostatic, and transport properties of this universal solvent are in turn controlled by its equation of state. As a result, development of an accurate function relating state variables of H_2O is of central importance to quantitative analysis of the hydrothermal environment.

Four thermodynamically equivalent functional descriptions for the equation of state can be derived from the Gibbs-Duhem equation: $V_m(T, P)$, $P(T, V_m)$, $\rho(T, \mu)$, and $\mu(T, \rho)$. The explicit form of the state function is, in principal, arbitrary and may be theroretical or empirical. The most useful expressions, however, are readily integrable to obtain the specific-volume or molar Helmholtz free energy from which all other thermodynamic functions are obtained by appropriate differentiation. Following choice of independent variables and functional form, the regression coefficients inherent to the equation are obtained by numerical fitting to

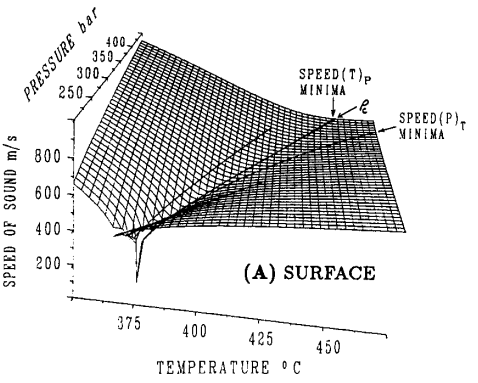

Figure 35: Speed of sound (m/s) as a function of **(A)** temperature ($°C$) and pressure (bar); **(B)** temperature at constant pressure, and **(C)** pressure at constant temperature; computed from eqs (37), (48), (49), (51), (52), (73), (74), (77), (78), (111), and requisite derivatives of (33) and (37).

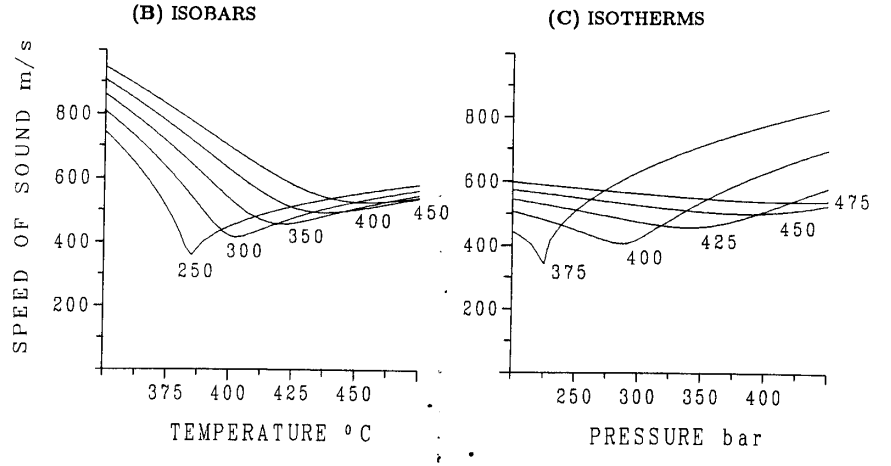

TABLE 35

Sound velocity (m/s) *as a function of pressure* (bars) *and temperature* (°C)*; computed from eqs (37), (48), (49), (51), (52), (73), (74), (77), (78), (111), and requisite derivatives of (33) and (37)*

$P \backslash T$	375	400	425	450	475
250	506.08	448.63	510.40	549.65	579.70
300	628.99	419.66	473.59	525.32	561.96
350	710.23	536.07	457.83	504.93	546.46
400	773.70	627.26	507.20	500.71	536.82
450	826.74	697.95	579.23	525.34	538.54

experimental data. Because of this ultimate dependence on experiment, most equations of state are of $V_m(P, T)$ or $P(T, V_m)$ form as a consequence of data availability; examples include all van der Waals and virial equations. In the critical region, however, it is advantageous to cast the equation of state as $\rho(T, \mu)$ or $\mu(T, \rho)$ because these descriptions provide symmetry features in real fluids analogous to those predicted by theoretical models of critical-point phase transition developed from statistical mechanics.

The global region of the $P(T, \rho)$ surface can be represented to within experimental accuracy by a modified version of the Ursell-Mayer virial equation augmented with a minimum number of residual terms (Haar, Gallagher, and Kell, 1984). In contrast, the divergence of compressibility and expansivity to $\pm\infty$ at the critical point cannot be modeled precisely, in theory or practice, by virial or other classical equations of state that presume critical-point analyticity. These critical anomalies are, however, accurately predicted by a revised and extended scaled equation of state that incorporates asymptotic power laws, nonclassical critical exponents, and critical-point singularity (Levelt Sengers and others, 1983). Because the HGK and LS equations yield nearly equivalent results along their near-coincident validity perimeters, the two formulations can be used together with dependent electrostatic and transport functions to provide comprehensive prediction of fluid H_2O properties within and near the critical region.

Divergence of partial derivatives of the equation of state to $\pm\infty$ at the critical point causes the development of local isobaric temperature and isothermal pressure extrema in other dependent H_2O properties. These extrema asymptotically decay in magnitude according to their governing critical exponent along unique P–T projections that themselves asymptotically depart unequally from the critical isochore with increasing temperature and pressure. P–T projections of isobaric temperature and isothermal pressure extrema for several properties of particular importance in transport models and solution chemistry are summarized in figures 36 and 37.

Local extrema in α, c_p, and ν have an important effect on the nature of heat and mass transport processes in hydrothermal systems (Norton and Knight, 1977). For a given rock permeability, fluid flux predicted from Darcy's law with imposed Boussinesq approximation (Tritton, 1977) is proportional to α and inversely proportional to ν. Maximum flow rates therefore occur at state conditions intermediate to α maxima and ν minima. Because $\alpha\ [^\circ K^{-1}] \approx 10^2\ \nu\ [cm^2/s]$, these conditions are, in fact, closely approximated by those of α maxima. The local rate of convective heat transfer is proportional to both fluid flux and c_p. Because c_p is a dependent function of α, their extrema projections are nearly coincident. As a result, *fluid flux and convective heat transfer rates in hydrothermal systems attain local maxima within the critical region in the vicinity of* α *extrema. Magnitudes of these maxima increase exponentially through the near-critical*

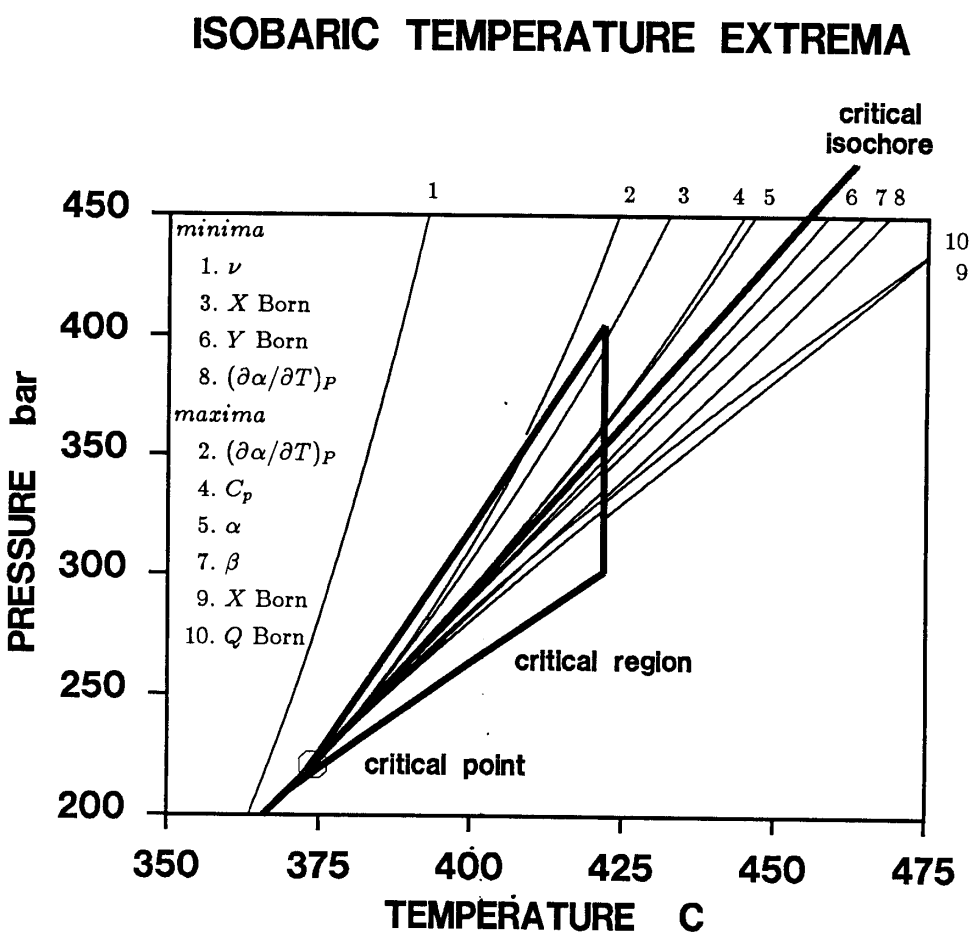

Fig. 36. Summary of isobaric temperature extrema in α, β, $(\partial\alpha/\partial T)_P$, c_p, ν, Q, Y, and X. Also included, for reference, are the critical isochore and critical-region outline.

region and in the context of permeable media become infinite at the critical point. (Johnson and Norton, 1986).

Divergence of the Q, Y, and X Born functions to $\pm\infty$ at the critical point controls the thermodynamic behavior of aqueous ions, complexes, and electrolytes in the critical region. Specifically, solvation contributions to the standard partial molal enthalpies and entropies of these aqueous species are functionally dependent on $Y(-\alpha)$, which diverges to $-\infty$ at criticality; corresponding volumes and heat capacities are similarly dependent on, respectively, $-Q(\beta)$, which diverges to $-\infty$ at the critical point, and $X(-(\partial\alpha/\partial T)_P)$, which also diverges to $-\infty$ for paths of critical-point approach where $\rho > \rho_c$, but to ∞ along analogous paths where $\rho < \rho_c$

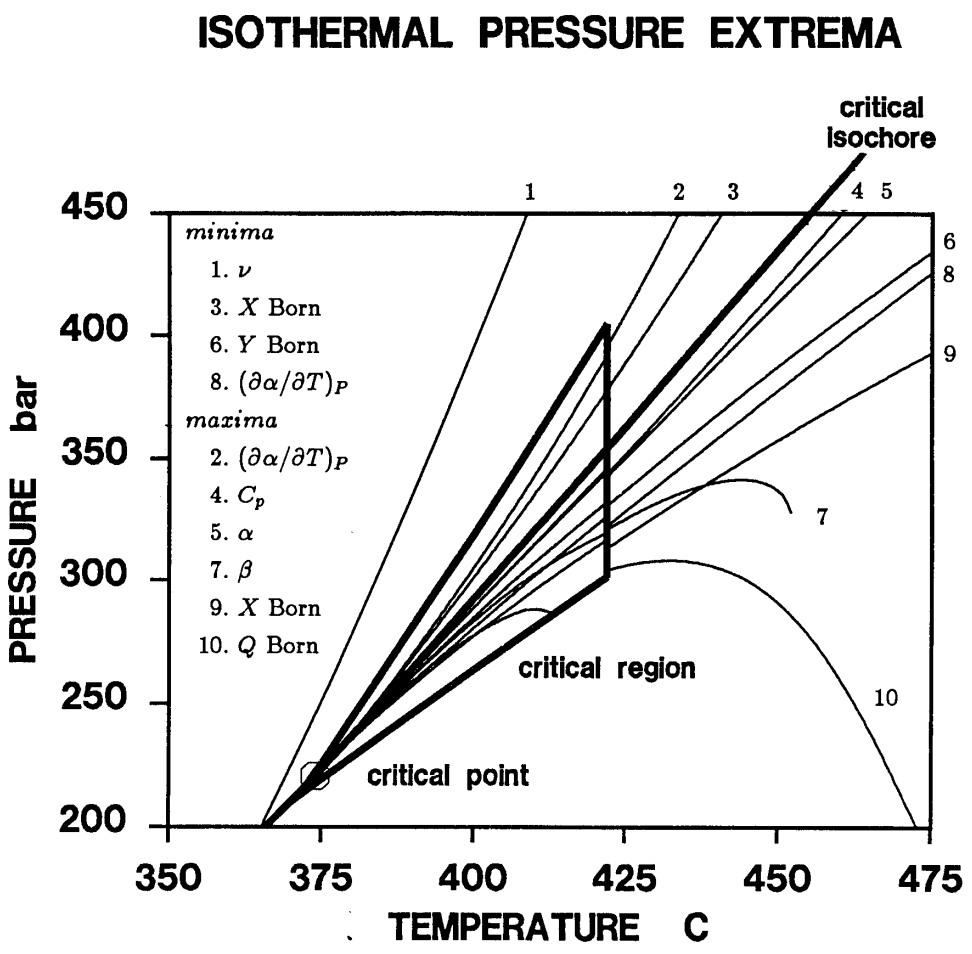

Fig. 37. Summary of isothermal pressure extrema in α, β, $(\partial\alpha/\partial T)_P$, c_p, ν, Q, Y, and X. Also included, for reference, are the critical isochore and critical-region outline.

(Helgeson, Kirkham, and Flowers, 1981). Intimate functional dependence of these Born functions on the indicated equation-of-state derivatives is evidenced by near-coincidence of Y, α; Q, β; and X, $(\partial\alpha/\partial T)_P$ extrema in the critical region (figs. 36 and 37). *At critical-region conditions, this dependence causes the solvation contributions to dominate those of all other contributing processes, thereby controlling the composite standard partial molal properties of aqueous species (Helgeson and Kirkham, 1974a; Helgeson, Kirkham, and Flowers, 1981). In the near-critical region, these properties attain sufficient magnitude to render corresponding properties of minerals, gases, and the solvent*

negligible; hence, they effectively dictate the thermodynamic behavior of fluid-mineral reactions (Johnson, 1987).

In summary, the critical region can be viewed as a funnelform, *P–T* sector of extreme behavior in the properties of H_2O (figs. 36 and 37). These property extrema are of sufficient magnitude to control a variety of transport and chemical processes in hydrothermal systems during transient attainment of critical-region conditions. In the near-critical region, the extent of this control is such that certain of these processes — for example, local variations in fluid mass flux and the state of chemical equilibrium — can be closely approximated by accounting only for contributions of the α- and β- and $(\partial\alpha/\partial T)_P$-dependent terms. With the development of an accurate scaled equation of state for near-critical H_2O (Levelt Sengers and others, 1983), it is now possible to quantitatively assess these transport and chemical consequences of critical phenomena in hydrothermal systems (Johnson and Norton, 1986; Johnson, 1987, Helgeson, 1991).

ACKNOWLEDGMENTS

Much of the present contribution derives from the senior author's Ph.D. dissertation at the University of Arizona. This research was supported by the National Science Foundation (NSF grants EAR-8440670, EAR-8503114, EAR-841680, and EAR-9007101) with additional funds for technical support provided through a geohydrology project funded by the State of Arizona. Many friends and colleagues have made important contributions to this work; the senior author wishes to acknowledge those of Jibamitra Ganguly, Harold C. Helgeson, Webb Miller, Dick Beane, J. M. H. Levelt Sengers, L. Haar, John Walther, Dennis Bird, Tim Loomis, Arend Meijer, Spencer Titley, John Guilbert, Krishna Vemulapalli, L. Steve Sorenson, Eric Oelkers, Rob Drabek, Chris Beattie, Gary Levin, Regina Capuano, Tom Brikowski, Jeanne Woodward, and Becki Oddone. Very special thanks go to L. Steve Sorenson, software engineer and consultant *par excellence,* for access to his versatile graphics toolbox and computational expertise, and to Harold C. Helgeson and Eric Oelkers, for numerous insightful discussions regarding the electrostatic properties of water. We are also deeply indebted to Jibamitra Ganguly, John Walther, and especially to J. M. H. Levelt Sengers, each of whom carefully reviewed earlier drafts of the manuscript and offered many useful suggestions, insightful comments, and technical corrections, all of which were invaluable in preparing the final product.

Note added in proof.—Our introductory remarks alluded to the inevitability of subsequent improvements in the far-decimal reaches of skeleton tables reported herein; two recent publications (Hill, 1990; Archer and Wang, 1990) may provide such improvement. Hill (1990) has sagaciously revised and extended the Helmholtz formulation of Keenan and others (1969) and developed an associated blending function that facilitates confluence of this formulation with the scaled description of Levelt

Sengers and others (1983) through the critical region. Although Hill's (1990) approach incorporates selected elements from earlier strategies (Chapola and Rowlinson, 1974; Woolley, 1983; Levelt Sengers, Kamgar-Parsi, and Sengers, 1983), his is the first unified equation of state for H_2O that smoothly meshes nonclassical behavior near the critical point with classical behavior beyond the critical region. Archer and Wang (1990) have used experimental $\epsilon(T, P)$ data, the Hill (1990) and Kirkwood (1939) equations, and nonlinear least-squares analysis to develop a new empirical revision of the Kirkwood equation that facilitates calculation of $\epsilon(T, P, \rho)$ to 5000 *bars* and 550°*C*. Although their methodology follows closely the trail blazed by Franck (1956), Quist and Marshall (1965), Helgeson and Kirkham (1974a), Heger, Uematsu, and Franck (1980), and Pitzer (1983), Archer and Wang (1990) note that their equation can be used over a slightly larger range of conditions than its predecessors and demonstrate that it provides more accurate representation of experimental $(\partial^2\epsilon/\partial T^2)_P$ and $(\partial^2\epsilon/\partial P^2)_T$ values than do the Helgeson-Kirkham (1974a) and Uematsu-Franck (1980) equations for temperatures below approx 70°*C* at one *bar*.

Whether or not the Hill (1990) and Archer-Wang (1990) equations permit improved prediction of H_2O properties over the range of conditions considered in the present study is a debate beyond the scope of this note. More importantly, the difference between properties calculated using these new equations and those obtained from the formulations employed above is typically less than two percent (table 36) — a discrepancy of insignificant magnitude for most practical applications. In fact, examination of table 36 indicates that one would have difficulty distinguishing the two sets of calculations in a side-by-side comparison of the figures presented herein. Hence, substitution of the Hill (1990) and Archer-Wang (1990) equations for their counterparts used in the present study would not modify the functional behavior of H_2O properties as illustrated and analyzed above, nor would it alter the noted effects of this behavior on transport and chemical processes in hydrothermal systems.

On the other hand, it is important to recognize the significant advances embodied in these new equations. In addition to achieving the inaugural unification of nonclassical and classical behavior, Hill's (1990) equation of state "permits regular extrapolation of property estimations" to approx 250,000 *bars,* based on comparison with ultra high pressure *P-T-*ρ data derived from shock tube measurements. This upper limit far exceeds the analogous boundary of 30,000 *bars* for the HGK equation, although their associated temperature limits are similar (approx 2000° and 2200°*C* for the Hill (1990) and HGK formulations, respectively). As a result, the Hill (1990) equation represents a crucial first step toward expanding the physical limits of geochemical calculations involving H_2O from the lower crust to considerable depths within the upper mantle. Unfortunately, the analogous extrapolation of dielectric equations, including the Archer-Wang (1990) formulation, to pressures beyond 5000 *bars* (and temperatures above 550°*C*) remains largely paralyzed by the dearth•

TABLE 36

Comparison of $\rho(g/cm^3)$, $\beta(bar^{-1})$, $\alpha(°K^{-1})$, ϵ(dimensionless), $Q(bar^{-1})$, *and* $Y(°K^{-1})$ *calculated as a function of pressure* (bars) *and temperature* (°C) *over the range of conditions considered in the present study using (A) the equations presented above and (B) equations developed by Hill (1990) and Archer and Wang (1990). Note that over this range of conditions (and particularly within the critical region, represented by the 300* bar, *400*°C *comparison), the magnitude of discrepancy between the two sets of predictions is uniformly less than one percent for* ρ, β, *and* α, *and typically less than two percent for* ϵ, Q, *and* Y. *Exponentiations are shorthand for* $\times 10^{[-4,-3,-2,-1,1,2]}$

P, T	eqs	ρ	β	α	ϵ	Q	Y
200, 350	A	0.60078	0.10094^{-2}	0.70281^{-2}	0.14252^{2}	0.10472^{-3}	-0.86933^{-3}
	B	0.60079	0.99991^{-3}	0.69771^{-2}	0.13961^{2}	0.10844^{-3}	-0.89647^{-3}
200, 475	A	0.72546^{-1}	0.64397^{-2}	0.29809^{-2}	0.15240^{1}	0.17318^{-2}	-0.11483^{-2}
	B	0.72484^{-1}	0.64366^{-2}	0.29849^{-2}	0.14901^{1}	0.17602^{-2}	-0.11258^{-2}
300, 400	A	0.35838	0.11996^{-1}	0.37789^{-1}	0.62851^{1}	0.24803^{-2}	-0.80815^{-2}
	B	0.35836	0.11988^{-1}	0.37767^{-1}	0.61762^{1}	0.25185^{-2}	-0.81843^{-2}
450, 350	A	0.68333	0.30999^{-3}	0.29892^{-2}	0.17260^{2}	0.26827^{-4}	-0.37288^{-3}
	B	0.68318	0.31137^{-3}	0.29907^{-2}	0.16984^{2}	0.28079^{-4}	-0.38884^{-3}
450, 475	A	0.26170	0.41082^{-2}	0.91929^{-2}	0.38635^{1}	0.11651^{-2}	-0.29229^{-2}
	B	0.26166	0.41168^{-2}	0.92043^{-2}	0.38330^{1}	0.11817^{-2}	-0.29525^{-2}

of experimental dielectric-constant measurements at these conditions. Experimental data of this kind are essential if the intriguing possibility of geochemical calculations involving H_2O and other aqueous species at conditions found in the upper mantle is to become reality. Should these data become available in the near future, they might well be represented most easily with a modified version of the Archer-Wang (1990) expression owing to its implicit and explicit links to the Hill (1990) equation of state.

APPENDIX
GLOSSARY OF SYMBOLS

Symbol	*Definition*
a_{sc}	— Dimensionless scaling function parameter in eqs (21), (25), (26), (44), and (45).
$a_{[T,\rho]}$	— Dimensionless parameters in eq (19); defined in associated text.
$a_{\eta,i}$	— Dimensionless coefficients used to compute $\eta_0(\overline{T}, \overline{\rho})$ in eq (93).
$a_{\eta,i,j}$	— Dimensionless coefficients used to compute $\eta_1(\overline{T}, \overline{\rho})$ in eq (94).
$a_{\lambda,i}$	— Dimensionless coefficients used to compute $\lambda_0(\overline{T}, \overline{\rho})$ in eq (100).
$a_{\lambda,i,j}$	— Dimensionless coefficients used to compute $\lambda_1(\overline{T}, \overline{\rho})$ in eq (101).
A	— Helmholtz free energy (*cal*); defined by eq (59).
A_{ca}	— Universal, dimensionless critical amplitude for the asymptotic power law associated with c_v^* along the critical isochore: eq (17).

A_m — Helmholtz free energy per mole (*cal/mol*); computed with eqs (33) and (60).

$A_{m,base}$ — Base function contribution to Helmholtz free energy per mole (*cal/mol*) in the virial equation of state given by Haar, Gallagher, and Kell (1984); defined by eq (34).

$A_{m,ideal}$ — Ideal gas function contribution to Helmholtz free energy per mole (*cal/mol*) in the virial equation of state given by Haar, Gallagher, and Kell (1984); defined by eq (36).

$A_{m,resid}$ — Residual function contribution to Helmholtz free energy per mole (*cal/mol*) in the virial equation of state given by Haar, Gallagher, and Kell (1984); defined by eq (35).

$A_{m,tr}$ — Helmholtz free energy per mole (*cal/mol*) at the H_2O triple point; defined in table 6.

A_v — Helmholtz free energy per unit volume (cal/cm^3); defined by eq (5).

A_{vij} — Coefficients for near-critical Taylor expansion of A_v^*; defined by eq (13).

A_v^* — Dimensionless Helmholtz free energy per unit volume (normalized with respect to appropriate critical parameters); defined by eq (11).

ΔA_m — Apparent molal Helmholtz free energy (*cal/mol*); defined by eq (47).

b_j — Coefficients (cm^3/g) used to compute $b_{v,2}$ in eq (31).

b_{sc} — Dimensionless scaling function parameter in eqs (21), (42), (43), and (45).

$b_{v,2}$ — Second virial coefficient (cm^3/g) for the hard-sphere equation of state in the formulation developed by Haar, Gallagher, and Kell (1984); defined by eq (31).

$B_{ca,[l,v]}$ — Universal, dimensionless critical amplitudes for asymptotic power laws associated with the liquid (l) and vapor (v) branches of the near-critical vaporization boundary; eq (15).

B_j — Coefficients (cm^3/g) used to compute $B_{v,2}$ in eq (32).

$B_{v,2}$ — Second virial coefficient (cm^3/g) associated with the equation of state given by Haar, Gallagher, and Kell (1984); defined by eq (32).

c_i — Dimensionless coefficients used to compute $A_{m,ideal}$ in eq (36).

c_p — Isobaric heat capacity ($cal\ mol^{-1}\ °K^{-1}$); defined by eq (75) and computed with eqs (77) and (78).

c_{sc} — Dimensionless scaling function parameter in eq (45).

c_v — Isochoric heat capacity ($cal\ mol^{-1}\ °K^{-1}$); defined by eq (72) and computed with eqs (73) and (74).

c_v^* — Dimensionless isochoric heat capacity; defined in text describing the associated asymptotic power law; eq (17).

C — Conversion factor: $0.02390054\ cal\ bar^{-1}\ cm^{-3}$.

$\overline{C}$ — Conversion factor: $10^{-4}\ bar\ cm\ s^2\ g^{-1}$.

$\hat{C}$ — Conversion factor: $4.814\ J/cal$.

$C_{K,[1,2]}$ — Combined variables from eq (80); defined by eq (81).

D_{ca} — Universal, dimensionless critical amplitude for the asymptotic power law associated with the critical isotherm; eq (14).

e_i — Coefficients (*dimensionless*) used to compute $k_i(\hat{T})$ in eq (84).

$e_{i,j}$ — Coefficients ($T^{-i}\ \rho^{-j}$) used to compute $\epsilon(T, \rho)$ in eq (79).

E — Internal energy (*cal*); defined by eq (64).

E_m — Internal energy per mole (*cal/mol*); computed with eqs (65) and (66).

$E_{m,tr}$ — Internal energy per mole (*cal/mol*) at the H_2O triple point; defined in table 6.

ΔE_m — Apparent molal internal energy (*cal/mol*); defined by eq (47).

$f_{\lambda,co}$ — Crossover function used to compute the relative contribution of $\lambda_2(\overline{T}, \overline{\rho})$ to λ; defined by eq (103).

g_K — Kirkwood coefficient that accounts for local geometric structure of the H_2O molecule in eq (80); defined by eq (82).

g^* — Modified Kirkwood-coefficient variable; defined by eq (81).

$g(i)$ — Coefficients (J/g) used to compute P_{resid} in eq (30).

$g_i(x)$ — Scaling ($i = 0$) and corrections-to-scaling ($i = 1$) functions used to compute $\Delta\tilde{P}$ in the scaled equation of state given by Levelt Sengers and others (1983); defined by eq (42).

G — Gibbs free energy (*cal*); defined by eq (61).

G_m — Gibbs free energy per mole (*cal/mol*); computed with eqs (62) and (63).

$G_{m,tr}$ — Gibbs free energy per mole (*cal/mol*) at the H_2O triple point; defined in table 6.

ΔG_m — Apparent molal Gibbs free energy (*cal/mol*); defined by eq (47).

$h(1, x/x_o)$ — Scaling function defined by eq (20).

$h_o(x)$ — Scaling function used to compute $\tilde{P}_{sc}$ in eq (25).

$h_i(x)$ — i^{th} scaling function used to compute $\tilde{P}_{corr}$ in eq (26).

H — Enthalpy (*cal*); defined by eq (67).

H_m — Enthalpy per mole (*cal/mol*); computed with eqs (68) and (69).

$H_{m,tr}$ — Enthalpy per mole (*cal/mol*) at the H_2O triple point; defined in table 6.

ΔH_m — Apparent molal enthalpy (*cal/mol*); defined by eq (47).

k_B — Boltzmanns constant: 3.29957 (10^{-24}) *cal/°K*.

$k_i(\hat{T})$ — Temperature polynomials defined by eq (84).

$k_{sc,i}$ — i^{th} scaling function parameter in eqs (21), (25), (26), and (37).

$k(i)$ — Integer constants used to compute P_{resid} in eq (30).

k_λ — Numerical constant in eq (100): 2.39 (10^{-3}) *cal* cm^{-1} s^{-1} $°K^{-1}$.

k_η — Numerical constant in eq (93): 10^{-5} *g* cm^{-1} s^{-1}.

k_ρ — Numerical constant in eqs (30) and (35): 1 cm^3/g.

$l(i)$ — Integer constants used to compute P_{resid} in eq (30).

L — Numerical constant in eq (104): 9.103 (10^{-10}) *cal g* cm^{-2} s^{-2} $°K^{-1}$.

M — Molecular weight of H_2O: 18.0152 *g/mol*.

n — Number of moles (*mol*).

N_A — Avogardro's number: 6.02252(10^{23}) mol^{-1}.

$p_i(\theta)$ — Polynomials used to compute $g_i(x)$ in eq (42); defined by eq (46).

p_{ji} — Coefficients used to compute $p_i(\theta)$; defined by eq (46).

P — Pressure (*bars*).

P^* — Dimensionless pressure variable (P_c-normalized).

$\tilde{P}$ — Dimensionless, temperature-normalized pressure variable (also normalized with respect to T_c, P_c); defined by eqs (22), (23), and (37).

P_{base} — Base function contribution to pressure (*bar*) in the virial equation of state given by Haar, Gallagher, and Kell (1984); defined by eq (29).

P_c — Pressure at the H_2O critical point: 220.46 *bar*.

P_o — Pressure constant in eq (34): 1.01325 *bar*.

P_{resid} — Residual function contribution to pressure (*bar*) in the virial equation of state given by Haar, Gallagher, and Kell (1984); defined by eq (30).

P_c^* — Pressure constant in dynamic viscosity and thermal conductivity equations: 221.15 *bar*.

$\tilde{P}_{corr}$ — Correction-to-scaling function contribution to $\tilde{P}$; defined by eq (26).

$\tilde{P}_{reg}$ — Analytic conbtribution to $\tilde{P}$; defined by eqs (24) and (37).

$\tilde{P}_{sc}$ — Scaling function contribution to $\tilde{P}$; defined by eq (25).

$\tilde{P}_i$ — Pressure background parameters for $\tilde{P}_{reg}$ in eqs (37) and (41).

$\tilde{P}_o(\tilde{T})$ — Polynomial representing the background $\tilde{P}$ contribution to $\tilde{P}_{reg}$; defined by eq (41).

$\Delta\tilde{P}$ — Sum of asymptotic scaling and correction-to-scaling contributions to $\tilde{P}$ in the scaled equation of state given by Levelt Sengers and others (1983); defined by eq (37).

Pr — Dimensionless Prandtl number; defined by eq (107).

q — System-dependent wave parameter in eq (95): 3.76 (10^8) m.

Q — Q Born function (bar^{-1}); defined by eq (86).

r — Variable representing distance from the critical point in the linear-model parametric equation of state; see eq (21) and associated text.

R — Gas constant: 1.9872 $cal\ mol^{-1}\ °K^{-1}$.

$\hat{R}$ — Gas constant ($\equiv R/C$): 83.145 $bar\ cm^3\ mol^{-1}\ °K^{-1}$.

$\overline{R}$ — Gas constant ($\equiv RC^{-1}\ M^{-1}$): 4.6152 $bar\ cm^3\ g^{-1}\ °K^{-1}$.

S — Entropy ($cal/°K$).

S_m — Entropy per mole ($cal\ mol^{-1}\ °K^{-1}$); computed with eqs (70) and (71).

$S_{m,tl}$ — Third law molal entropy ($cal\ mol^{-1}\ °K^{-1}$); defined by eq (47).

$S_{m,tr}$ — Entropy per mole ($cal\ mol^{-1}\ °K^{-1}$) at the H_2O triple point; defined in table 6.

S_v — Entropy per unit volume ($cal\ cm^{-3}\ °K^{-1}$).

T — Temperature in $°K$; where specified, in $°C$.

T_c — Temperature at the H_2O critical point: 647.067°K = 373.917°C.

T_i — Temperature constants ($°K$) used to compute τ_i in eqs (30) and (35); defined in associated text.

T_o — Temperature constant in eqs (30) through (32) and (35): 647.074°K.

T_R — Dimensionless temperature variable in eq (36): $T°K/100°K$.

T^* — Dimensionless temperature variable (T_c-normalized); defined by eq (11).

$\overline{T}$ — Dimensionless temperature variable in dynamic viscosity and thermal conductivity equations: $T°K/647.27°K$.

$\hat{T}$ — Dimensionless temperature variable (298.15°K-normalized) used in eqs (83) and (84).

$\tilde{T}$ — Dimensionless temperature variable (T_c-normalized); defined by eq (22).

T_c^* — Temperature constant used in dynamic viscosity and thermal conductivity equations: 647.27°K.

ΔT^* — Dimensionless temperature variable (normalized and reduced with respect to T_c); defined by eq (11).

$\Delta\tilde{T}$ — Dimensionless temperature variable (normalized and reduced with respect to T_c) in the scaled equation of state given by Levelt Sengers and others (1983); defined by eq (38).

u — Molecular dipole moment of H_2O (1.84 (10^{-18}) esu) in eq (80).

$u_{[t,\mu]}$ — Scaling fields introduced in eq (24) and associated text; defined by eqs (44) and (45) in the context of the scaled equation of state given by Levelt Sengers and others (1983).

V — Volume (cm^3).

V_m — Molar volume (cm^3/mol).

$V_{m,c}$ — Molar volume at the H_2O critical point: 55.8130 (cm^3/mol).

x — Scaling variable introduced in eq (20); defined in associated text and by eqs (27) and (43).

x_o — Numerical constant in eq (19); defined in associated text.

X — X Born function ($°K^{-2}$); defined by eq (90).

y — Dimensionless density parameter ($\equiv b_{v,2\rho}/4$) in eqs (29) and (34).

Y — Y Born function ($°K^{-1}$); defined by eq (88).

Z — Dimensionless Z Born function; defined by eq (85).

α — Coefficient of isobaric expansivity ($°K^{-1}$); defined by eq (53) and computed with eqs (54) and (55).

$[\alpha, \alpha', \alpha'']_{cr}$ — Universal, dimensionless critical exponents for asymptotic power laws associated with c_v^* along the critical isochore, vaporization boundary, and sub-T_c analytic extension of the critical isochore: eq (17).

α_i — Integer constants in eqs (30) and (35).

α_k — Molecular polarizibility of H_2O ($1.444\ (10^{-24}\ cm^3/mol)$ in eq (80).

β — Coefficient of isothermal compressibility (bar^{-1}); defined by eq (50) and computed with eqs (51) and (52).

β_{ce} — Universal, dimensionless critical exponent for the asymptotic power law associated with the near-critical vaporization boundary; eq (15).

β_i — Integer constants in eqs (30) and (35).

$[\gamma, \gamma']_{ce}$ — Universal, dimensionless critical exponent for the asymptotic power law associated with χ_T^* along the critical isochore and vaporization boundary; eq (16).

$\hat{\gamma}$ — Dimensionless geometric constant (=13) representing ellipsoid eccentricity in the hard-ellipse equation of state employed in the formulation developed by Haar, Gallagher, and Kell (1984); see eq (29).

Γ_{ca} — Universal, dimensionless critical amplitude for the asymptotic power law associated with χ_T^* along the critical isochore; eq (16).

δ_{ce} — Universal, dimensionless critical exponent for the asymptotic power law associated with the critical isotherm; eq (14).

δ_i — Dimensionless density variable in eqs (30) and (35); defined in associated text.

Δ_i — Correction-to-scaling ("gap") exponents in eqs (26) and (37).

ϵ — Dimensionless dielectric constant; computed using eqs (79) and (81) through (84).

η — Dynamic viscosity ($g\ cm^{-1}\ s^{-1}$); computed with eq (92).

$\eta_0(\overline{T})$ — Polynomial representing the ideal gas contribution to η; defined by eq (93).

$\eta_1(\overline{T}, \overline{\rho})$ — Polynomial representing η in the global region; defined by eq (94).

$\eta_2(\overline{T}, \overline{\rho})$ — Function accounting for anomalous enhancement of η very near the critical point; defined by eqs (95) and (96).

θ — Variable representing location on an r-contour in the linear-model parametric equation of state; see eq (21) and associated text.

κ — Thermal diffusivity (cm^2/s); defined by eq (106).

λ — Thermal conductivity ($cal\ cm^{-1}\ s^{-1} \circ K^{-1}$); computed with eq (99).

λ_h — Dimensionless parameter in eq (19); defined in associated text.

$\lambda_0(\overline{T})$ — Polynomial representing the ideal gas contribution to λ; defined by eq (100).

$\lambda_1(\overline{T}, \overline{\rho})$ — Polynomial representing λ in the global region; defined by eq (101).

$\lambda_2(\overline{T}, \overline{\rho})$ — Function accounting for anomalous enhancement of λ in the critical region; defined by eqs (102) and (104).

Λ — Dimensionless constant in eq (102).

μ — Chemical potential (*cal/mol*).

μ_{ij} — Dimensionless coefficients for near-critical Taylor expansion of μ^*; defined by eq (13).

μ^* — Dimensionless chemical potential variable (normalized per appropriate critical parameters); defined by eq (11).

$\tilde{\mu}$ — Dimensionless, temperature-normalized, chemical potential variable (also normalized with respect to appropriate critical parameters); defined by eq (22).

$\tilde{\mu}_i$ — Dimensionless chemical potential background parameters in eq (40).

$\tilde{\mu}_0(\tilde{T})$ — Polynomial representing $\tilde{\mu}$ along the vaporization boundary and its supercritical analytic extension; defined by eq (40).

$\Delta\mu^*$ — Dimensionless chemical potential variable (normalized and reduced with respect to appropriate critical parameters); defined by eq (11). Associated asymptotic power law defined by eq (14).

$\Delta\tilde{\mu}$ — Dimensionless chemical potential variable (normalized and reduced with respect to appropriate critical parameters) in the scaled equation of state given by Levelt Sengers and others (1983); defined by eq (38).

ν — Kinematic viscosity (cm^2/s); defined by eq (105).

ν_{ce} — Universal critical exponent in eqs (95) and (102).

ξ — Correlation length representing the range of near-critical density fluctuations in eq (95).

ξ_0 — System-dependent amplitude ($1.31\ (10^{-10})\ m$) in eqs (95) and (102).

ρ — Density (g/cm^3).

ρ_i — Density constants (g/cm^3) used to compute δ_i in eqs (30) and (35); defined in associated text.

ρ_c — Density at the H_2O critical point: 0.322778 (g/cm^3).

ρ^* — Dimensionless density variable (ρ_c-normalized); defined by eq (11).

$\overline{\rho}$ — Dimensionless density variable in dynamic viscosity and thermal conductivity equations: $\rho[kg/m^3]/317.763\ [kg/m^3]$.

$\hat{\rho}$ — Dimensionless density variable used in eq (83) and referenced in discussion of critical-region approximations to Q and Y.

ρ_c^* — Density constant in dynamic viscosity and thermal conductivity equations: $317.763\ kg/m^3$.

$\Delta\rho^*$ — Dimensionless density variable (normalized and reduced with respect to ρ_c); defined by eq (11). Associated asymptotic power law defined by eq (15).

τ_i — Dimensionless temperature variable in eqs (30) and (35); defined in associated text.

ϕ_{ce} — Universal critical exponent in eq (95).

Φ — Combination of eq (80) variables; defined by eq (81).

χ_T^* — Dimensionless isothermal compressibility; defined in text describing the associated asymptotic power law: eq (16).

$\overline{\chi}_T$ — Dimensionless isothermal compressibility ($\overline{\rho}^2\ P_c^*\ \beta$) in eqs (95) through (97).

ω_s — Speed of sound in fluid H_2O (cm/s); defined by eq (111).

REFERENCES

Albright, P. C., Sengers, J. V., Nicoll, J. F., and Ley-Koo, M., 1986, A crossover description for the thermodynamic properties of fluids in the critical region: International Journal of Thermophysics, v. 7, n. 1, p. 75–85.

Aleksandrov, A. A., Ivanov, A. I., and Matveev, A. B., 1975, The dynamic viscosity of water and steam within a wide region of temperatures and pressures: Thermal Engineering, v. 22, n. 4, p. 77–83.

Aleksandrov, A. A., and Matveev, A. B., 1978, The thermal conductivity of water and steam within a wide range of temperature and pressure: Thermal Engineering, v. 25, n. 8, p. 58–64.

Archer, D. G., and Wang, P., 1990, The dielectric constant of water and Debye-Huckel limiting law slopes: Journal of Physical and Chemical Reference Data, v. 19, p. 371–411.

Baker, G. A., 1977, Analysis of hyperscaling in the Ising model by the high-temperatures series method: Physical Review B, v. 15, p. 1552–1559.

Balfour, F. W., Sengers, J. V., and Levelt Sengers, J. M. H., 1980, A revised and extended scaled fundamental equation for the thermodynamic behavior of steam in the critical region, *in* Straub, J., and Scheffler, K., editors, Water and Steam: Their Properties and Current Industrial Applications: New York, Pergamon, p. 128–137.

Balfour, F. W., Sengers, J. V., Moldover, M. R., and Levelt Sengers, J. M. H., 1978, Universality, revisions of and corrections to scaling in fluids: Physics Letters, v. 65A, n. 3, p. 223–225.

Basu, R. S., and Sengers, J. V., 1977, Thermal conductivity of steam in the critical region, *in* Cezairliyan, A., editor, Proceedings of the Seventh Symposium on Thermophysical Properties: New York, American Society of Mechanical Engineers, p. 822–830.

Basu, R. S., Sengers, J. V., and Kestin, J., 1980, Prandtl number of water and steam, *in* Straub, J., and Scheffler, K., editors, Water and Stream: Their Properties and Current Industrial Applications: New York, Pergamon, p. 445–452.

Basu, R. S., Sengers, J. V., and Watson, J. T. R., 1980, Viscosity of steam in the critical region: International Journal of Thermophysics, v. 1, n. 1, p. 33–50.

Bjerrum, N., 1929, Neuere anschauungen uber elektrolyte: Deutsche Chemische Gesellschaft, Berichte der Deutschen Chemischen Gesellschraft, v. 62, p. 1091–1103.

Born, Von M., 1920, Volumen und hydratationswarme der ionen: Zeitschrift fuer Physik, v. 1, p. 45–48.

Bradley, D. J., and Pitzer, K. S., 1979, Thermodynamics of electrolytes. 12. Dielectric properties of water and Debye-Huckel parameters to 350°C and 1 kbar: Journal of Physical Chemistry, v. 83, n. 12, p. 1599–1603.

Brush, S. G., 1967, History of the Lenz-Ising model: Reviews of Modern Physics, v. 39, n. 4, p. 883–893.

Cailletet, L., and Mathias, E., 1886, Recherches sur les densites des gaz liquefies et de leurs vapeurs saturees: Comptes Rendus des Seances de L'Academie des Sciences, v. 102, p. 1202–1207.

Camp, W. J., Saul, D. M., Van Dyke, J. P., and Wortis, M., 1976, Series analysis of corrections to scaling for the spin pair correlations of the spin-s Ising model: confluent singularities, universality, and hyperscaling: Physical Review B, v. 14, n. 9, p. 3990–4001.

Chang, R. F., and Levelt Sengers, J. M. H., 1986, Behavior of dilute mixtures near the solvent's critical point: Journal of Physical Chemistry, v. 90, p. 5921–5927.

Chang, R. F., Morrison, G., and Levelt Sengers, J. M. H., 1984, The critical dilemma dilute mixtures: Journal of Physical Chemistry, v. 88, p. 3389–3391.

Chapela, G. A., and Rowlinson, J. S., 1974, Accurate representation of thermodynamic properties near the critical point: Journal of the Chemical Society: Faraday Transactions I, v. 70, n. 3, p. 584–593.

de Boor, C., 1978, A practical guide to splines: New York, Springer-Verlag, 392 p.

Domb, C., 1974, Ising model, *in* Domb, C., and Green, M. S., editors, Critical Phenomena and Phase Transitions: New York, Academic Press, v. 3, p. 357–484.

Draper, N. R., and Smith, H., 1981, Applied Regression Analysis: New York, Wiley & Sons, 2d ed., 709 p.

Eck, H., 1939, Untersuchungen im saettigungzustand des wassers von 350 C bis zur kritischen temperatur: Physik un Unserer Zeit, v. 40, p. 3–15.

Edwards, C., Lipa, J. A., and Buckingham, M. J., 1968, Specific heat of xenon near the critical point: Physical Review Letters, v. 20, p. 496–499.

Erokhin, N. F., and Kal'yanov, B. I., 1979, Experimental investigation of the velocity of ultrasound in the critical region of water: High Temperature, v. 17, p. 245–251.

———— 1980, Extreme behavior of ultrasonic velocity and of some other quantities in the supercritical region of water: Thermal Engineering, v. 27, n. 11, p. 634–636.

Few, G. A., and Rigby, M., 1973, Equation of state for systems of hard non-spherical molecules: Chemical Physics Letters, v. 20, p. 433–435.

Fisher, M. E., 1964, Correlation functions and the critical region of simple fluids: Journal of Mathematical Physics, v. 5, p. 944–962.

———— 1971, The theory of critical point singularities, *in* Green, M. S., editor, Critical Phenomena: Proceedings of the International School of Physics (Enrico Fermi), Course LI: New York, Academic Press, p. 1–99.

Fox, J. R., 1983, Method for construction of non-classical equations of state: Fluid Phase Equilibria, v. 14, p. 45–53.

Franck, E. U., 1956, Hochverdichteter wasserdampf II. Ionendissoziation von KCl in H_2O bis 750°C: Zeitschrift fuer Physikalische Chemie, v. 8, p. 107–126.

Gasparini, F., and Moldover, M. R., 1969, Specific heat of He^3–He^4 mixtures very near the λ-line: Physical Review, v. 23, p. 749–752.

Gaunt, D. S., and Sykes, M. F., 1979, The critical exponent γ for the three-dimensional Ising model: Journal of Physics A, v. 12, n. 1, p. L25–L28.

Gibbons, R. M., 1969, The scaled particle theory for particles of arbitrary shape: Molecular Physics, v. 17, p. 81–86.

Gill, P. E., Murray, W., and Wright, M. H., 1981, Practical Optimization: New York, Academic Press, 401 p.

Green, M. S., Cooper, M. J., and Levelt Sengers, J. M. H., 1971, Extended thermodynamic scaling from a generalized parametric form: Physical Review Letters, v. 26, p. 492–495.

Greer, S. C., and Moldover, M. R., 1981, Thermodynamic anomalies at critical points of fluids: Annual Review of Physical Chemistry, v. 32, p. 233–265.
Griffiths, R. B., 1965a, Ferromagnets and simple fluids near the critical point: some thermodynamic inequalities: Journal of Chemical Physics, v. 43, p. 1958–1968.
———— 1965b, Thermodynamic inequality near the critical point for ferromagnets and fluids: Physical Review Letters, v. 14, p. 623–624.
———— 1967, Thermodynamic functions for fluids and ferromagnets near the critical point: Physical Review, v. 158, p. 176–187.
———— 1970, Dependence of critical indices on a parameter: Physical Review Letters, v. 24, p. 1479–1482.
Griffiths, R. B., and Wheeler, J. C., 1970, Critical points in multicomponent systems: Physical Review A, v. 2, p. 1047–1064.
Guggenheim, E. A., 1945, The principal of corresponding states: Journal of Chemical Physics, v. 13, p. 253–261.
Haar, L., and Shenker, S. H., 1971, Equation of state for dense gases: Journal of Chemical Physics, v. 55, p. 4951–4958.
Haar, L., Gallagher, J. G., and Kell, G. S., 1980, Thermodynamic properties for fluid water, *in* Straub, J., and Scheffler, K., editors, Water and Steam: Their Properties and Current Industrial Applications: New York, Pergamon, p. 69–82.
———— 1982a. The equation of state of water at high temperatures and pressures, *in* Somiya, S., editor, International Symposium on Hydrothermal Reactions, 1st, Tokyo, Proceedings, p. 66–75.
———— 1982b, The anatomy of the thermodynamic surface of water: the formulation and comparisons with data, *in* Sengers, J. V., editor, Proceedings of the Eighth Symposium on Thermophysical Properties, Vol. 2: Thermophysical Properties of Solids and of Selected Fluids for Energy Technology: New York, American Society of Mechanical Engineers, p. 298–302.
———— 1984, NBS/NRC Steam Tables: Washington, D.C., Hemisphere Pub., 320 p.
Hanafusa, H., Tsuchida, T., Araki, M., Sato, H., Uematsu, M., Watanabe, K., 1983, Volumetric properties of water in the critical region: High Temperatures—High Pressures, v. 15, p. 311–320.
Heger, K., ms, 1969, Die statische dielektrizitatskonstante von wasser und methylalkohol im uberkritischebn temperatur und druckbereich: Ph.D. dissertation, University of Karlsruhe, F. R. Germany.
Heger, K., Uematsu, M., and Franck, E. U., 1980, The static dielectric constant of water at high pressures and temperatures to 500 MPa and 550°C: Berichte der Bunsen-Gesellschaft fur Physikalische Chemie, v. 84, p. 758–762.
Helgeson, H. C., 1964, Complexing and Hydrothermal Ore Deposition: Oxford, Pergamon, 128 p.
———— 1970, Description and interpretation of phase relations in geochemical processes involving aqueous solutions: American Journal of Science, v. 268, p. 415–438.
———— 1991, Effects of complex formation on the hydrothermal solubilities of minerals as functions of fluid pressure and temperature in the critical and supercritical regions of the system H_2O: Geochimica et Cosmochimica Acta, v. 55, in press.
Helgeson, H. C., Delany, J. M. Nesbitt, H. W., and Bird, D. K., 1978, Summary and critique of the thermodynamic properties of rock-forming minerals: American Journal of Science, v. 278-A, 229 p.
Helgeson, H. C., and Kirkham, D. H., 1974a, Theoretical prediction of the thermodynamic behavior of aqueous electrolytes at high pressures and temperatures. I. Summary of the thermodynamic/electrostatic properties of the solvent: American Journal of Science, v. 274, p. 1089–1198.
———— 1974b, Theoretical prediction of the thermodynamic behavior of aqueous electrolytes at high pressures and temperatures. II. Debye-Huckel parameters for activity coefficients and relative partial molal properties: American Journal of Science, v. 274, p. 1199–1261.
———— 1976, Theoretical prediction of the thermodynamic behavior of aqueous electrolytes at high pressures and temperatures. III. Equation of state for aqueous species at infinite dilution: American Journal of Science, v. 276, p. 97–240.
Helgeson, H. C., Kirkham, D. H., and Flowers, G. C., 1981, Theoretical prediction of the thermodynamic behavior of aqueous electrolytes at high pressures and temperatures: IV. Calculation of activity coefficients, osmotic coefficients, and apparent molal and standard and relative partial molal properties to 600°C and 5 kb: American Journal of Science, v. 281, p. 1249–1516.

Hill, P. G., 1990, A unified fundamental equation for the thermodynamic properties of H_2O: Journal of Physical and Chemical Reference Data, v. 19, n. 5, p. 1233–1274.
Hocken, R., and Moldover, M. R., 1976, Ising critical exponents in real fluids: an experiment: Physical Review Letters, v. 37, p. 29–32.
Hohenberg, P. C., and Barmatz, M., 1972, Gravity effects near the gas-liquid critical point: Physical Review A, v. 6, p. 289–313.
Hohenberg, P. C., and Halperin, B. I., 1977, Theory of dynamical critical phenomena: Reviews of Modern Physics, v. 49, p. 435–479.
Ising, E., 1925, Beitrag zur theorie des ferromagnetismus: Zeitschrift fuer Physik, v. 31, p. 253–258.
James, W. R., ms, 1968, Development and application of nonlinear regression models in geology: Ph.D. dissertation, Northwestern University, Evanston, Illinois.
Jasnow, D., and Wortis, M., 1968, High-temperature critical indicies for the classical anisotropic Heisenberg Model: Physical Review, v. 176, p. 739–750.
Johnson, J. W., 1987, Chemical equilibria in the H_2O critical region: Geological Society of America Abstracts with Programs, v. 19, p. 718.
Johnson, J. W., and Norton, D., 1986, Transport and chemical consequences of critical phenomena in magma-hydrothermal systems: A preliminary assessment: Geological Society of America Abstracts with Programs, v. 18, p. 647.
Josephson, B. D., 1969, Equation of state near the critical point: Journal of Physics C, v. 2, p. 1113–1115.
Juza, J., 1966, An equation of state for water and steam: Prague, Ceskoslovenske Akademie Ved, Akademie Nakladatelstvi, p. 131–142.
Kac, M., Uhlenbeck, G. E., and Hemmer, P. C., 1963, On the van der Waals theory of the vapor-liquid equilibrium. I. Discussion of a one-dimensional models: Journal of Mathematical Physics, v. 4, p. 216–228.
Kadanoff, L. P., 1966, Scaling laws for Ising models near T_c: Physics, v. 2, n. 6, p. 263–272.
———— 1971, Critical Behavior. Universality and scaling., *in* Green, M. S., editor, Critical Phenomena: Proceedings of the Intenational School of Physics (Enrico Fermi), Course LI: New York, Academic Press, p. 100–117.
Keenan, J. H., Keyes, F. G., Hill, P. G., and Moore, J. G., 1969, Steam Tables: New York, John Wiley & Sons, 162 p.
Kerimov, A. M., 1968, Investigation of the isochoric specific heat of water and steam near the critical point: Teploenergetika, v. 15, p. 60–65.
Kestin, J., and Sengers, J. V., 1986, New international formulations for the thermodynamnic properties of light and heavy water: Journal of Physical and Chemical Reference Data, v. 15, p. 305.
Kestin, J., Sengers, J. V., Kamgar-Parsi, B., and Levelt Sengers, J. M. H., 1984, Thermophysical properties of fluid H_2O: Journal of Physical and Chemical Reference Data, v. 13, p. 175–183.
Kirkwood, J. G., 1939, The dielectric polarization of polar liquids: Journal of Chemical Physics, v. 7, p. 911–919.
Knapp, R. B., and Knight, J. E., 1977, Differential thermal expansion of pore fluids: fracture propogation and microearthquake production in hot pluton environments: Journal of Geophysical Research, v. 82, p. 2515–2522.
Le Guillou, J. C., and Zinn-Justin, 1980, Critical exponents from field theory: Physical Review B, v. 21, p. 3976–3998.
Le Neindre, B., Tufeu, R., Bury, P., and Sengers, J. V., 1973, Thermal conductivity of carbon dioxide and steam in the supercritical region: Berichte der Bunsen-Gesellschaft fur Physikalische Chemie, v. 77, p. 262–275.
Lee, T. D., and Yang, C. N., 1952, Statistical theory of equations of state and phase transitions. II. Lattice gas and Ising Model: Physical Review, v. 87, p. 410–419.
Levelt Sengers, J. M. H., 1970, Scaling predictions for thermodynamic anomalies near the gas-liquid critical point: Industrial and Engineering Chemistry Fundamentals, v. 9, p. 470–481.
———— 1974, From van der Waals' equation to the scaling laws: Physica, v. 73, p. 73–106.
———— 1979, Liquidons and gasons: controversies about the continuity of states: Physica, v. 98A, p. 363–402.
———— 1983, The state of the critical state of fluids: Pure and Applied Chemistry, v. 55, p. 437–453.
Levelt Sengers, J. M. H., Everhart, C. M. Morrison, G., and Chang, R. F., 1984, Impure Steam near the critical point, *in* Proceedings of the 10th International Conference on the Properties of Steam: Moscow, MIR Publ., p. 277–288.

Levelt Sengers, J. M. H., Everhart, C. M., Morrison, G., and Pitzer, K. S., 1986, Thermodynamic anomalies in near-critical aqueous NaCl solutions: Chemical Engineering Communications, v. 47, p. 315–328.

Levelt Sengers, J. M. H., and Greer, S. C., 1972, Thermodynamic anomalies near the critical point of steam: International Journal of Heat and Mass Transfer, v. 15, p. 1865–1886.

Levelt Sengers, J. M. H., Greer, W. L., and Sengers, J. V., 1976, Scaled equation of state parameters for gases in the critical region: Journal of Physical and Chemical Reference Data, v. 5, p. 1–51.

Levelt Sengers, J. M. H., Kamgar-Parsi, B., Balfour, F. W., and Sengers, J. V., 1983, Thermodynamic properties of steam in the critical region: Journal of Physical and Chemical Reference Data, v. 12, p. 1–28.

Levelt Sengers, J. M. H., Kamgar-Parsi, B., and Sengers, J. V., 1983, Thermodynamic properties of isolutane in the critical region: Journal of Chemical and Engineering Data, v. 28, p. 354–362.

Levelt Sengers, J. M. H., Morrison, G., and Chang, R. F., 1983, Critical behavior in fluids and fluid mixtures: Fluid Phase Equilibria, v. 14, p. 19–44.

Levelt Sengers, J. M. H., and Sengers, J. V., 1975, Universality of critical behavior in gases: Physical Review A, v. 12, p. 2622–2627.

———— 1981, How close is "close to the critical point"?, *in* Ravoche, H. J., editor, Perspectives in Statistical Physics: New York, North-Holland, p. 239–271.

Ley-Koo, M., and Green, M. S., 1977, Revised and extended scaling for coexisting densities of SF_6: Physical Review A, v. 16, p. 2483–2487.

———— 1981, Consequences of the renormalization group for the thermodynamics of fluids near the critical point: Physical Review A, v. 23, p. 2650–2659.

Ley-Koo, M., and Sengers, J. V., 1982, On corrections to scaling in the thermodynamic properties of fluids near the critical point, *in* Sengers, J. V., editor, Proceedings of the Eighth Symposium on Thermophysical Properties, Vol. 1: Thermophysical Properties of Fluids: New York, American Society of Mechanical Engineers, p. 358–364.

Liberman, D. A., 1966, Another relation between thermodynamic functions near the critical point of a simple fluid: Journal of Chemical Physics, v. 44, p. 419–420.

Lipa, J. A., Edwards, C., and Buckingham, M. J., 1970, Precision measurement of the specific heat of CO_2 near the critical point: Physical Review Letters, v. 25, p. 1086–1090.

Lorentzen, H. L., 1953, Studies of critical phenomena in carbon dioxide contained in vertical tubes: Acta Chemica Scandinavica, v. 7, p. 1335–1346.

Marshall, W. L., and Jones, E. V., 1974, Liquid-vapor critical temperatures of aqueous electrolyte solutions: Journal of Inorganic Nuclear Chemistry, v. 36, p. 2313–2318.

Mayer, J. E., and Mayer, M. A., 1940, Statistical Mechanics: New York, John Wiley & Sons, 495 p.

Mermin, N. D., and Rehr, J. J., 1971, Generality of the singular diameter of the liquid-vapor coexistence curve: Physical Review Letters, v. 26, p. 1155–1156.

McKenzie, W. F., and Helgeson, H. C., 1984, Estimation of the dielectric constant of H_2O from experimental solubilities of quartz, and calculation of the thermodynamic properties of aqueous species to 900°C and 2 kb: Geochimica et Cosmochimica Acta, v. 48, p. 2167–2177.

Michels, A., Blaisse, B., and Michels, C., 1937, The isotherms of CO_2 in the neighborhood of the critical point and round the coexistence line: Proceedings of the Royal Society of London, Series A, v. 160, p. 358–375.

Michels, A., Levelt, J. M., and Graaff, W. de, 1958, Compressibility isotherms of argon at temperatures between −25°C and −155°C, and at densities up to 640 amagat (pressures up to 1050 atmospheres): Physica, v. 24, p. 659–671.

Miller, W., 1984, The engineering of numerical software: Englewood Cliffs, N.J., Prentice-Hall 167 p.

Moldover, M. R., 1969, Scaling of the specific-heat singularity of He^4 near its critical point: Physical Review, v. 182, p. 342–352.

———— 1978, Implementation of scaling and extended scaling equations of state for the critical point of fluids: Journal of Research of the National Bureau of Standards, v. 83, n. 4, p. 329–334.

———— 1982, Thermodynamic anomalies near the liquid-vapor critical point: A review of experiments, *in* Levy, M., Le Guillou, J. C., and Zinn-Justin, J., editors, Phase Transitions: New York, Plenum, p. 63–94.

Moldover, M. R., and Little, W. A., 1966, The specific heat of He^3 and He^4 in the neighborhood of their critical points, *in* Green, M. S., and Sengers, J. V., editors, Critical Phenomena: Proceedings of a Conference: Washington, National Bureau of Standards Miscellaneous Publications, n. 273, p. 79–85.

Norton, D., 1984, Theory of hydrothermal systems: Annual Review of Earth and Planetary Sciences, v. 12, p. 155–177.

Norton, D., and Cathles, L. M., 1979, Thermal aspects of ore deposition, *in* Barnes, H. L., editor, Geochemistry of Hydrothermal Ore Deposition: New York, John Wiley & Sons, p. 611–631.

Norton, D., and Knight, J. E., 1977, Transport phenomena in hydrothermal systems: Cooling plutons: American Journal of Science, v. 277, p. 937–981.

Oltermann, G., ms, 1977, Measurement of the viscosity of steam in the vicinity of the critical state: Ph.D. dissertation, Technical University, Hanover, Germany.

Onnes, H. K., 1901, Proceedings of the Section of Sciences: Akademie Wetenschappen, Amsterdam, v. 4, p. 125.

Onsager, L. 1936, Electric moments of molecules in liquids: Journal of the American Chemical Society, v. 58, p. 1486–1493.

———— 1944, Crystal statistics. I. A two-dimensional model with an order-disorder transition: Physical Review, v. 65, p. 117–149.

Osborne, N. S., Stimson, H. F., Fiock, E. F., and Ginnings, D. C. 1933, The pressure of saturated water vapor in the range 100° to 374°C: Journal of Research of the National Bureau of Standards, v. 10, p. 155–188.

Osborne, N. S., Stimson, H. F., and Ginnings, D. C., 1937, Calorimetric determination of the thermodynamic properties of saturated water in both the liquid and gaseous states from 100° to 374°C: Journal of Research of the National Bureau of Standards, v. 18, p. 389–447.

Oshry, H. I., ms, 1949, The dielectric constant of saturated water from the boiling point to the critical point: Ph.D. dissertation, University of Pittsburgh, Pittsburgh, Penn., 13 p.

Oster, G., and Kirkwood, J. G., 1943, The influence of hindered molecular rotation on the dielectric constants of water, alcohols, and other polar liquids: Journal of Chemical Physics, v. 11, p. 175–178.

Owen, B. B., Miller, R. C., Milner, C. E., and Cogan, H. L., 1961, The dielectric constant of water as a function of temperature and pressure: Journal of Physical Chemistry, v. 65, p. 2065–2070.

Percus, J. K., and Yevick, G. J., 1958, Analysis of classical statistical mechanics by means of collective coordinates: Physical Review, v. 110, p. 1–13.

Pings, C. J., and Teague, R. K., 1968, Experimental study of the shape of the coexistence curve of argon near the critical state: Physics Letters, v. 26A, p. 496–497.

Pitzer, K. S., 1983, Dielectric constant of water at very high temperature and pressure: Proceedings of the National Academy of Sciences, v. 80, p. 4575–4576.

Powell, E. G., Wilmot, G., Haar, L., and Klein, M., 1979, Equations of state and thermodynamic data for interior ballistics calculations, *in* Krier, H., and Summerfield, M., editors, Interior Ballistics of Guns: New York, American Institute of Aeronautics and Astronautics, p. 325–348.

Quist, A. S., and Marshall, W. L., 1965, Estimation of the dielectric constant of water to 800°C: Journal of Physical Chemistry, v. 69, n. 9, p. 3165–3167.

Rehr, J. J., and Mermin, N. D., 1973, Revised scaling equation of state at the liquid-vapor critical point: Physical Review A, v. 8, p. 472–480.

Rivkin, S. L., and Akhundov, T. S., 1962, Experimental investigation of the specific volume of water: Teploenergetika, v. 9, p. 57–65.

———— 1963, Experimental determination of the specific volume of water at temperatures in the range 374.15–500°C and pressures up to 600 kg/cm^2: Teploenergetika, v. 10, p. 66–71.

———— 1966, A study of the specific volumes of water in the region close to the critical point: Teploenergetika, v. 13, p. 59–62.

Rivkin, S. L., Levin, A. Ya., Izrailevsky, L. B., 1976, Experimental study of the viscosity of water near the critical point: Teplofizicheskie Svoistva Veshchestv i Materialov, v. 10, p. 232–241.

Rivkin, S. L., Levin, A. Ya., Izrailevsky, L. B., and Kharitonov, K. G., 1975, Experimental investigation of viscosity of light water near the critical point and of heavy water in liquid phase and in supercritical region, *in* Bury, P., Perdon, H., and Vodar, B., editors, Proceedings of the Eighth International Conference on the Properties of Water and Steam: Paris, Editions Europeennes Thermiques et Industries, p. 153–162.

Rivkin, S. L., and Troianovskaia, G. V., 1964, Determination of the specific volume near the critical region: Teploenergetika, v. 11, p. 72–75.
Roach, P. R., 1968, Pressure-temperature-density surface of He^4 near the critical point: Physical Review, v. 170, p. 213–223.
Robie, R. A., Hemingway, B. S., and Fisher, J. R., 1978, Thermodynamic properties of minerals and related substances at 298.15°*K* and 1 *bar* (10^5 *Pascals*) pressure and at higher temperatures: United States Geological Survey Bulletin 1452, 456 p.
Roedder, E., 1972, Composition of fluid inclusions: United States Geological Survey Professional Paper 440 JJ.
———— 1979, Fluid inclusions as samples of ore fluids, *in* Barnes, H. L., editor, Geochemistry of Hydrothermal Ore Deposition: New York, John Wiley & Sons, p. 684–737.
———— 1984, Fluid Inclusions: Reviews in Mineralogy, v. 12: Washington, D.C., Mineralogical Society of America, 646 p.
Rowlinson, J. S., 1969, Liquids and Liquid Mixtures, 2d ed., London, Butterworth, 371 p.
Rushbrooke, G. S., 1963, On the thermodynamics of the critical region for the Ising problem: Journal of Chemical Physics, v. 39, p. 842–843.
Schofield, P., 1969, Parametric representation of the equation of state near a critical point: Physical Review Letters, v. 22, p. 606–608.
Sengers, J. V., 1973, Transport properties of gases and binary liquids near the critical state, *in* Kestin, J., editor, Transport Phenomena—1973: American Institute of Physics Conference Proceedings Number 11: New York, American Institute of Physics, p. 229–277.
———— 1982, Universality of critical phenomena in classical fluids, *in* Levy, M., Le Guillou, J. C., and Zinn-Justin, J., editors, Phase Transitions: New York, Plenum, p. 95–136.
———— 1985, Transport properties of fluids near critical points: International Journal of Thermophysics, v. 6, p. 203–232.
Sengers, J. V., and Kamgar-Parsi, B., 1984, Representative equations for the viscosity of water substance: Journal of Physical and Chemical Reference Data, v. 13, p. 185–205.
Sengers, J. V., and Levelt Sengers, J. M. H., 1978, Critical phenomena in classical fluids, *in* Croxton, C. A., editor, Progress in Liquid Physics: New York, John Wiley & Sons, p. 103–174.
———— 1984, A universal representation of the thermodynamic properties of fluids in the critical region: International Journal of Thermophysics, v. 5, p. 195–208.
———— 1986, Thermodynamic behavior of fluids near the critical point: Annual Review of Physical Chemistry, v. 37, p. 189–222.
Sengers, J. V., and Watson, J. T. R., 1986, Improved international formulations for the viscosity and thermal conductivity of water substance: Journal of Physical and Chemical Reference Data, v. 15, p. 1291–1314.
Sengers, J. V., Watson, J. T. R., Basu, R. S., Kamgar-Parsi, B., and Hendricks, R. C., 1984, Representative equations for the thermal conductivity of water substance: Journal of Physical and Chemical Reference Data, v. 13, p. 893–933.
Shock, E. L., and Helgeson, H. C., 1988, Calculation of the thermodynamic and transport properties of aqueous species at high pressures and temperatures: Correlation algorithms for ionic species and equation of state predictions to 5 kb and 1000°C: Geochimica et Cosmochimica Acta, v. 52, p. 2009–2036.
———— 1990, Calculation of the thermodynamic and transport properties of aqueous species at high pressures and temperatures: Standard partial molal properties of organic species: Geochimica et Cosmochimica Acta, v. 54, p. 915–945.
Shock, E. L., Helgeson, H. C., and Sverjensky, D. A., 1989, Calculation of the thermodynamic and transport properties of aqueous species at high pressures and temperatures: Standard partial molal properties of inorganic neutral species: Geochimica et Cosmochimica Acta, v. 53, p. 2157–2183.
Silvester, L. F., and Pitzer, K. S., 1977, Thermodynamics of electrolytes. 8. High-temperature properties, including enthalpy and heat capacity, with application to sodium chloride: Journal of Physical Chemistry, v. 81, n. 19, p. 1822–1828.
Sirota, A. M., and Mal'tsev, B. K., 1962, Experimental determination of the specific heat of water in the critical region: Teploenergetika, v. 9, p. 52–57.
Smith, L. B., Keyes, F. G., and Gerry, H. T., 1934, The vapor pressure of water: Proceedings of the American Academy of Arts and Sciences, v. 69, p. 137–168.
Smith, L. B., and Keyes, F. G., 1934, The volumes of unit mass of liquid water and their correlation as a function of pressure and temperature: Proceedings of the American Academy of Arts and Sciences, v. 69, p. 285–312.

Stanley, H. E., 1971, Introduction to Phase Transitions and Critical Phenomena:New York, Oxford Univ. Press, 308 p.

Stimson, H. F., 1969, Some precise measurements of the vapor pressure of water in the range from 25 to 100°C: Journal of Research of the National Bureau of Standards, v. 73A, p. 493–496.

Straus, J. M., and Schubert, G., 1977, Thermal convection of water in a porous medium: Effects of temperature- and pressure-dependent thermodynamic and transport properties: Journal of Geophysical Research, v. 82, p. 325–333.

Tanger, J. C., and Helgeson, H. C., 1988, Calculation of the thermodynamic and transport properties of aqueous species at high pressures and temperatures: revised equations of state for the standard partial molal properties of ions and electrolyes: American Journal of Science, v. 288, p. 19–98.

Thiele, E., 1963, Equation of state for hard spheres: Journal of Chemical Physics, v. 39, p. 474–479.

Tisza, L., and Chase, C. E., 1965, Equation of state of ^4He in the critical region: Physical Review Letters, v. 15, p. 4–6.

Tritton, D. J., 1977, Physical Fluid Dynamics: New York, Van Nostrand Reinhold, 362 p.

Uematsu, M., and Franck, E. U., 1980, Static dielectric constant of water and steam: Journal of Physical and Chemical Reference Data, v. 9, p. 1291–1304.

van der Waals, J. D., ms, 1873, Over de continuiteit van den gas-en vloeistoftoestand, Ph.D. dissertation, University of Leiden.

Verschaffelt, J. E., 1900, On the critical isothermal line and the densities of liquified carbonic acid near the critical temperature: Communications from the Kamerlingh Onnes Laboratory of the University of Leiden, n. 55.

Vicentini-Missoni, M., Levelt Sengers, J. M. H., and Green, M. S., 1969a, Thermodynamic anomalies of CO_2, *Xe* and He^4 in the critical region: Physical Review Letters, v. 22, p. 389–393.

———— 1969b, Scaling analysis of thermodynamic properties in the critical region of fluids: Journal of Research of the National Bureau of Standards, v. 73A, p. 563–583.

Voronel, A. V., 1976, Thermal measurements and critical phenomena in liquids, *in* Domb, C., and Green, M. S., editors, *Critical Phenomena and Phase Transitions:* New York, Academic Press, v. 5B, p. 344–394.

Voronel, A. V., Chashkin, Yu. R., Popov, V. A., and Simkin, V. G., 1964, Measurements of the specific heat C_v of oxygen near the critical point: Soviet Physics JETP, v. 18, p. 568–569.

Voronel, A. V., Snigirev, V. G., and Chashkin, Yu. R., 1965, Behavior of the specific heat C_v of pure substances near the critical point: Soviet Physics JETP, v. 21, p. 653–655.

Vukalovich, M. P., Vargaftik, N. B., Rivkin, S. L., and Aleksandrov, A. A., 1967, Report of the International Committee on the formulation for water and saturated steam: Teploenergetika, v. 14, p. 91–93.

Wallace, B., Jr., and Meyer, H., 1970a, Equation of state of He^3 close to the critical point: Physical Review A, v. 2, p. 1563–1575.

———— 1970b, Critical isotherm of He^3: Physical Review A, v. 2, p. 1610–1612.

Wardell, J. R., Wilmot, G. B., Haar, L., and Klein, M., 1975, Thermodynamic data for interior ballistics calculations, *in* 12th JANNAF Combustion Meeting: Chemical Propulsion Information Agency, Publication 273, v. 1, p. 363–390.

Watson, J. T. R., 1977, The thermal conductivity of water substance—final release to IAPS on 8 June 1977: Techical Report Y1/173, National Engineering Laboratory, U.K.

Watson, J. T. R., Basu, R. S., and Sengers, J. V., 1980a, An improved equation for the viscosity of water and steam, *in* Straub, J., and Scheffler, K., editors, Water and Steam: Their Properties and Current Industrial Applications: New York, Pergamon, p. 336–343.

———— 1980b, An improved representative equation for the dynamic viscosity of water substance: Journal of Physical and Chemical Reference Data, v. 9, p. 1255–1290.

Waxman, M., and Gallagher, J. S, 1983, Thermodynamic properties of isobutane for temperatures from 250–600° *K* and pressures from 0.1–40 *MPa*: Journal of Chemical and Engineering Data, v. 28, p. 224–241.

Weber, L. A., 1970, Density and compressibility of oxygen in the critical region: Physical Review A2, p. 2379–2388.

Wegner, F. J., 1972, Corrections to scaling laws: Physical Review B, v. 5, p. 4529–4536.

Wertheim, M. S, 1963, Exact solution of the Percus-Yevick integral equation for hard spheres: Physical Review Letters, v. 10, p. 321–323.

———— 1964, Analytic solution of the Percus-Yevick equation: Journal of Mathematical Physics, v. 5, p. 643–651.

Widom, B., 1965, Equation of state in the neighborhood of the critical point: Journal of Chemical Physics, v. 43, p. 3898–3905.

———— 1974, The critical point and scaling theory: Physica, v. 73, p. 107–118.

Widom, B., and Rice, O. K., 1955, Critical isotherm and the equation of state of liquid-vapor systems: Journal of Chemical Physics, v. 23, p. 1250–1255.

Wilson, K. G., 1971a, Renormalization group and critical phenomena. I. Renormalization group and the Kadanoff scaling picture: Physical Review B4, p. 3174–3183.

———— 1971b, Renormalization group and critical phenomena. II. Phase-space cell analysis of critical behavior: Physical Review, B4, p. 3184–3205.

———— 1983, The renormalization group and critical phenomena: Reviews of Modern Physics, v. 55, p. 583–600.

Woolley, H. W., 1980, Thermodynamic properties for H_2O in the ideal gas state, *in* Straub, J., and Scheffler, K., editors, Water and Steam: Their Properties and Current Industrial Applications: New York, Pergamon, p. 166–175.

———— 1983, A switch function applied to the thermodynamic properties of steam near and not near the critical point: International Journal of Thermophysics, v. 4, p. 51–95.

Zinn-Justin, J., 1979, Analysis of Ising model critical exponents from high temperature series expansion: Journal de Physique, v. 40, p. 969–975.